Tight-binding treatment of conjugated polymers

Lynge, Thomas Bastholm

Publication date:
2004

Document Version
Publisher's PDF, also known as Version of record

Thomas Bastholm Lynge

Tight-Binding Treatment of Conjugated Polymers

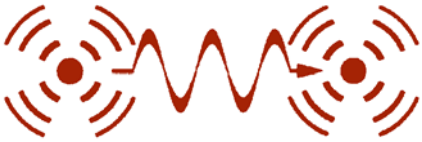

Institute of Physics and Nanotechnology
Aalborg University, Denmark

TIGHT-BINDING TREATMENT OF CONJUGATED POLYMERS

TIGHT-BINDING BESKRIVELSE AF KONJUGEREDE POLYMERER

Published and distributed by
Institute of Physics and Nanotechnology, Aalborg University
Pontoppidanstræde 103, DK–9220 Aalborg Øst.
Phone +45 96 35 80 80. Fax +45 98 15 65 02.

Typeset in LaTeX2$_\varepsilon$ by the author.

Printed in Denmark by Centertrykkeriet, Aalborg University.

ISBN 87-89195-24-8

Preface

This PhD thesis is based on the results obtained during my PhD studies from September 1st 2001 to August 31st 2004 at the Institute of Physics and Nanotechnology, Aalborg University, Denmark, under the skilled supervision of Dr. Thomas Garm Pedersen. The thesis has been submitted to the Faculty of Engineering and Science at Aalborg University.

Outline

The motivation for studying the conjugated polymers *trans*-polyacetylene (tPA), poly(*para*-phenylene) (PPP) and poly(*para*-phenylene vinylene) (PPV) is given in Part I which also contains a description of the physical characteristics of a conjugated polymer.

Part II contains the theoretical text book foundation for this work, while Parts III-IV are based on the scientific papers [1, 2, 3, 4] which constitute the basis of this thesis. Part III is concerned with optical susceptibility with Chap. 8 containing an analytic derivation of the linear optical susceptibility of tPA and PPP, while Chap. 9 deals with the electro-optic susceptibility of PPP. In Part IV, the Density Functional-based Tight-Binding (DFTB) approach is applied to phonons in tPA and PPP (Chap. 10) and to polarons in tPA, PPP and PPV (Chap. 11). Part V contains a summary of conclusions and an outlook.

It has been the ambition to make this thesis accessible to physics student from the bachelor level and up. The theoretical foundation in Part II is therefore quite elaborate and might easily be skipped by anyone with a background in condensed matter physics, maybe with the exception of Chap. 5 which describes the perhaps less well-known DFTB approach.

Acknowledgements

I am grateful to the Frauenheim Group at the Department of Theoretical Physics, University of Paderborn, for providing the DFTB code with which the results presented in Chap. 11 were obtained. I would especially like to thank Dr. Marcus Elstner and Dr. Thomas Niehaus for fruitful discussions in that relation.

Financial support from the Danish Technical Science Council STVF, talent Grant No. 56-00-0290, is also gratefully acknowledged.

Last, but certainly not least, I would like to thank my wife Helen Urban for her never-ending love and support. Without you, none of this would have mattered.

Aalborg, Denmark, August 2004 **Thomas Bastholm Lynge**

Contents

Part I

Motivation

Chapter 1

Conjugated Polymers

A monomer[1] is a small molecule that may become chemically bonded to other monomers to form oligomer[2] chains called dimers, trimers, tetramers, pentamers[3], etc. according to the number of monomers in the chain. A polymer[4] is a long chain of monomers put together through a chemical process known as polymerization, and polymers are often treated as being infinitely long. Polymers can be both organic (carbon based) as well as inorganic.

In a chemical terminology, conjugated means with alternating single and double covalent bonds. In general, conjugation leads to electron delocalization, and the term conjugated has consequently been somewhat generalized to characterize systems containing communities of delocalized electrons.

By the term conjugated polymer (CP), one generally understands an organic polymer in which the $2s$, $2p_x$ and $2p_y$ atomic carbon orbitals are tied up in sp^2-hybridized covalent bonds with the neighboring atoms while the $2p_z$ orbitals form delocalized orbitals with symmetry axes perpendicular to the plane of the unit cell in question. A CP is thus characterized by an unsaturated sp^2p_z-hybridization that leaves one unpaired, delocalized electron per carbon atom.

Because of their p-like symmetry, the delocalized orbitals are known as π-orbitals[5]. The delocalized π-electrons are the most loosely bound of the electrons in a CP and therefore dominate the electric and optical properties. Due to the relatively weak inter-chain interactions, the π-electrons are primarily delocalized along the polymer chain. Furthermore, overlap between the π-orbitals create occupied bonding π-orbitals and unoccupied anti-bonding π^*-orbitals that form valence and conduction bands, respectively. Therefore, chain-aligned samples

[1] *Mono* and *meros* are the greek words for "one" and "part", respectively.

[2] *Oligo* is greek for "a few".

[3] *Di, tri, tetra, penta* is greek for "two, three, four, five".

[4] *Poly* is greek for "many".

[5] More precisely, this type of conjugated system should be called π-conjugated as opposed to σ-conjugated systems in which the delocalized orbitals have s-like symmetry.

of CP are quasi-one-dimensional semiconductors with metal-sized conductivities obtainable through doping [5].

The simplest example of a CP is polyacetylene (PA) which is the polymerization of the monomer acetylene (C_2H_2). As shown in Fig. 1.1, acetylene can polymerize to either *cis*- or *trans*-polyacetylene. As these two polymers have the same chemical formula, they are known as isomers[6]. *Trans*-polyacetylene (tPA), which is treated in this work, is thermodynamically the most stable of the two isomers [6], and *cis* to *trans* isomerization can therefore be obtained by heating.

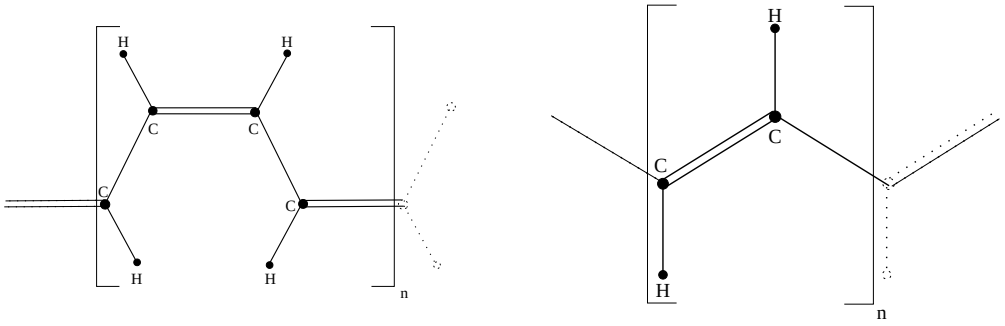

Figure 1.1: Left: The unit cell of *cis*-polyacetylene. Right: The unit cell of *trans*-polyacetylene.

Besides tPA, this work contains results obtained for the CP poly(*para*-phenylene) (PPP) and poly(*para*-phenylene vinylene) (PPV). The unit cells of tPA, PPP and PPV are shown in Fig. 1.2 where the π-orbitals have symmetry axes out of the plane of the paper. Notice that, as discussed in Secs. 8.3 and 10.1.2, the torsion between alternating benzene rings is ignored for PPP and PPV.

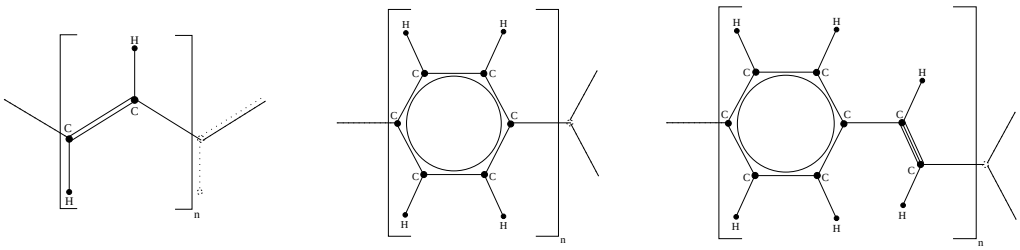

Figure 1.2: From left to right the unit cells of *trans*-polyacetylene, poly(*para*-phenylene) and poly(*para*-phenylene vinylene). One electron per carbon atom occupies a delocalized π-orbital with p-like symmetry axis out of the plane of the unit cell. For the phenyl rings, this electron community is indicated by a ring.

[6] *Iso* is greek for "same".

1.1 Conjugated Polymers in Modern Research

Due to the vast technological potentialities of CP, a lot of research effort has been invested in this area within the last few decades. One of the pioneering efforts leading to an overall interest in organic materials was the 1963 reporting of electroluminescence[7] from organic semiconductors [7]. Following the 1977 report of metal-sized conductivities in doped polyacetylene [8], a substantial part of that interest was devoted to CP. The recognition of CP as a fruitful area of research culminated when Alan J. Heeger, Alan G. MacDiarmid and Hideki Shirakawa were awarded The Nobel Prize in Chemistry 2000 "for the discovery and development of conductive polymers".

Today, solar cells [9] and polymer light emitting diodes (PLED) [10, 11] have been produced showing attractive device characteristics. Polymer-based solar cells are expected to reduce the production costs of solar cell arrays substantially, and PLED have already been implemented in various sorts of screen displays. In the future, colour screen displays based on PLED are expected to combine high quality with low production costs as well as practicability and low energy demands. Anno 2004, the market for computer and TV screens are still dominated by the bulky, energy demanding and low quality but also low cost cathode ray tubes that date as far back as 1928. As for the more modern flat screen alternatives in Liquid Screen Displays (LCD) and plasma screens, besides various technical imperfections, large production costs remain a problem. Therefore, along with screens based on carbon nano tubes, PLED-based screens are expected to assert their claim to the flat screen technology of tomorrow.

Solar cells and PLED owe their technological success to the following characteristics of CP [12]: 1) Charge transport ability, 2) High photon-to-current conversion efficiency (solar cells) and high-efficiency electroluminescence in the visible (PLED) with wavelengths tunable by chemical modification[8] and 3) The simple processing techniques, light weight and flexibility common to all plastics. Furthermore, the fast response times characteristic of organic materials in general make the use of CP appealing in connection with photo detection [13]. In short, CP combine the desirable properties of plastics with the electronic and optoelectronic properties of conventional inorganic semiconductors. When it comes to practically all semiconductor-based devices, therefore, organic devices in general and CP-based devices in particular have proved to be competitive with conventional inorganic devices. In addition to the abovementioned solar cells and PLED, such devices include plastic lasers [14] and field-effect transistors [15].

Being the simplest of all CP, the electronic, optical and structural properties of PA has been thoroughly investigated over the years [6, 16, 17, 18, 19, 20, 21, 22, 23, 24, 25], and tPA has been included in this work due to its status as

[7] Electroluminescence is the generation of light by electrical excitation and is the physical mechanism behind light emitting diodes.

[8] This process is known as band gap engineering

a well-studied model polymer for which comparable results are abundant. The phenyl-based CP PPP and PPV have been chosen as supplement to the linear polymer tPA because they are technologically promising. In 1990, PPV was the first CP to display electroluminescence in the visible [10, 26], and in 1992, PPP was the first CP to be used in a PLED showing blue light emission at room temperature [27, 28, 29]. PPP and PPV have also drawn substantial interest over the years [22, 30, 31, 32], but the obtained results have been somewhat less exhaustive than for PA.

1.2 Modeling Conjugated Polymers

The models used for the CP treated in this work have some common features:

- Due to weak inter-chain interactions, parallel non-interacting chains are treated.
- The treated chains are pristine (undoped).
- Torsion is disregarded in the phenyl-based polymers PPP and PPV.

Part II

Theoretical Foundation

Chapter 2

This chapter contains a description of the tight-binding approximation applied to a periodic crystal with Sec. 2.2.2 containing the extention to a finite molecule. In Sec. 2.1, the characteristics of a periodic potential are described.

2.1 Periodic Potential

In a perfect crystal[1], the atoms are arranged in a periodic lattice consisting of identical unit cells, and the effective one-electron potential V (see Sec. 4.6) has the same periodicity as the lattice:

$$V\left(\vec{r}+\vec{R}_{\mathrm{l}}\right)=V(\vec{r}) \quad , \; \forall \vec{R}_{\mathrm{l}}, \tag{2.1}$$

in which the lattice vector $\vec{R}_{\mathrm{l}}$ connects two identical lattice points.

For this time-independent potential, the solutions to the time-dependent Schrödinger equation

$$\hat{H}\,\Psi(\vec{r},t) = i\hbar\frac{\partial\Psi(\vec{r},t)}{\partial t} \tag{2.2a}$$

$$, \quad \hat{H}=-\frac{\hbar^2\nabla^2}{2m_e}+V(\vec{r}) \tag{2.2b}$$

can be written

$$\Psi(\vec{r},t) = e^{\frac{-i}{\hbar}\hat{H}t}\Psi(\vec{r},0) \tag{2.3a}$$

$$, \quad e^{\frac{-i}{\hbar}\hat{H}t}=1+\frac{\frac{-i}{\hbar}\hat{H}t}{1!}+\frac{\left(\frac{-i}{\hbar}\hat{H}t\right)^2}{2!}+\cdots \tag{2.3b}$$

for some initial state $\Psi(\vec{r},0)$.

[1] In all real crystals, periodicity is broken because of impurities, lattice imperfections, thermal vibrations of the atoms (phonons), etc.

The energy eigenfunctions $\psi(\vec{r})$ satisfy the time-independent Schrödinger equation

$$\hat{H}\psi(\vec{r}) = \epsilon\psi(\vec{r}). \tag{2.4}$$

If the initial state is an energy eigenfunction, $\Psi(\vec{r},0) = \psi(\vec{r})$, Eq. (2.3a) takes the much simpler form

$$\Psi(\vec{r},t) = e^{-i\omega t}\psi(\vec{r}) \quad , \quad \omega = \frac{\epsilon}{\hbar}. \tag{2.5}$$

2.1.1 The Bloch Theorem

Electrons moving in a periodic one-electron potential as described in Eq. (2.1) are known as Bloch electrons[2]. Due to the periodicity of the potential, the wave functions of Bloch electrons have some characteristics that are stated in the Bloch Theorem which will be derived in the following.

Since the electron density follows the periodicity of the lattice, one has

$$\left|\psi\left(\vec{r}+\vec{R}_\mathrm{l}\right)\right|^2 = \left|\psi(\vec{r})\right|^2, \tag{2.6}$$

such that the translation operator $\hat{T}_{\vec{R}_\mathrm{l}}$ defined by

$$\hat{T}_{\vec{R}_\mathrm{l}}\psi(\vec{r}) = \psi\left(\vec{r}+\vec{R}_\mathrm{l}\right) \tag{2.7}$$

satisfies the eigenvalue equation

$$\hat{T}_{\vec{R}_\mathrm{l}}\psi(\vec{r}) = e^{iT_{\vec{R}_\mathrm{l}}}\psi(\vec{r}) \tag{2.8}$$

for some real, $\vec{R}_\mathrm{l}$-dependent number $T_{\vec{R}_\mathrm{l}}$.

Writing

$$e^{iT_{\vec{R}_\mathrm{l}}} = e^{i\vec{k}\cdot\vec{R}_\mathrm{l}}, \tag{2.9}$$

one has introduced the crystal wave vector $\vec{k}$ as a quantum number associated with the translation operator.

Since, due to the periodicity of the potential, the Hamiltonian and the translation operator commute:

$$\left[\hat{H},\hat{T}\right] = 0, \tag{2.10}$$

simultaneous eigenfunctions exist for the two operators. Therefore, the solutions to Eq. (2.4) can be written

$$\psi_{a\vec{k}}(\vec{r}+\vec{R}_\mathrm{l}) = e^{i\vec{k}\cdot\vec{R}_\mathrm{l}}\psi_{a\vec{k}}(\vec{r}), \tag{2.11}$$

[2]Free electrons occur for the simplest imaginable periodic potential $V(\vec{r}) = 0$.

where the band number a characterizes different solutions with same $\vec{k}$, and where $e^{i\vec{k}\cdot\vec{R}_\mathrm{l}}$ is known as the Bloch factor.

Eq. (2.11) implies that the energy eigenfunctions can be written as a plane wave multiplied by a so-called Bloch function which has the periodicity of the lattice:

$$\psi_{a\vec{k}}(\vec{r}) = e^{i\vec{k}\cdot\vec{r}} u_{a\vec{k}}(\vec{r}) \tag{2.12a}$$

$$, \quad u_{a\vec{k}}\left(\vec{r}+\vec{R}_\mathrm{l}\right) = u_{a\vec{k}}(\vec{r}) \quad , \; \forall \vec{R}_\mathrm{l}. \tag{2.12b}$$

Eqs. (2.11) and (2.12) are two equivalent statements of the same result known as the Bloch Theorem.

2.1.2 Periodic Boundary Conditions

The Bloch electrons are assumed to be confined to the crystal. This corresponds to the potential being infinite for $\vec{r}$ outside the crystal or, equivalently, that the wave functions $\psi(\vec{r})$ vanish outside the crystal. This condition can be satisfied by two different choices of boundary conditions: Either the wave functions are simply assumed to vanish outside the lattice, which leads to standing wave solutions and an assumption of the electrons being reflected from the surfaces. Alternatively, an electron leaving the lattice at one end is assumed to appear instantaneously at the corresponding point at the opposite end of the crystal. The latter, which is known as periodic boundary conditions or Born-von Karman boundary conditions, corresponds to the surfaces being disregarded altogether and leads to running wave solutions. Since running wave solutions turn out to be more convenient, periodic boundary conditions have been applied throughout this work.

The periodic boundary conditions correspond to

$$\psi(\vec{r}+N_i\vec{a}_i) = \psi(\vec{r}) \quad , \quad N_i \in \mathbb{N} \quad , \quad i \in \{1,2,3\}, \tag{2.13}$$

where the $\vec{a}_i$ are the primitive lattice vectors spanning the lattice[3], and where $N_i\vec{a}_i$ is the shortest vector mapping $\vec{r}$ onto itself if the crystal is repeated in the direction defined by $\vec{a}_i$. The product $N_\mathrm{uc} = N_1N_2N_3$ is thus the number of primitive unit cells[4].

Combining the Bloch Theorem from Eq. (2.11) with Eq. (2.13), one obtains

$$\psi_{a\vec{k}}(\vec{r}+N_i\vec{a}_i) = e^{iN_i\vec{k}\cdot\vec{a}_i}\psi_{a\vec{k}}(\vec{r}) = \psi_{a\vec{k}}(\vec{r}) \tag{2.14}$$

and thus

$$e^{iN_i\vec{k}\cdot\vec{a}_i} = 1. \tag{2.15}$$

[3] All lattice points can be written as an integral linear combination of these primitive lattice vectors: $\vec{R}_\mathrm{l} = a_1\vec{a}_1 + a_2\vec{a}_2 + a_3\vec{a}_3 \; , \; a_i \in \mathbb{Z}$.

[4] The primitive unit cells are spanned by the $\vec{a}_i$ and are the smallest repetitive unit of the lattice.

Expanding $\vec{k}$ in the primitive reciprocal lattice vectors $\vec{b}_1, \vec{b}_2, \vec{b}_3$:

$$\vec{k} = b_1\vec{b}_1 + b_2\vec{b}_2 + b_3\vec{b}_3 \tag{2.16a}$$

$$, \quad \vec{b}_i \cdot \vec{a}_j = 2\pi\delta_{ij}, \tag{2.16b}$$

in which δ_{ij} is the Kronecker delta, Eq. (2.15) corresponds to

$$e^{i2\pi N_i b_i} = 1, \tag{2.17}$$

and consequently

$$b_i = \frac{n_i}{N_i} \quad , \quad n_i \in \mathbb{Z}. \tag{2.18}$$

Since the plane wave fase $\vec{k} \cdot \vec{R}_\mathrm{l} = 2\pi(a_1b_1 + a_2b_2 + a_3b_3)$ is defined modulus 2π, one can limit the n_i in Eq. (2.18) to $n_i \in \{0, 1, \ldots, N_i - 1\}$.

Under the periodic boundary conditions, the $N_\mathrm{uc} = N_1N_2N_3$ physically different crystal wave vectors are thus given by

$$\vec{k} = \sum_{i=1}^{3} \frac{n_i}{N_i}\vec{b}_i \quad , \quad n_i \in \{0, 1, \ldots, N_i - 1\}. \tag{2.19}$$

Cubic Lattice

In a cubic lattice with

$$\vec{a}_1 = l_x\hat{x} \ , \ \vec{a}_2 = l_y\hat{y} \ , \ \vec{a}_3 = l_z\hat{z}, \tag{2.20}$$

in which the l_i are the 3 lattice constants, Eq. (2.16b) leads to

$$\vec{b}_1 = \frac{2\pi}{l_x}\hat{x} \ , \ \vec{b}_2 = \frac{2\pi}{l_y}\hat{y} \ , \vec{b}_3 = \frac{2\pi}{l_z}\hat{z}, \tag{2.21}$$

such that Eq. (2.19) takes the form

$$\vec{k} = \frac{2\pi}{N_x l_x}n_x\hat{x} + \frac{2\pi}{N_y l_y}n_y\hat{y} + \frac{2\pi}{N_z l_z}n_z\hat{z} \quad , \quad n_i \in \{0, 1, \ldots, N_i - 1\}. \tag{2.22}$$

2.2 Tight-Binding Approximation

In an imaginary crystal with macroscopic distances between neighbouring atoms, the electron orbitals in the lattice are identical to the atomic orbitals. As the neighbour distances are reduced to a natural scale, the atomic orbitals begin to overlap and consequently become altered. In the Tight-Binding (TB) approximation, the lattice orbitals are recognized as being different from the the atomic orbitals but assumed to be close enough in resemplance to make the atomic orbitals a sensible starting point for a description of the crystal states.

In the TB approximation, it is convenient to write the crystal Halmiltonian $\hat{H}$ as the atomic Hamiltonian $\hat{H}^0_{\text{at}}$ of an atom placed at the origin plus a correction potential $\Delta V(\vec{r})$ containing all corrections to the atomic potential required to produce the full crystal potential:

$$\hat{H} = \hat{H}^0_{\text{at}} + \Delta V(\vec{r}). \tag{2.23}$$

Regarding $\psi_{a\vec{k}}(\vec{r})$ as a periodic function of $\vec{k}$ for fixed a and $\vec{r}$, one has the Fourier expansion

$$\psi_{a\vec{k}}(\vec{r}) = \sum_{\vec{R}_{\text{l}}} \Phi_{a\vec{r}}(\vec{R}_{\text{l}}) e^{i\vec{k}\cdot\vec{R}_{\text{l}}} \tag{2.24a}$$

$$\Phi_{a\vec{r}}(\vec{R}_{\text{l}}) = \frac{1}{V_{\text{BC}}} \int_{\text{BC}} \psi_{a\vec{k}}(\vec{r}) e^{-i\vec{k}\cdot\vec{R}_{\text{l}}} d\vec{k}, \tag{2.24b}$$

where the integral is over the volume V_{BC} of the 1st Brillouin zone[5].

Shifting $\vec{r}$ and $\vec{R}_{\text{l}}$ with an arbitrary lattice vector in Eq. (2.24b) and using the Bloch Theorem from Eq. (2.11), it can be seen that $\Phi_{a\vec{r}}(\vec{R}_{\text{l}})$ only depends on the difference $\vec{r} - \vec{R}_{\text{l}}$. Without loss of generality, one can therefore write

$$\psi_{a\vec{k}}(\vec{r}) = \frac{1}{\sqrt{N_{\text{uc}}}} \sum_{\vec{R}_{\text{l}}} e^{i\vec{k}\cdot\vec{R}_{\text{l}}} \phi_a\big(\vec{r} - \vec{R}_{\text{l}}\big), \tag{2.25}$$

with $1/\sqrt{N_{\text{uc}}}$ being a normalization factor[6].

Using the fact that the atomic orbitals constitute a complete set, one has

$$\phi_a(\vec{r} - \vec{R}_{\text{l}}) = \sum_{\beta} a_\beta(\vec{k})\ \psi_\beta(\vec{r} - \vec{R}_{\text{l}}) + \int n_m \Upsilon(m, \vec{r} - \vec{R}_{\text{l}}) dm, \tag{2.26}$$

in which ψ_β and Υ are bound and ionized atomic orbitals, respectively, and where the $\vec{k}$-dependence of $a_\beta(\vec{k})$ allows the β-sum to be limited to the bound atomic orbitals belonging to the same unit cell as $\vec{R}_{\text{l}}$.

Changing now to Dirac notation

$$\left|a\vec{k}\right\rangle \leftrightarrow \psi_{a\vec{k}}(\vec{r}), \tag{2.27a}$$

$$\left|\beta\vec{R}_{\text{l}}\right\rangle \leftrightarrow \psi_\beta(\vec{r} - \vec{R}_{\text{l}}), \tag{2.27b}$$

[5] The 1st Brillouin zone consists of all points in reciprocal space that are closer to the origo $\vec{k} = 0$ than to all other reciprocal lattice points $\vec{k} = b_1\vec{b}_1 + b_2\vec{b}_2 + b_3\vec{b}_3 \neq \vec{0}\ ,\ b_i \in \mathbb{Z}$.

[6] The ϕ_a are known as Wannier functions.

and discarding the bound states in Eq. (2.26), Eq. (2.25) reads

$$\begin{aligned} \left|a\vec{k}\right\rangle &= \frac{1}{\sqrt{N_{\rm uc}}}\sum_{\beta,\vec{R}_{\rm l}} a_\beta(\vec{k}) e^{i\vec{k}\cdot\vec{R}_{\rm l}} \left|\beta\vec{R}_{\rm l}\right\rangle, \\ &= \sum_\beta a_\beta(\vec{k}) \left|\beta\vec{k}\right\rangle \qquad (2.28a) \\ , \quad |\beta\vec{k}\rangle &= \frac{1}{\sqrt{N_{\rm uc}}}\sum_{\vec{R}_{\rm l}} e^{i\vec{k}\cdot\vec{R}_{\rm l}} \left|\beta\vec{R}_{\rm l}\right\rangle \qquad (2.28b) \end{aligned}$$

in which the $|\beta\vec{k}\rangle$ are called the Bloch sums. The above expansion of a crystal wave function in bound atomic orbitals is called Linear Combination of Atomic Orbitals (LCAO) and is the hallmark of the TB approximation. Notice that the Bloch sums serve as basis functions, so that there is one basis function for each (bound) atomic orbital β centered on the different atoms in the unit cell.

As there are infinitely many atomic orbitals, it would be convenient if a reasonable approximation could be obtained by limiting the β-sum in Eq. (2.28a) to a finite number of orbitals. To this end, assume for simplicity that the unit cell consists of one atom only[7], and consider the crystal Schrödinger equation

$$\hat{H}\left|a\vec{k}\right\rangle = \epsilon_a(\vec{k})\left|a\vec{k}\right\rangle, \qquad (2.29)$$

in which the $\epsilon_a(\vec{k})$ are the energy bands.

Applying the atomic orbital $\left|\alpha\vec{0}\right\rangle \leftrightarrow \psi_\alpha(\vec{r})$ from the left yields

$$\left\langle\alpha\vec{0}\right| \hat{H}^0_{\rm at} + \Delta V \left|a\vec{k}\right\rangle = \epsilon_a(\vec{k}) \left\langle\alpha\vec{0}\middle|a\vec{k}\right\rangle. \qquad (2.30)$$

Using the fact that $\hat{H}^0_{\rm at}$ is a Hermitian operator, such that

$$\left\langle\alpha\vec{0}\right| \hat{H}^0_{\rm at} \left|a\vec{k}\right\rangle = \hat{H}^0_{\rm at} \left\langle\alpha\vec{0}\middle|a\vec{k}\right\rangle = \epsilon_\alpha \left\langle\alpha\vec{0}\middle|a\vec{k}\right\rangle, \qquad (2.31)$$

Eq. (2.30) yields

$$\left(\epsilon_a(\vec{k}) - \epsilon_\alpha\right) \left\langle\alpha\vec{0}\middle|a\vec{k}\right\rangle = \left\langle\alpha\vec{0}\right| \Delta V \left|a\vec{k}\right\rangle, \qquad (2.32)$$

and, since $\langle\alpha\vec{R}_{\rm l}|\beta\vec{R}_{\rm l}\rangle = \delta_{\alpha\beta}$, one obtains the following eigenvalue equations for $\epsilon_a(\vec{k})$ and corresponding eigenvector components $a_\alpha(\vec{k})$:

$$\begin{aligned} \left[\epsilon_a(\vec{k}) - \epsilon_\alpha\right] a_\alpha(\vec{k}) &= \left[\epsilon_\alpha - \epsilon_a(\vec{k})\right] \sum_{\beta,\vec{R}_{\rm l}\neq\vec{0}} e^{i\vec{k}\cdot\vec{R}_{\rm l}} \left\langle\alpha\vec{0}\middle|\beta\vec{R}_{\rm l}\right\rangle a_\beta(\vec{k}) \\ &\quad + \sum_{\beta,\vec{R}_{\rm l}} e^{i\vec{k}\cdot\vec{R}_{\rm l}} \left\langle\alpha\vec{0}\right| \Delta V \left|\beta\vec{R}_{\rm l}\right\rangle a_\beta(\vec{k}) \quad , \forall\alpha. \qquad (2.33) \end{aligned}$$

[7] The obtained results can be generalized to unit cells containing an arbitrary number of atoms.

The TB approximation is based on the following two assumptions:

- The overlap $\langle \alpha\vec{0}|\beta\vec{R}_{\rm l}\rangle$ between atomic orbitals placed on different atomic sites is small, i.e. the atomic orbitals are well localized with respect to the atomic spacing in the lattice.

- The product $\Delta V|\alpha\vec{0}\rangle$ is small, i.e. the correction potential $\Delta V(\vec{r})$ is significant only at points $\vec{r}$ where the atomic wave function $\psi_\alpha(\vec{r})$ is negligible[8].

Within the TB approximation, the right-hand side of Eq. (2.33) is small, and $a_\alpha(\vec{k})$ is consequently only significant, when $\epsilon_a(\vec{k}) - \epsilon_\alpha$ is small. This means that the significantly contributing atomic orbitals are those whose energy levels are within the same range as the energy bands of interest, and these are the orbitals that should be included in the β-sum in Eq. (2.28a). Furthermore, due to the assumption of small overlaps, the $\vec{R}_{\rm l}$-sum in Eqs. (2.28) will in practice be limited to the neighbouring unit cells.

In some cases the atomic levels give rise to separate energy bands with an s-level giving rise to an s-band, a p-level to a p-band, etc. In other cases, the bands are coupled, such that so-called hybridized sp, sp^2 or sp^3 bands are formed from an s-level and one, two or three of the degenerate p-levels in the same shell. In case of such sp-mixing or sp-hybridization, which is prominent in Group IV elements such as C and Si or in Group III-IV compounds such as $GaAs$, a TB model must include atomic orbitals with both s- and p-symmetry. Notice that in all TB models, the number of included atomic orbitals is proportional to the number of atoms in the unit cell.

2.2.1 The Matrix Eigenvalue Problem

The eigenvalue equations in Eq. (2.33) correspond to the generalized matrix eigenvalue equation

$$\left(\overleftrightarrow{H} - \epsilon_a(\vec{k})\overleftrightarrow{S}\right)\vec{a}(\vec{k}) = 0, \tag{2.34}$$

where the eigenvector $\vec{a}$ has components a_β, and where

$$H_{\alpha\beta} = \sum_{\vec{R}_{\rm l}} e^{i\vec{k}\cdot\vec{R}_{\rm l}} \left\langle \alpha\vec{0}\left|\hat{H}\right|\beta\vec{R}_{\rm l}\right\rangle, \tag{2.35a}$$

$$S_{\alpha\beta} = \sum_{\vec{R}_{\rm l}} e^{i\vec{k}\cdot\vec{R}_{\rm l}} \left\langle \alpha\vec{0}\middle|\beta\vec{R}_{\rm l}\right\rangle \tag{2.35b}$$

are the Hamilton and overlap matrix elements, respectively.

[8] In the extreme case $\Delta V(\vec{r})\psi_\alpha(\vec{r}) = 0$, Eq. (2.29) degenerates to the atomic Schrödinger equation leading to atomic eigenfunctions for the crystal electrons and non-dispersive energy bands $\epsilon_\alpha(\vec{k}) = \epsilon_\alpha$.

Eq. (2.34) can be orthogonalized:

$$\left(\overleftrightarrow{H}' - \epsilon_a(\vec{k})\overleftrightarrow{I}\right)\vec{a}'(\vec{k}) = 0, \tag{2.36}$$

with $\overleftrightarrow{I}$ being the identity matrix, and[9]

$$\overleftrightarrow{H}' = \overleftrightarrow{Z}^{\dagger}\overleftrightarrow{H}\overleftrightarrow{Z}, \tag{2.37a}$$

$$\vec{a} = \overleftrightarrow{Z}\vec{a}', \tag{2.37b}$$

where † denotes Hermitian conjugation, and where the column vectors of $\overleftrightarrow{Z}$ consist of the orthonormal eigenvectors of $\overleftrightarrow{S}$ divided by the square roots of the corresponding eigenvalues:

$$\overleftrightarrow{S}\vec{s}_i = s_i\vec{s}_i \quad , \quad \vec{s}_i\vec{s}_j^{\,*} = \delta_{ij}, \tag{2.38a}$$

$$\overleftrightarrow{Z} = \left[\ldots, \frac{1}{\sqrt{s_i}}\vec{s}_i, \ldots\right], \tag{2.38b}$$

with * denoting complex conjugation.

The matrix eigenvalue problem in Eq. (2.36) has a dimension given by the number of included atomic orbitals in the unit cell, and its solution yields the energy bands $\epsilon_a(\vec{k})$ and corresponding eigenvectors $\vec{a}'(\vec{k})$ with the number of bands being equal to the number of included atomic orbitals, taking account of possible degeneration.

2.2.2 Finite Molecule

In a finite molecule, the potential is not periodic, and the Bloch description is consequently invalid. Therefore, the LCAO expansion in Eq. (2.28a) is replaced by

$$|a\rangle = \sum_{\beta} a_\beta\,|\beta\rangle\,, \tag{2.39}$$

where the β-sum is over atomic orbitals $|\beta\rangle$.

The matrix eigenvalue problem of Eq. (2.36) corresponds to

$$\left(\overleftrightarrow{H}' - \epsilon_a\overleftrightarrow{I}\right)\vec{a}' = 0, \tag{2.40}$$

with Eqs. (2.37) still valid, and

$$H_{\alpha\beta} = \left\langle \alpha \left| \hat{H} \right| \beta \right\rangle, \tag{2.41a}$$

$$S_{\alpha\beta} = \langle\alpha|\beta\rangle\,. \tag{2.41b}$$

The dimension of the matrix eigenvalue problem in Eq. (2.40) is equal to the number of included atomic orbitals in the molecule.

[9] This orthogonalization corresponds to a change of basis from the non-orthogonal Bloch sums from Eq. (2.28b) to orthogonal Löwdin states $|\nu\vec{k}\rangle = \sum_\beta Z_{\beta\nu}|\beta\vec{k}\rangle$.

Chapter 3

Optical Susceptibility

Information about optical properties such as index of refraction, absorption, etc. can be derived from the optical susceptibility tensor $\overleftrightarrow{\chi}$, and the derivation of optical properties thus typically amounts to calculating components of either the optical susceptibility tensor or, alternatively, the dielectric tensor

$$\overleftrightarrow{\varepsilon} = \varepsilon_0 \left(\overleftrightarrow{I} + \overleftrightarrow{\chi} \right), \tag{3.1}$$

in which ε_0 is the vacuum permittivity, and $\overleftrightarrow{I}$ is the identity matrix.

The index of refraction tensor $\overleftrightarrow{n}$ is related to $\overleftrightarrow{\varepsilon}$ and $\overleftrightarrow{\chi}$ through

$$n_{ij} = \sqrt{\varepsilon_{ij}} = \sqrt{\varepsilon_0 \left(1 + \chi_{ij} \right)}. \tag{3.2}$$

In Sec. 3.1, the concept of optical susceptibility is presented as the intermediary between an electric field and its induced polarization, while Secs. 3.2 and 3.3 deal with the linear optical susceptibility and the electro-optic effect, respectively.

3.1 Optical Susceptibility

The polarization $\vec{P}$ induced by an electric field $\vec{E}$ is given by

$$\vec{P}(\vec{r}, t) = \varepsilon_0 \iint_{-\infty}^{t} \overleftrightarrow{\chi}(\vec{r}, \vec{r}'; t, t') \vec{E}(\vec{r}', t') dt' d\vec{r}', \tag{3.3}$$

where the response function $\overleftrightarrow{\chi}(\vec{r}, \vec{r}'; t, t')$ describes the response of the system to the electric fields existing at earlier times. The upper limit of the time integration is thus due to causality.

In a local medium, the response in a point $\vec{r}$ is determined by the field in that point. This corresponds to $\overleftrightarrow{\chi}(\vec{r}, \vec{r}'; t, t') = \overleftrightarrow{\chi}(\vec{r}; t, t')\delta(\vec{r}' - \vec{r})$ and thus to

$$\vec{P}(\vec{r}, t) = \varepsilon_0 \int_{-\infty}^{t} \overleftrightarrow{\chi}(\vec{r}; t, t') \vec{E}(\vec{r}, t') dt'. \tag{3.4}$$

As the polarization is a macroscopic quantity, so is the response function. In a macroscopically homogeneous medium, therefore, the response function is independent of $\vec{r}$:

$$\vec{P}(\vec{r},t) = \varepsilon_0 \int_{-\infty}^{t} \overleftrightarrow{\chi}(t,t')\vec{E}(\vec{r},t')dt'. \tag{3.5}$$

In a medium in equilibrium, the response function depends only on the time difference $\tau \equiv t - t'$:

$$\begin{aligned} \vec{P}(\vec{r},t) &= \varepsilon_0 \int_{-\infty}^{t} \overleftrightarrow{\chi}(t-t')\vec{E}(\vec{r},t')dt' \\ &= \varepsilon_0 \int_{0}^{\infty} \overleftrightarrow{\chi}(\tau)\vec{E}(\vec{r},t-\tau)d\tau. \end{aligned} \tag{3.6}$$

Fourier transforming Eq. (3.6) from the time domain into the frequency domain, one has

$$\begin{aligned} \vec{P}(\vec{r},\omega) &= \varepsilon_0 \int_{-\infty}^{\infty}\int_{0}^{\infty} \overleftrightarrow{\chi}(\tau)\vec{E}(\vec{r},t-\tau)e^{i\omega t}d\tau dt \\ &= \varepsilon_0 \int_{0}^{\infty} \overleftrightarrow{\chi}(\tau)e^{i\omega\tau}\int_{-\infty}^{\infty} \vec{E}(\vec{r},t-\tau)e^{i\omega(t-\tau)}d(t-\tau)d\tau \\ &= \varepsilon_0 \overleftrightarrow{\chi}(\omega)\vec{E}(\vec{r},\omega), \end{aligned} \tag{3.7}$$

with

$$\overleftrightarrow{\chi}(\omega) = \int_{0}^{\infty} \overleftrightarrow{\chi}(\tau)e^{i\omega\tau}d\tau. \tag{3.8}$$

The Fourier transformation thus converts the convolution in Eq. (3.6) to the product in Eq. (3.7). Again, the lower limit of the integration in Eq. (3.8) is due to causality.

For frequencies in the optical range, $\overleftrightarrow{\chi}(\omega)$ is known as the optical susceptibility. Note, that whereas the response function relates the real functions $\vec{P}(\vec{r},t)$ and $\vec{E}(\vec{r},t)$ and therefore is a real function itself, the optical susceptibility is a complex function.

Expanding $\vec{P}(\vec{r},\omega)$ in a power series of the electric field, one has

$$\begin{aligned} P_i(\vec{r},\omega) &= \varepsilon_0 \sum_j \chi_{ij}^{(1)}(\omega)E_j(\vec{r},\omega) \\ &+ \varepsilon_0 \sum_{j,k}\sum_{(m,n)} \chi_{ijk}^{(2)}(\omega=\omega_m+\omega_n)E_j(\vec{r},\omega_m)E_k(\vec{r},\omega_n) \\ &+ \varepsilon_0 \sum_{j,k,l}\sum_{(m,n,o)} \chi_{ijkl}^{(3)}(\omega=\omega_m+\omega_n+\omega_o)E_j(\vec{r},\omega_m)E_k(\vec{r},\omega_n)E_l(\vec{r},\omega_o) \\ &+ \cdots \quad , \quad i,j,k,l \in \{x,y,z\}, \end{aligned} \tag{3.9}$$

in which $\sum_{(m,n)}$ means summing over m and n under the condition $\omega_m+\omega_n=\omega$. Eq. (3.9) thus serves as the definition of the linear optical susceptibility tensor $\overleftrightarrow{\chi}^{(1)}$ as well as the higher-order optical susceptibility tensors $\overleftrightarrow{\chi}^{(2)}$, $\overleftrightarrow{\chi}^{(3)}$, ... Note that optical susceptibility tensors of different order have different units.

Note also that in a medium with inversion symmetry, inverting the fields ($E \to -E$) will physically lead to the inversion of the polarization. Inspection of Eq. (3.9) thus shows that all even-order susceptibilities must be zero in inversion-symmetrical media.

For small electric fields, the polarization is approximately proportional to the electric field. This corresponds to the optical susceptibility in Eq. (3.7) being independent of $\vec{E}$ or, equivalently, that $\overleftrightarrow{\chi} = \overleftrightarrow{\chi}^{(1)}$. As the electric field grows larger, the higher-order terms in Eq. (3.9) become an increasingly important correction.

3.2 Linear Optical Susceptibility

In this section, an expression for the linear optical susceptibility is obtained by deriving an expression for that part of the polarization which is linear in the electric field.

3.2.1 Dipole Approximation

In the dipole approximation, the wavelength of a light wave is assumed to be large compared with the extent of any atoms with which the light wave interacts. This has the following consequences:

- Displaced atomic electrons can be treated as point dipoles over which the electromagnetic field of the light wave is constant.

- Photon momentum can be disregarded.

3.2.2 The Electric Dipole Moment

In the dipole approximation, a classical, monochromatic, linearly polarized, electric light field can be written

$$\begin{aligned} \vec{E}(t) &= E(t)\hat{z} = E(\omega)\cos(\omega t)e^{\gamma t}\hat{z} \\ &= \frac{1}{2}E(\omega)\left(e^{i(\omega-i\gamma)t}+e^{-i(\omega+i\gamma)t}\right)\hat{z}, \end{aligned} \tag{3.10}$$

with $\hat{z}$ being a unit vector, and the so-called switch-on parameter $\gamma > 0$ being introduced partly in order to have

$$\lim_{t\to-\infty} E(t) = 0, \tag{3.11}$$

and partly because γ will be seen to correspond to a classical damping/broadening parameter. The role of γ as a damping parameter will be commented on in Sec. 3.2.4.

The time-dependent Schrödinger equation for an electron interacting with the electric field is given by

$$\left(\hat{H}_0 + \hat{H}_I\right) \Phi(\vec{r}, t) = i\hbar \frac{\partial \Phi(\vec{r}, t)}{\partial t}, \tag{3.12}$$

where the unperturbed Hamiltonian is given by

$$\hat{H}_0 = -\frac{\hbar^2 \nabla^2}{2m_\mathrm{e}} + V(\vec{r}), \tag{3.13}$$

and where, in the dipole approximation, the interaction Hamiltonian is given by[1]

$$\begin{aligned} \hat{H}_I &= -\vec{d} \cdot \vec{E}(t) \\ &= eE(t)z, \end{aligned} \tag{3.14}$$

in which e is the elementary charge, and

$$\vec{d} = -e\vec{r} \tag{3.15}$$

is the electric dipole moment operator.

In a periodic potential as described in Eq. (2.1), the unperturbed solutions to Eq. (3.12) are the Bloch wave functions

$$\Psi_{a\vec{k}}(\vec{r}, t) = e^{-i\omega_{a\vec{k}} t} \psi_{a\vec{k}}(\vec{r}) \tag{3.16}$$

described in Sec. 2.1. As eigen functions of the Hermitian operator $\hat{H}_0$, these Bloch wave functions constitute a complete set in which the field perturbed wave functions Φ can be expanded:

$$\Phi(\vec{r}, t) = \sum_{a', \vec{k}'} b_{a'\vec{k}'}(t) \Psi_{a'\vec{k}'}(\vec{r}, t) \tag{3.17a}$$

$$= \sum_{a', \vec{k}'} b_{a'\vec{k}'}(t) e^{-i\omega_{a'\vec{k}'} t} \psi_{a'\vec{k}'}(\vec{r}), \tag{3.17b}$$

in which the $\vec{k}$-sum runs over the values indicated in Eq. (2.19).

Inserting Eq. (3.17b) in Eq. (3.12), one has

$$\sum_{a', \vec{k}'} eE(t) z b_{a'\vec{k}'}(t) e^{-i\omega_{a'\vec{k}'} t} \psi_{a'\vec{k}'}(\vec{r}) = i\hbar \sum_{a', \vec{k}'} \frac{\partial b_{a'\vec{k}'}(t)}{\partial t} e^{-i\omega_{a'\vec{k}'} t} \psi_{a'\vec{k}'}(\vec{r}). \tag{3.18}$$

[1] To include photon momentum, use $\hat{H} = \hat{H}_0 + \hat{H}_I = \frac{1}{2m_\mathrm{e}} \left(\hat{\vec{\mathcal{P}}} - e\hat{\vec{\mathcal{A}}}\right)^2$ in which $\hat{\vec{\mathcal{P}}}$ and $\hat{\vec{\mathcal{A}}}$ are the operators for the vector momentum and vector potential, respectively.

Multiplying Eq. (3.18) from the left with $\Psi^*_{a\vec{k}}(\vec{r},t) = e^{i\omega_{a\vec{k}}t}\psi^*_{a\vec{k}}(\vec{r})$ and integrating over all space, one obtains the following due to the orthonormality of the $\Psi_{a\vec{k}}(\vec{r},t)$:

$$i\hbar\frac{\partial b_{a\vec{k}}(t)}{\partial t} = -E(t)\sum_{a',\vec{k}'} b_{a'\vec{k}'}(t)e^{i\omega_{a\vec{k},a'\vec{k}'}t}d^z_{a\vec{k},a'\vec{k}'} \tag{3.19a}$$

$$, \quad \omega_{a\vec{k},a'\vec{k}'} = \omega_{a\vec{k}} - \omega_{a'\vec{k}'} \tag{3.19b}$$

$$, \quad d^z_{a\vec{k},a'\vec{k}'} = \int \psi^*_{a\vec{k}}(\vec{r})(-ez)\psi_{a'\vec{k}'}(\vec{r})d\vec{r} \quad , \quad d^z_{a\vec{k},a'\vec{k}'} = d^{z^*}_{a'\vec{k}',a\vec{k}} \ , \tag{3.19c}$$

where $d^z_{a\vec{k},a'\vec{k}'}$ is the z-component of the electic dipole matrix element.

The solution to the differential equation in Eq. (3.19a) is

$$b_{a\vec{k}}(t) = \lim_{t'\to-\infty} b_{a\vec{k}}(t') + \frac{i}{\hbar}\int_{-\infty}^{t} E(t')\sum_{a',\vec{k}'} b_{a'\vec{k}'}(t')e^{i\omega_{a\vec{k},a'\vec{k}'}t'}d^z_{a\vec{k},a'\vec{k}'}dt'. \tag{3.20}$$

Because of Eq. (3.11), the system was initially in some eigen state

$$\Psi_{a_0\vec{k}_0}(\vec{r},t) = e^{-i\omega_{a_0\vec{k}_0}t}\psi_{a_0\vec{k}_0}(\vec{r}) \tag{3.21}$$

of the unperturbed Hamiltonian, and therefore

$$\lim_{t\to-\infty} b_{a\vec{k}}(t) = \delta_{aa_0}\delta_{\vec{k}\vec{k}_0}. \tag{3.22}$$

An expansion of $b_{a\vec{k}}(t)$ in powers of $E(t)$ can be written

$$b_{a\vec{k}}(t) = b^{(0)}_{a\vec{k}}(t) + b^{(1)}_{a\vec{k}}(t) + b^{(2)}_{a\vec{k}}(t) + \cdots \tag{3.23}$$

with $b^{(n)}_{a\vec{k}}(t)$ proportional to the nth power of $E(t)$.

Inserting Eqs. (3.10), (3.22) and (3.23) in Eq. (3.20) and equating terms with equal powers in $E(t)$, one has

$$b^{(0)}_{a\vec{k}}(t) = \delta_{aa_0}\delta_{\vec{k}\vec{k}_0}, \tag{3.24a}$$

$$\begin{aligned} b^{(1)}_{a\vec{k}}(t) &= i\frac{E(\omega)}{2\hbar}d^z_{a\vec{k},a_0\vec{k}_0}\int_{-\infty}^{t} e^{i\left(\omega_{a\vec{k},a_0\vec{k}_0}+(\omega-i\gamma)\right)t'} + e^{i\left(\omega_{a\vec{k},a_0\vec{k}_0}-(\omega+i\gamma)\right)t'}dt' \\ &= \frac{E(\omega)}{2\hbar}d^z_{a\vec{k},a_0\vec{k}_0}\left[\frac{e^{i\left(\omega_{a\vec{k},a_0\vec{k}_0}+(\omega-i\gamma)\right)t}}{\omega_{a\vec{k},a_0\vec{k}_0}+(\omega-i\gamma)} + \frac{e^{i\left(\omega_{a\vec{k},a_0\vec{k}_0}-(\omega+i\gamma)\right)t}}{\omega_{a\vec{k},a_0\vec{k}_0}-(\omega+i\gamma)}\right], \end{aligned} \tag{3.24b}$$

$$b^{(2)}_{a\vec{k}}(t) = \cdots \tag{3.24c}$$

For a weak electric field, $b_{a\vec{k}}(t)$ can be assumed to depend linearly on $E(t)$ corresponding to vanishing higher-order terms $b^{(2)}_{a\vec{k}}(t), b^{(3)}_{a\vec{k}}(t), \ldots$.

The electric dipole moment of a field-perturbed crystal electron is given by

$$\begin{aligned}\vec{p}(t) &= \int \Phi^*(\vec{r},t)\ \vec{d}\ \Phi(\vec{r},t)d\vec{r} \\ &= \sum_{a,a',\vec{k},\vec{k}'} b^*_{a'\vec{k}'}(t)b_{a\vec{k}}(t)e^{i\omega_{a'\vec{k}',a\vec{k}}t}\vec{d}_{a'\vec{k}',a\vec{k}} \qquad (3.25a)\end{aligned}$$

$$, \quad \vec{d}_{a'\vec{k}',a\vec{k}} = \int \psi^*_{a'\vec{k}'}(\vec{r})\ \vec{d}\ \psi_{a\vec{k}}(\vec{r})d\vec{r}, \qquad (3.25b)$$

where Eq. (3.17a) has been used.

Expanding $\vec{p}(t)$ in powers of $E(t)$ and using Eqs. (3.24) to equate terms of equal power, one obtains

$$\vec{p}^{(0)}(t) = \vec{d}_{a_0\vec{k}_0,a_0\vec{k}_0}, \qquad (3.26a)$$

$$\begin{aligned}\vec{p}^{(1)}(t) &= \frac{E(\omega)}{2\hbar}\sum_{a,\vec{k}}\left[\frac{e^{i\omega t}e^{\gamma t}}{\omega_{a\vec{k},a_0\vec{k}_0}+(\omega-i\gamma)}+\frac{e^{-i\omega t}e^{\gamma t}}{\omega_{a\vec{k},a_0\vec{k}_0}-(\omega+i\gamma)}\right]d^z_{a\vec{k},a_0\vec{k}_0}\vec{d}_{a_0\vec{k}_0,a\vec{k}} \\ &\quad + \ c.c., \qquad (3.26b)\end{aligned}$$

$$\vec{p}^{(2)}(t) = \cdots \qquad (3.26c)$$

where *c.c.* denotes the complex conjugate of the preceding terms.

Eq. (3.26a) is the permanent electric dipole moment of an electron in the unperturbed state $\Psi_{a_0\vec{k}_0}$, whereas Eq. (3.26b) is the first-order field-induced electric dipole moment.

Writing $\vec{p}^{(1)}$ in the same form as Eq. (3.10):

$$\begin{aligned}\vec{p}^{(1)}(t) &= \frac{1}{2}\vec{p}^{(1)}(\omega)\left(e^{i(\omega-i\gamma)t}+e^{-i(\omega+i\gamma)t}\right) \\ &= \frac{1}{2}\vec{p}^{(1)}(\omega)e^{-i\omega t}e^{\gamma t}+c.c., \qquad (3.27)\end{aligned}$$

comparison with Eq. (3.26b) yields

$$\vec{p}^{(1)}(\omega) = \frac{E(\omega)}{\hbar}\sum_{a,\vec{k}}\left[\frac{d^z_{a\vec{k},a_0\vec{k}_0}\vec{d}_{a_0\vec{k}_0,a\vec{k}}}{\omega_{a\vec{k},a_0\vec{k}_0}-(\omega+i\gamma)}+\frac{d^z_{a_0\vec{k}_0,a\vec{k}}\vec{d}_{a\vec{k},a_0\vec{k}_0}}{\omega_{a\vec{k},a_0\vec{k}_0}+(\omega+i\gamma)}\right]. \qquad (3.28)$$

3.2.3 Linear Optical Susceptibility

Since the polarization is the total electric dipole moment per volume V, combining Eqs. (3.9) and (3.10) one has

$$\vec{p}^{(1)}(\omega) = \varepsilon_0 V E(\omega)\begin{pmatrix}\chi^{(1)}_{xz}(\omega)\\ \chi^{(1)}_{yz}(\omega)\\ \chi^{(1)}_{zz}(\omega)\end{pmatrix}. \qquad (3.29)$$

The linear optical susceptibility contribution $\chi_{ij}^{e(1)}$ from the above treated crystal electron is thus found by comparison of Eqs. (3.28) and (3.29):

$$\chi_{ij}^{e(1)}(\omega) = \frac{1}{\varepsilon_0 V} \sum_{a,\vec{k}} \left[\frac{d^i_{a_0\vec{k}_0,a\vec{k}} d^j_{a\vec{k},a_0\vec{k}_0}}{\hbar\omega_{a\vec{k},a_0\vec{k}_0} - (\hbar\omega + i\hbar\gamma)} + \frac{d^j_{a_0\vec{k}_0,a\vec{k}} d^i_{a\vec{k},a_0\vec{k}_0}}{\hbar\omega_{a\vec{k},a_0\vec{k}_0} + (\hbar\omega + i\hbar\gamma)} \right], \quad (3.30)$$

where V is the volume of the crystal, and where the first and second terms are called the resonant and anti-resonant contributions, respectively.

In an independent electron picture (see Sec. 4.6), the total linear optical susceptibility in a semiconductor is found by summing the one-electron susceptibility contribution in Eq. (3.30) over all occupied valence band states $\Psi_{\mathrm{v}\vec{k}_0}$ and letting the $a,\vec{k}$-sum run over all unoccupied conduction band states[2] $\mathrm{c},\vec{k}$:

$$\chi_{ij}^{(1)}(\omega) = \frac{2}{\varepsilon_0 V} \sum_{\mathrm{v},\mathrm{c},\vec{k},\vec{k}'} \left[\frac{d^i_{\mathrm{v}\vec{k},\mathrm{c}\vec{k}'} d^j_{\mathrm{c}\vec{k}',\mathrm{v}\vec{k}}}{\hbar\omega_{\mathrm{c}\vec{k}',\mathrm{v}\vec{k}} - (\hbar\omega + i\hbar\gamma)} + \frac{d^j_{\mathrm{v}\vec{k},\mathrm{c}\vec{k}'} d^i_{\mathrm{c}\vec{k}',\mathrm{v}\vec{k}}}{\hbar\omega_{\mathrm{c}\vec{k}',\mathrm{v}\vec{k}} + (\hbar\omega + i\hbar\gamma)} \right], \quad (3.31)$$

where the factor of 2 has been included because of spin degeneracy[3].

As photon momentum is disregarded in the dipole approximation, conservation of momentum requires $\vec{k} = \vec{k}'$, and Eq. (3.31) thus reduces to

$$\chi_{ij}^{(1)}(\omega) = \frac{2}{\varepsilon_0 V} \sum_{\mathrm{v},\mathrm{c},\vec{k}} \left[\frac{d^i_{\mathrm{vc}}(\vec{k}) d^j_{\mathrm{cv}}(\vec{k})}{E_{\mathrm{cv}}(\vec{k}) - \hbar\Omega} + \frac{d^j_{\mathrm{vc}}(\vec{k}) d^i_{\mathrm{cv}}(\vec{k})}{E_{\mathrm{cv}}(\vec{k}) + \hbar\Omega} \right], \quad (3.32a)$$

$$, \quad d^i_{\mathrm{cv}}(\vec{k}) = d^i_{\mathrm{c}\vec{k},\mathrm{v}\vec{k}}\ , \quad (3.32b)$$

$$, \quad E_{\mathrm{cv}}(\vec{k}) = E_{\mathrm{c}}(\vec{k}) - E_{\mathrm{v}}(\vec{k}) = \hbar\omega_{\mathrm{c}\vec{k},\mathrm{v}\vec{k}}, \quad (3.32c)$$

$$, \quad \Omega = \omega + i\gamma. \quad (3.32d)$$

and if the electric dipole matrix elements are real $\left(d^i_{\mathrm{vc}} = d^i_{\mathrm{cv}}\right)$, Eq. (3.32a) can be simplified

$$\chi_{ij}^{(1)}(\omega) = \frac{4}{\varepsilon_0 V} \sum_{\mathrm{v},\mathrm{c},\vec{k}} d^i_{\mathrm{cv}}(\vec{k})\ d^j_{\mathrm{cv}}(\vec{k})\ \frac{E_{\mathrm{cv}}(\vec{k})}{E^2_{\mathrm{cv}}(\vec{k}) - \hbar^2\Omega^2}. \quad (3.33)$$

[2]Strictly speaking, all valence band states are only occupied and all conduction band states only unoccupied at a temperature of absolute zero. However, even at room temperature, the deviation from this picture will be insignificant in any semiconductor.

[3]Between every two spatial states $\Psi_{v\vec{k}}$ and $\Psi_{c\vec{k}'}$, spin up-spin up and spin down-spin-down transitions can occur. Spin flip transitions spin up-spin down or spin down-spin up do not occur in this context due to the orthogonality of the spin up- and spin-down states. Generalizing Eq. (3.25b) to include spin states σ, one would have $\vec{d}_{a'\vec{k}'\sigma',a\vec{k}\sigma} = \int \psi^*_{a'\vec{k}'}(\vec{r})\vec{d}\psi_{a\vec{k}}(\vec{r})d\vec{r}\ \delta_{\sigma\sigma'}$.

3.2.4 Broadening

In the limit $\gamma \to 0$, the spectrum in Eq. (3.33) is seen to contain singularities occurring when the photon energy $\hbar\omega$ exactly matches the energy difference $E_{\mathrm{cv}}(\vec{k})$ between an occupied and an unoccupied state. This infinitely sharp resonance condition is unphysical for a number of reasons. First of all, the energy levels are not infinitely sharp but subject to quantum mechanical uncertainties, and this so-called lifetime broadening leads to a softening of the resonance condition corresponding to a spectral broadening of the susceptibility spectrum. In addition, nature displays numerous different broadening mechanisms, such as e.g. Doppler shifted energy levels, which all serve as the physical basis for the inclusion of the empirical broadening parameter γ.

3.2.5 One-dimensional Crystal

According to Eq. (2.22), the allowed k-values in a one-dimensional (1D) crystal are equally spaced:

$$k = \frac{2\pi}{N_{\mathrm{uc}} l} n \quad , \quad n \in \{0, 1, \ldots, N_{\mathrm{uc}} - 1\}. \tag{3.34}$$

In a macroscopic 1D crystal, for which N_{uc} is very large and $\Delta k = 2\pi / N_{\mathrm{uc}} l$ thus very small, the allowed k-values constitute a quasi-continuous set, and the $\vec{k}$-sum in Eq. (3.33) can be written

$$\sum_k = \sum_k \frac{\Delta k}{\Delta k} = \frac{N_{\mathrm{uc}} l}{2\pi} \sum_k \Delta k \approx \frac{N_{\mathrm{uc}} l}{2\pi} \int_k dk. \tag{3.35}$$

As $L = N_{\mathrm{uc}} l$ is the length of the crystal, Eq. (3.33) takes the 1D form

$$\chi^{(1)}_{ij}(\omega) = \frac{2}{\pi \varepsilon_0 A} \sum_{\mathrm{v,c}} \int_{-\frac{\pi}{l}}^{\frac{\pi}{l}} d^i_{\mathrm{cv}}(k)\; d^j_{\mathrm{cv}}(k)\; \frac{E_{\mathrm{cv}}(k)}{E^2_{\mathrm{cv}}(k) - \hbar^2 \Omega^2}\; dk, \tag{3.36}$$

where A is the cross-sectional area of the crystal.

3.3 Electro-optic Effect

The electro-optic effect is the change in the optical properties, here described through the optical susceptibility $\overleftrightarrow{\chi}$, induced by a static (or very low-frequency) electric field $\vec{F}$.

In non-inversion-symmetrical media, the electro-optic effect will be dominantly described by the second-order optical susceptibility $\overleftrightarrow{\chi}^{(2)}$. As $\overleftrightarrow{\chi}^{(2)}$ vanishes in inversion-symmetrical media (see the comment following Eq. (3.9)), $\overleftrightarrow{\chi}^{(3)}$ is the dominant electro-optic susceptibility for inversion-symmetrical media. In any case, the components $\chi^{(2)}_{ijk}$ and $\chi^{(3)}_{ijkl}$ are known as the electro-optic functions.

3.3.1 Pockels Effect

That the electro-optic effect is described by $\overleftrightarrow{\chi}^{(2)}$ corresponds to the change in the optical susceptibility depending linearly on the static electric field[4]:

$$\begin{aligned}
\vec{P}(\vec{r},\omega) &\simeq \varepsilon_0 \overleftrightarrow{\chi}^{(1)}(\omega)\vec{E}(\vec{r},\omega) + \varepsilon_0 \overleftrightarrow{\chi}^{(2)}(\omega)\vec{E}(\vec{r},\omega)\vec{F}(\vec{r}) \\
&= \varepsilon_0 \left(\overleftrightarrow{\chi}^{(1)}(\omega) + \overleftrightarrow{\chi}^{(2)}(\omega)\vec{F}(\vec{r}) \right) \vec{E}(\vec{r},\omega) \\
&\Downarrow \\
\overleftrightarrow{\chi}(\vec{r},\omega) &\simeq \overleftrightarrow{\chi}^{(1)}(\omega) + \overleftrightarrow{\chi}^{(2)}(\omega)\vec{F}(\vec{r}),
\end{aligned} \tag{3.37}$$

in which $\overleftrightarrow{\chi}(\vec{r},\omega)$ depends on $\vec{r}$, as the in general spatially variant static electric field $\vec{F}(\vec{r})$ breaks the assumed intrinsic homogeneity of the medium.

This linear electro-optic effect is also known as the Pockels effect.

3.3.2 Kerr Effect

An electro-optic effect described by $\overleftrightarrow{\chi}^{(3)}$ corresponds to a quadratic dependence on the static electric field:

$$\overleftrightarrow{\chi}(\vec{r},\omega) \simeq \overleftrightarrow{\chi}^{(1)}(\omega) + \overleftrightarrow{\chi}^{(3)}(\omega)\vec{F}(\vec{r})\vec{F}(\vec{r}). \tag{3.38}$$

The quadratic electro-optic effect is also known as the Kerr effect.

[4] The order of $\vec{E}(\vec{r},\omega)$ and $\vec{F}(\vec{r})$ can be interchanged according to the intrinsic permutation symmetry of the susceptibility: $\chi^{(2)}_{ijk}(\omega = \omega + 0) = \chi^{(2)}_{ikj}(\omega = 0 + \omega)$.

Chapter 4

Density Functional Theory

Since the formulation of quantum mechanics in the mid 1920ies by Heisenberg [33], Schrödinger [34] and others, there have existed two competing ways of describing an electron system: By electron density $\rho(\vec{r})$ or by many-electron wave function $\Phi(\vec{r}_1, \vec{r}_2, \ldots, \vec{r}_N)$.

After a description of the Born-Oppenheimer approximation, which will be applied throughout this work, this chapter gives a historical introduction to the evolution of Density Functional Theory (DFT) as an alternative to the wave function based Hartree and Hartree-Fock models.

4.1 The Born-Oppenheimer Approximation

Due to the large difference between nuclear and electron masses, it is a widespread assumption within condensed matter physics that nuclear and electron dynamics occur on different time scales. This assumption of decoupled nuclear and electron dynamics, which is known as the Born-Oppenheimer (BO) approximation [35], has the following consequences:

- When describing electron dynamics, the nuclei can be treated as fixed, i.e. the positions of the nuclei enter the calculations as parameters rather than variables.

- For all processes occuring on the time scale of nuclear dynamics, the electrons can be assumed to be in the ground state.

4.2 Thomas-Fermi Model

In terms of a normalized many-electron wave function $\Phi(\vec{r}_1, \vec{r}_2, \ldots, \vec{r}_N)$, the electron density is given by

$$\begin{aligned} \rho(\vec{r}) &= \sum_{i=1}^{N} \big\langle \Phi \big| \delta(\vec{r} - \vec{r}_i) \big| \Phi \big\rangle \\ &= \sum_{i=1}^{N} \underbrace{\int \cdots \int}_{N-1} \big| \Phi(\vec{r}_1, \ldots, \vec{r}_{i-1}, \vec{r}, \vec{r}_{i+1}, \ldots, \vec{r}_N) \big|^2 d\vec{r}_1 \cdots d\vec{r}_{i-1} d\vec{r}_{i+1} \cdots d\vec{r}_N, \end{aligned} \tag{4.1}$$

where N is the number of electrons.

Note that

$$\int \rho(\vec{r}) d\vec{r} = N. \tag{4.2}$$

If Φ describes a single electron, Eq. (4.1) reduces to

$$\rho(\vec{r}) = \big| \Phi(\vec{r}) \big|^2. \tag{4.3}$$

The idea of discarding the many-electron wave function, which depends on $3N$ parameters, in favour of the electron density, which depends on just 3 parameters, was first presented by Thomas [36] and Fermi [37] (TF) in 1927. In the TF-model, the electrons are treated as particles forming an electron gas, and each electron is assumed to move independently of other electrons in the Coulomb field created by the fixed nuclei and the averaged electron charge density. Such an independent-electron model is a significant simplification from the true picture of pairwise electron-electron interaction. In reality, of course, electrons do not move independently of one another, but have to correlate their movements in accordance with their mutual Coulomb repulsion. Indeed, the TF-model was not very successful when it came to quantitative predictions in neither atomic, molecular nor solid-state physics and was therefore viewed as an oversimplified model without quantitative significance.

4.3 Hartree Model

A more successful approach was the wave function based Hartree-Fock (HF) model that was based on the Hartree model put forward by Hartree [38] in 1928 and a few years later improved by Fock [39], Slater [40], and others.

In the BO approximation, the electron Hamiltonian is given by

$$\hat{H} = \hat{T} + \hat{V}_{\text{ext}} + \hat{U}_{\text{ee}}, \tag{4.4}$$

where $\hat{T}$, $\hat{V}_{\text{ext}}$ and $\hat{U}_{\text{ee}}$ are the operators for the kinetic energy of the electrons, the external potential (e.g. the repulsion potential of the nuclei) and the electron-electron interaction, respectively.

In atomic units, distance is measured in units of Bohr radii $a_{\text{B}} \doteq 0.529\text{Å}$, charge is measured in units of elementary charge $e = 1.602 \cdot 10^{-19} C$, and energy is measured in units of Hartrees H (= 2 Rydbergs):

$$1H = \frac{\hbar^2}{m_{\text{e}} a_{\text{B}}^2} = \frac{e^2}{4\pi\varepsilon_0 a_{\text{B}}} \doteq 27.2eV. \tag{4.5}$$

In the following, the external potential is limited to an electrostatic nuclear potential. In this case, one has in atomic units

$$\hat{T} = \sum_{i=1}^{N} -\frac{1}{2}\nabla_i^2 \quad , \quad \nabla_i^2 = \frac{\partial^2}{\partial x_i^2} + \frac{\partial^2}{\partial y_i^2} + \frac{\partial^2}{\partial z_i^2} \ , \tag{4.6a}$$

$$\hat{V}_{\text{ext}} = \sum_{i=1}^{N} \hat{V}_i \quad , \quad \hat{V}_i(\vec{r}_i) = \left(-\sum_{\alpha=1}^{N_{\text{nuc}}} \frac{Z_\alpha}{|\vec{r}_i - \vec{R}_\alpha|} \right), \tag{4.6b}$$

$$\hat{U}_{\text{ee}} = \sum_{i<j}^{N} \frac{1}{|\vec{r}_i - \vec{r}_j|}, \tag{4.6c}$$

where N_{nuc} is the number of nuclei, and where Z_α and $\vec{R}_\alpha$ is the charge and the coordinate vector of the αth nucleus, respectively.

Inserting Eqs. (4.6) in Eq. (4.4), one has

$$\hat{H} = \sum_{i=1}^{N} \hat{H}_i + \hat{U}_{\text{ee}} \tag{4.7a}$$

$$, \quad \hat{H}_i = -\frac{1}{2}\nabla_i^2 + \hat{V}_i, \tag{4.7b}$$

where $\hat{H}_i$ is an operator concerning the ith electron only, and where the electron-electron interaction $\hat{U}_{\text{ee}}$ couples the movement of the electrons.

Had it not been for this coupling, one could have written

$$\hat{H} = \sum_{i=1}^{N} \hat{H}_i' \tag{4.8}$$

for some one-electron Hamiltonian $\hat{H}_i'$. For such a separable Hamiltonian, the solution to the many-electron Schrödinger equation

$$\hat{H}\Phi(\vec{r}_1, \ldots, \vec{r}_N; s_1, \ldots, s_N) = E\Phi(\vec{r}_1, \ldots, \vec{r}_N; s_1, \ldots, s_N), \tag{4.9}$$

in which the s_i are the spin parameters, would be factorizable:

$$\Phi(\vec{r}_1, \ldots, \vec{r}_N; s_1, \ldots, s_N) = \phi_1(\vec{r}_1)\sigma_1(s_1) \cdots \phi_N(\vec{r}_N)\sigma_N(s_N), \tag{4.10}$$

where the σ_i are the spin wave functions corresponding to either spin up or spin down, and where ϕ_i is that orthonormalized[1] solution to the one-electron Schrödinger equation

$$\hat{H}'_\alpha \phi_\alpha(\vec{r}_\alpha) = E'_\alpha \phi_\alpha(\vec{r}_\alpha) \quad , \quad \langle \phi_\alpha | \phi_\beta \rangle = \delta_{\alpha\beta}, \tag{4.11}$$

that characterizes the ith electron[2]. The spatial one-electron wave functions $\phi_i(\vec{r}_i)$ are known as orbitals, while the full one-electron wave functions $\phi_i(\vec{r}_i)\sigma_i(s_i)$ are known as spin orbitals.

In the 1920ies, Eq. (4.9) was in practice insoluble for all but the smallest systems, and Hartree therefore adopted an independent-electron approximation in which the ith electron interacts with the charge density of the remaining electrons.

Inserting Eq. (4.10) in Eq. (4.1), one obtains the following density of independent electrons:

$$\rho(\vec{r}) = \sum_{i=1}^{N} \left| \phi_i(\vec{r}) \right|^2. \tag{4.12}$$

Hartree's independent-electron approximation thus corresponds to

$$\hat{U}_{\mathrm{ee}} = \sum_{i=1}^{N} \hat{U}_i \tag{4.13a}$$

$$, \quad \hat{U}_i(\vec{r}_i) = \int \sum_{\substack{j=1 \\ j \neq i}}^{N} |\phi_j(\vec{r}')|^2 \frac{1}{|\vec{r}_i - \vec{r}'|} d\vec{r}', \tag{4.13b}$$

where $\hat{U}_i$ is known as the Hartree potential.

Within this independent-electron approximation, the desirable form in Eq. (4.8) is obtained with

$$\hat{H}'_i = \hat{H}_i + \hat{U}_i = -\frac{1}{2}\nabla_i^2 + \hat{V}_i + \hat{U}_i. \tag{4.14}$$

In Eq. (4.11), both E'_i and E'_j contain the Coulomb interaction between the ith and the jth electrons. Therefore, correcting for double counting of electron-electron interactions, the Hartree model has the following for the total energy in a system of N electrons:

$$E = \sum_{i=1}^{N} E'_i - \sum_{i<j}^{N} J_{ij}, \tag{4.15}$$

[1] For a Hermitian operator, eigenfunctions corresponding to different eigenvalues are orthogonal, and degenerate eigenfunctions can be orthogonalized, e.g. by applying the Gram-Schmidt algorithm.

[2] Notice the somewhat confusing notation here: ϕ_α is the αth solution to Eq. (4.11) whereas ϕ_i is that solution which characterizes the ith electron. Since a spatial orbital can hold two electrons (with opposite spin), it it possible to have $\phi_i = \phi_j$, whereas $\phi_\alpha \neq \phi_\beta$ unless $\alpha = \beta$.

where the Coulomb integral

$$\begin{aligned} J_{ij} &= \iint |\phi_i(\vec{r})|^2 \frac{1}{|\vec{r}-\vec{r}'|} |\phi_j(\vec{r}')|^2 d\vec{r} d\vec{r}' \\ &= \left\langle \phi_i(\vec{r}) \middle| \left\langle \phi_j(\vec{r}') \middle| \frac{1}{|\vec{r}-\vec{r}'|} \middle| \phi_i(\vec{r}) \right\rangle \middle| \phi_j(\vec{r}') \right\rangle \end{aligned} \tag{4.16}$$

represents the Coulomb interaction between the ith and jth electrons.

Within the Hartree model, a many-electron problem is solved iteratively in the following manner: The starting point is a reasonable choice of approximate orbitals $\phi_i^{(0)}$ (e.g. solutions to the one-electron problem of the hydrogen atom). Inserting these in Eq. (4.13b), one obtains an initial approximation to the Hartree potential $\hat{U}_i^{(0)}$ which by insertion in Eq. (4.14) leads to new solutions $\phi_i^{(1)}$ to Eq. (4.11). This algorithm is continued until the ϕ_i are sufficiently converged to satisfy the need for accuracy. The converged ϕ_i are the Hartree orbitals of Eq. (4.10) which are said to have been found self-consistently since, inserted in the Schrödinger equation, the Hartree potential yields the same orbitals as have been used to construct it. Accordingly, Eqs. (4.11), (4.12) and (4.13b) are known as the self-consistent Hartree equations.

4.4 Hartree-Fock Model

The Hartree wave function in Eq. (4.10) violates the Pauli principle for fermions which states that the many-electron wave function has to be anti-symmetric with respect to the exchange of any two parameter indices. Examplified by a 3-electron system, this amounts to

$$\Phi(\vec{r}_1,\vec{r}_2,\vec{r}_3;s_1,s_2,s_3) = -\Phi(\vec{r}_2,\vec{r}_1,\vec{r}_3;s_2,s_1,s_3) = \Phi(\vec{r}_3,\vec{r}_1,\vec{r}_2;s_3,s_1,s_2). \tag{4.17}$$

In 1930, Fock [39] and Slater [40] independently of one another proposed a correction to this deficiency by replacing Eq. (4.10) with an anti-symmetric sum of all the products of one-electron orbitals that can be achieved by index exchange. This sum is conveniently written as a Slater determinant:

$$\Phi(\vec{r}_1,\ldots,\vec{r}_N;s_1,\ldots,s_N) = \frac{1}{\sqrt{N!}} \begin{vmatrix} \phi_1(\vec{r}_1)\sigma_1(s_1) & \phi_2(\vec{r}_1)\sigma_2(s_1) & \cdots & \phi_N(\vec{r}_1)\sigma_N(s_1) \\ \phi_1(\vec{r}_2)\sigma_1(s_2) & \phi_2(\vec{r}_2)\sigma_2(s_2) & \cdots & \phi_N(\vec{r}_2)\sigma_N(s_2) \\ \vdots & \vdots & \vdots & \vdots \\ \phi_1(\vec{r}_N)\sigma_1(s_N) & \phi_2(\vec{r}_N)\sigma_2(s_N) & \cdots & \phi_N(\vec{r}_N)\sigma_N(s_N) \end{vmatrix}, \tag{4.18}$$

in which $1/\sqrt{N!}$ is a normalization factor.

As exchange of parameter indices is seen to correspond to row exchange, the Slater determinant implies an a priori satisfaction of the Pauli principle in

Eq. (4.17). Specifically, one has $\Phi = 0$ if $\phi_i = \phi_j$ and $\sigma_i = \sigma_j$ for any two indices i and j. The Pauli principle, or the Pauli exclusion principle, thus states that two fermions cannot occupy the same quantum state. The fact that $\phi_i = \phi_j$ implies $\sigma_i \neq \sigma_j$ corresponds to the well-known statement that any spatial electron state can contain two electrons with opposite spin.

4.4.1 Exchange Energy

Consider, for simplicity, a system of two electrons with

$$\Phi(\vec{r}_1, \vec{r}_2; s_1, s_2) = \frac{1}{\sqrt{2}}\Big[\phi_1(\vec{r}_1)\sigma_1(s_1)\phi_2(\vec{r}_2)\sigma_2(s_2) - \phi_1(\vec{r}_2)\sigma_1(s_2)\phi_2(\vec{r}_1)\sigma_2(s_1)\Big] \quad (4.19)$$

according to Eq. (4.18).

If the two electrons have parallel spin ($\sigma_1 = \sigma_2$), the total spin has three possible projections on an arbitrary axis. If the two electrons have opposite spin ($\sigma_1 \neq \sigma_2$), the total spin is zero, leaving only one possible projection[3]. With these two cases, one therefore associates the terms triplet state and singlet state, respectively.

In the following, $\Phi_{\uparrow,\downarrow}$ is short for the state $\Phi(\vec{r}_1, \vec{r}_2; s_1, s_2)$ with $\sigma_1 = \uparrow$ and $\sigma_2 = \downarrow$. Furthermore, $|\uparrow_1\rangle$ and $|\downarrow_2\rangle$ denote electron 1 in a spin up state and electron 2 in a spin down state, respectively.

Assuming the energy, and thus the Hamilton operator, to be independent of spin, and using the orthonormality of the spin states and the fact that $\hat{H}$ is symmetrical with respect to the parameter index exchange $1 \leftrightarrow 2$ [4], the energy of a singlet state is given by

$$\begin{aligned}
E_{\mathrm{S}} &= \left\langle \Phi_{\uparrow,\downarrow} \middle| \hat{H} \middle| \Phi_{\uparrow,\downarrow} \right\rangle \\
&= \frac{1}{2}\Bigg[\left\langle \phi_1(\vec{r}_1) \middle| \left\langle \uparrow_1 \middle| \left\langle \phi_2(\vec{r}_2) \middle| \left\langle \downarrow_2 \middle| \hat{H} \middle| \phi_1(\vec{r}_1) \right\rangle \middle| \uparrow_1 \right\rangle \middle| \phi_2(\vec{r}_2) \right\rangle \middle| \downarrow_2 \right\rangle \\
&\quad - \left\langle \phi_1(\vec{r}_1) \middle| \left\langle \uparrow_1 \middle| \left\langle \phi_2(\vec{r}_2) \middle| \left\langle \downarrow_2 \middle| \hat{H} \middle| \phi_1(\vec{r}_2) \right\rangle \middle| \uparrow_2 \right\rangle \middle| \phi_2(\vec{r}_1) \right\rangle \middle| \downarrow_1 \right\rangle \\
&\quad + \left\langle \phi_1(\vec{r}_2) \middle| \left\langle \uparrow_2 \middle| \left\langle \phi_2(\vec{r}_1) \middle| \left\langle \downarrow_1 \middle| \hat{H} \middle| \phi_1(\vec{r}_2) \right\rangle \middle| \uparrow_2 \right\rangle \middle| \phi_2(\vec{r}_1) \right\rangle \middle| \downarrow_1 \right\rangle \\
&\quad - \left\langle \phi_1(\vec{r}_2) \middle| \left\langle \uparrow_2 \middle| \left\langle \phi_2(\vec{r}_1) \middle| \left\langle \downarrow_1 \middle| \hat{H} \middle| \phi_1(\vec{r}_1) \right\rangle \middle| \uparrow_1 \right\rangle \middle| \phi_2(\vec{r}_2) \right\rangle \middle| \downarrow_2 \right\rangle \Bigg] \\
&= \left\langle \phi_1(\vec{r}_1) \middle| \left\langle \phi_2(\vec{r}_2) \middle| \hat{H} \middle| \phi_1(\vec{r}_1) \right\rangle \middle| \phi_2(\vec{r}_2) \right\rangle . \qquad (4.20)
\end{aligned}$$

[3] The spin angular momentum vector of each of the two electrons has the magnitude $S_1 = S_2 = \sqrt{\left(\frac{1}{2}\right)\left(\frac{1}{2}+1\right)}\,\hbar = \frac{\sqrt{3}}{2}\hbar$. In the case of parallel spin, the total spin angular momentum vector has the magnitude $S = \sqrt{(1)(1+1)}\,\hbar = \sqrt{2}\hbar$ with the three possible projections $S_z \in \{-\hbar, 0, \hbar\}$. In the case of opposite spin, $S = \sqrt{(0)(0+1)}\,\hbar = 0$ with $S_z = 0$ being the only possible projection.

[4] Since the two electrons are indistinguishable, all physical entities must be invariant under such an index exchange. Note in that connection that a wave function does not itself represent a physically measurable entity.

Analogously, the energy of a triplet state is given by

$$\begin{aligned} E_{\mathrm{T}} &= \Big\langle \Phi_{\uparrow,\uparrow} \Big| \hat{H} \Big| \Phi_{\uparrow,\uparrow} \Big\rangle \\ &= \Big\langle \phi_1(\vec{r}_1) \Big| \Big\langle \phi_2(\vec{r}_2) \Big| \hat{H} \Big| \phi_1(\vec{r}_1) \Big\rangle \Big| \phi_2(\vec{r}_2) \Big\rangle \\ &\quad - \Big\langle \phi_1(\vec{r}_1) \Big| \Big\langle \phi_2(\vec{r}_2) \Big| \hat{H} \Big| \phi_1(\vec{r}_2) \Big\rangle \Big| \phi_2(\vec{r}_1) \Big\rangle . \end{aligned} \tag{4.21}$$

Comparison of Eqs. (4.20) and (4.21) shows that the triplet energy is smaller than the singlet energy by an amount

$$E_{\mathrm{ex}} = \Big\langle \phi_1(\vec{r}_1) \Big| \Big\langle \phi_2(\vec{r}_2) \Big| \hat{H} \Big| \phi_1(\vec{r}_2) \Big\rangle \Big| \phi_2(\vec{r}_1) \Big\rangle . \tag{4.22}$$

This energy is known as the exchange energy. The term has its origin in the exchange of indices between the different terms in the Slater determinant wave function.

That the triplet energy is smaller than the singlet energy can be understood by the following argument: The linear combination between the indistinguishable states $\Phi_{\uparrow,\downarrow}$ and $\Phi_{\downarrow,\uparrow}$:

$$\begin{aligned} \big|\Phi_{\mathrm{S}}\big\rangle &= \frac{1}{\sqrt{2}}\Big(\Phi_{\uparrow,\downarrow} - \Phi_{\downarrow,\uparrow}\Big) \\ &= \frac{1}{2}\Big[\big|\phi_1(\vec{r}_1)\big\rangle \,|\uparrow_1\rangle\, \big|\phi_2(\vec{r}_2)\big\rangle \,|\downarrow_2\rangle - \big|\phi_1(\vec{r}_2)\big\rangle \,|\uparrow_2\rangle\, \big|\phi_2(\vec{r}_1)\big\rangle \,|\downarrow_1\rangle \\ &\quad - \big|\phi_1(\vec{r}_1)\big\rangle \,|\downarrow_1\rangle\, \big|\phi_2(\vec{r}_2)\big\rangle \,|\uparrow_2\rangle + \big|\phi_1(\vec{r}_2)\big\rangle \,|\downarrow_2\rangle\, \big|\phi_2(\vec{r}_1)\big\rangle \,|\uparrow_1\rangle\Big] \\ &= \frac{1}{2}\Big[\big|\phi_1(\vec{r}_1)\big\rangle\big|\phi_2(\vec{r}_2)\big\rangle + \big|\phi_1(\vec{r}_2)\big\rangle\big|\phi_2(\vec{r}_1)\big\rangle\Big]\,\big[\,|\uparrow_1\rangle\,|\downarrow_2\rangle - |\downarrow_1\rangle\,|\uparrow_2\rangle\,\big] \end{aligned} \tag{4.23}$$

shows that singlet states can be written as the product of a symmetrical spatial state and an anti-symmetrical spin state. Conversely, the three degenerate triplet states

$$\begin{aligned} \big|\Phi_{\mathrm{T}}^{S_z=+\hbar}\big\rangle &= \Phi_{\uparrow,\uparrow} \\ &= \frac{1}{\sqrt{2}}\Big[\big|\phi_1(\vec{r}_1)\big\rangle\big|\phi_2(\vec{r}_2)\big\rangle - \big|\phi_1(\vec{r}_2)\big\rangle\big|\phi_2(\vec{r}_1)\big\rangle\Big]\,|\uparrow_1\rangle\,|\uparrow_2\rangle\,, \end{aligned} \tag{4.24a}$$

$$\begin{aligned} \big|\Phi_{\mathrm{T}}^{S_z=-\hbar}\big\rangle &= \Phi_{\downarrow,\downarrow} \\ &= \frac{1}{\sqrt{2}}\Big[\big|\phi_1(\vec{r}_1)\big\rangle\big|\phi_2(\vec{r}_2)\big\rangle - \big|\phi_1(\vec{r}_2)\big\rangle\big|\phi_2(\vec{r}_1)\big\rangle\Big]\,|\downarrow_1\rangle\,|\downarrow_2\rangle\,, \end{aligned} \tag{4.24b}$$

$$\begin{aligned} \big|\Phi_{\mathrm{T}}^{S_z\,=\,0}\big\rangle &= \frac{1}{\sqrt{2}}\Big(\Phi_{\uparrow,\downarrow} + \Phi_{\downarrow,\uparrow}\Big) \\ &= \frac{1}{2}\Big[\big|\phi_1(\vec{r}_1)\big\rangle \,|\uparrow_1\rangle\, \big|\phi_2(\vec{r}_2)\big\rangle \,|\downarrow_2\rangle - \big|\phi_1(\vec{r}_2)\big\rangle \,|\uparrow_2\rangle\, \big|\phi_2(\vec{r}_1)\big\rangle \,|\downarrow_1\rangle \\ &\quad + \big|\phi_1(\vec{r}_1)\big\rangle \,|\downarrow_1\rangle\, \big|\phi_2(\vec{r}_2)\big\rangle \,|\uparrow_2\rangle - \big|\phi_1(\vec{r}_2)\big\rangle \,|\downarrow_2\rangle\, \big|\phi_2(\vec{r}_1)\big\rangle \,|\uparrow_1\rangle\Big] \\ &= \frac{1}{2}\Big[\big|\phi_1(\vec{r}_1)\big\rangle\big|\phi_2(\vec{r}_2)\big\rangle - \big|\phi_1(\vec{r}_2)\big\rangle\big|\phi_2(\vec{r}_1)\big\rangle\Big]\big[\,|\uparrow_1\rangle\,|\downarrow_2\rangle + |\downarrow_1\rangle\,|\uparrow_2\rangle\big] \end{aligned} \tag{4.24c}$$

can be written as the product of an anti-symmetrical spatial state and a symmetrical spin state. The anti-symmetrical spatial state of the triplet approaches zero as $\vec{r}_1$ approaches $\vec{r}_2$. The small propability of finding the two electrons close together corresponds to a repelling force between the two triplet state electrons. This repelling force is called the exchange force and has nothing to do with Coulomb repulsion, but is a consequence of the coupling between the spin and space variables introduced by the required anti-symmetry of the total wave function in Eq. (4.18). Inversely, the probability density of the symmetrical spatial state of the singlet approaches twice the average value when $\vec{r}_1$ approaches $\vec{r}_2$, corresponding to an attractive exchange force between two singlet electrons. In conclusion, as triplet electrons are farther apart than singlet electrons, the energy of the triplet state is smaller than the energy of the corresponding singlet state. As a consequence, $E_{\text{ex}} > 0$.

4.4.2 The Hartree-Fock Energy

Inserting the non-separable Hamiltonian of Eq. (4.7a) in Eqs. (4.20) and (4.21), for a system of 2 electrons one obtains

$$\begin{aligned} E_{\text{S}} &= \left\langle \phi_1(\vec{r}_1) \middle| \left\langle \phi_2(\vec{r}_2) \middle| \sum_{i=1}^{2} \hat{H}_i + \sum_{i<j}^{2} \frac{1}{|\vec{r}_i - \vec{r}_j|} \middle| \phi_1(\vec{r}_1) \right\rangle \middle| \phi_2(\vec{r}_2) \right\rangle \\ &= \sum_{i=1}^{2} E_i + \sum_{i<j}^{2} J_{ij} = E_1 + E_2 + J_{12}, \end{aligned} \tag{4.25}$$

with E_i being the solution to

$$\hat{H}_i \big| \phi_i(\vec{r}_i) \big\rangle = E_i \big| \phi_i(\vec{r}_i) \big\rangle. \tag{4.26}$$

Analogously

$$\begin{aligned} E_{\text{T}} &= \left\langle \phi_1(\vec{r}_1) \middle| \left\langle \phi_2(\vec{r}_2) \middle| \sum_{i=1}^{2} \hat{H}_i + \sum_{i<j}^{2} \frac{1}{|\vec{r}_i - \vec{r}_j|} \middle| \phi_1(\vec{r}_1) \right\rangle \middle| \phi_2(\vec{r}_2) \right\rangle \\ &\quad - \left\langle \phi_1(\vec{r}_1) \middle| \left\langle \phi_2(\vec{r}_2) \middle| \sum_{i=1}^{2} \hat{H}_i + \sum_{i<j}^{2} \frac{1}{|\vec{r}_i - \vec{r}_j|} \middle| \phi_1(\vec{r}_2) \right\rangle \middle| \phi_2(\vec{r}_1) \right\rangle \\ &= \sum_{i=1}^{2} E_i + \sum_{i<j}^{2} J_{ij} - \sum_{i<j}^{2} K_{ij} = E_1 + E_2 + J_{12} - K_{12}, \end{aligned} \tag{4.27}$$

where

$$\begin{aligned} K_{ij} &= \iint \phi_i^*(\vec{r}) \phi_j^*(\vec{r}') \frac{1}{|\vec{r} - \vec{r}'|} \phi_i(\vec{r}') \phi_j(\vec{r}) d\vec{r} d\vec{r}' \\ &= \left\langle \phi_i(\vec{r}) \middle| \left\langle \phi_j(\vec{r}') \middle| \frac{1}{|\vec{r} - \vec{r}'|} \middle| \phi_i(\vec{r}') \right\rangle \middle| \phi_j(\vec{r}) \right\rangle \end{aligned} \tag{4.28}$$

is called the exchange integral.

Generalizing Eqs. (4.25) and (4.27) to a system of N electrons, one obtains the following expression for the Hartree-Fock energy:

$$E = \sum_{i=1}^{N} E_i + \sum_{i<j}^{N} J_{ij} - \sum_{i<j}^{N} \delta_{\sigma_i \sigma_j} K_{ij}, \tag{4.29}$$

where $\delta_{\sigma_i \sigma_j}$ is the Kronecker delta for the spin. Since $J_{ii} = K_{ii}$, Eq. (4.29) can also be written

$$E = \sum_{i=1}^{N} E_i + \frac{1}{2} \sum_{i,j}^{N} J_{ij} - \frac{1}{2} \sum_{i,j}^{N} \delta_{\sigma_i \sigma_j} K_{ij}, \tag{4.30}$$

in which the self-interaction terms $J_{ii} - K_{ii}$ cancel out[5].

4.4.3 The Hartree-Fock Orbitals

The HF ground state orbitals can be found by applying the variational theorem (see App. A), but as Eq. (4.30) is based on an assumption of normalized orbitals, insertion in Eq. (A.3) will not lead to minimization, as arbitrarily small values of E could be obtained by choosing unnormalized orbitals. Therefore, the Lagrange method of undetermined multipliers is applied:

$$\delta \left(E - \sum_{i=1}^{N} \lambda_i \left(\int |\phi_i(\vec{r})|^2 d\vec{r} - 1 \right) \right) = 0, \tag{4.31}$$

in which the λ_i are called Lagrange multipliers. Eq. (4.31) is seen to be identical to Eq. (A.3) when the normalization condition is satisfied.

Insertion of Eq. (4.30) shows that Eq. (4.31) is satisfied for

$$\delta \left(E_i + \frac{1}{2} \sum_{j=1}^{N} J_{ij} - \frac{1}{2} \sum_{j=1}^{N} \delta_{\sigma_i \sigma_j} K_{ij} - \lambda_i \left(\int |\phi_i(\vec{r})|^2 d\vec{r} - 1 \right) \right) = 0 \quad , \quad \forall i. \tag{4.32}$$

For $\delta\phi_i(\vec{r})$ denoting a small change in $\phi_i(\vec{r})$, variation of E_i with respect to ϕ_i yields

$$\begin{aligned}
\delta(E_i) &= \delta \left(\int \phi_i^*(\vec{r}) \hat{H}_i(\vec{r}) \phi_i(\vec{r}) d\vec{r} \right) \\
&= \int \Big(\phi_i^*(\vec{r}) + \delta\phi_i^*(\vec{r}) \Big) \hat{H}_i(\vec{r}) \Big(\phi_i(\vec{r}) + \delta\phi_i(\vec{r}) \Big) d\vec{r} - \delta \left(\int \phi_i^*(\vec{r}) \hat{H}_i(\vec{r}) \phi_i(\vec{r}) d\vec{r} \right) \\
&\overset{\text{1st order}}{=} \int \phi_i^*(\vec{r})\ \hat{H}_i(\vec{r})\ \delta\phi_i(\vec{r})\ d\vec{r} + \int \delta\phi_i^*(\vec{r})\ \hat{H}_i(\vec{r})\ \phi_i(\vec{r})\ d\vec{r} \\
&= 2 \int \delta\phi_i^*(\vec{r})\ \hat{H}_i(\vec{r})\ \phi_i(\vec{r})\ d\vec{r},
\end{aligned} \tag{4.33}$$

[5] $J_{ii} = K_{ii}$ describes the Coulomb interaction of an electron with itself, and such self-interaction is not believed to occur in nature.

where it has been used that the ϕ_i may be chosen such that $\int \delta\phi_i^* \ \hat{H}_i \ \phi_i \ d\vec{r}$ is real.

Variation of J_{ij} yields

$$\begin{aligned}\delta\left(\iint \phi_i^*(\vec{r})\phi_i(\vec{r})\phi_j^*(\vec{r}')\phi_j(\vec{r}')\frac{d\vec{r}d\vec{r}'}{|\vec{r}-\vec{r}'|}\right) &= \iint \phi_i^*(\vec{r})\phi_i(\vec{r})\phi_j^*(\vec{r}')\delta\phi_j(\vec{r}')\frac{d\vec{r}d\vec{r}'}{|\vec{r}-\vec{r}'|} \\ &+ \iint \phi_i^*(\vec{r})\phi_i(\vec{r})\delta\phi_j^*(\vec{r}')\phi_j(\vec{r}')\frac{d\vec{r}d\vec{r}'}{|\vec{r}-\vec{r}'|} \\ &+ \iint \phi_i^*(\vec{r})\delta\phi_i(\vec{r})\phi_j^*(\vec{r}')\phi_j(\vec{r}')\frac{d\vec{r}d\vec{r}'}{|\vec{r}-\vec{r}'|} \\ &+ \iint \delta\phi_i^*(\vec{r})\phi_i(\vec{r})\phi_j^*(\vec{r}')\phi_j(\vec{r}')\frac{d\vec{r}d\vec{r}'}{|\vec{r}-\vec{r}'|} \\ &= 4\iint \delta\phi_i^*(\vec{r})\phi_i(\vec{r})\phi_j^*(\vec{r}')\phi_j(\vec{r}')\frac{d\vec{r}d\vec{r}'}{|\vec{r}-\vec{r}'|},\end{aligned} \tag{4.34}$$

where the invariance to the exchange $\vec{r} \leftrightarrow \vec{r}'$ has been used, and variation of K_{ij} yields

$$\delta\left(\iint \phi_i^*(\vec{r})\phi_i(\vec{r}')\phi_j^*(\vec{r}')\phi_j(\vec{r})\frac{d\vec{r}d\vec{r}'}{|\vec{r}-\vec{r}'|}\right) = 4\iint \delta\phi_i^*(\vec{r})\phi_i(\vec{r}')\phi_j^*(\vec{r}')\phi_j(\vec{r})\frac{d\vec{r}d\vec{r}'}{|\vec{r}-\vec{r}'|}. \tag{4.35}$$

Furthermore,

$$\delta\left(\int |\phi_i(\vec{r})|^2 d\vec{r} - 1\right) = 2\int \delta\phi_i^*(\vec{r})\phi_i(\vec{r})d\vec{r}. \tag{4.36}$$

Insertion of Eqs. (4.33)-(4.36) in Eq. (4.32) yields

$$\begin{aligned}\int \delta\phi_i^*(\vec{r})\Bigg[\hat{H}_i(\vec{r})\phi_i(\vec{r}) + \sum_{j=1}^{N}\int |\phi_j(\vec{r}')|^2\frac{d\vec{r}'}{|\vec{r}-\vec{r}'|}\ \phi_i(\vec{r}) \\ - \sum_{j=1}^{N}\delta_{\sigma_i\sigma_j}\int \phi_j^*(\vec{r}')\phi_i(\vec{r}')\frac{d\vec{r}'}{|\vec{r}-\vec{r}'|}\ \phi_j(\vec{r}) - \lambda_i\phi_i(\vec{r})\Bigg]d\vec{r} = 0 \quad , \forall i.\end{aligned} \tag{4.37}$$

Satisfying Eq. (4.37) for arbitrary $\delta\phi_i^*(\vec{r})$ amounts to

$$\left(\hat{H}_i(\vec{r}) + \sum_{j=1}^{N}\int \frac{|\phi_j(\vec{r}')|^2 d\vec{r}'}{|\vec{r}-\vec{r}'|}\right)\phi_i(\vec{r}) - \sum_{j=1}^{N}\delta_{\sigma_i\sigma_j}\int \frac{\phi_j^*(\vec{r}')\phi_i(\vec{r}')d\vec{r}'}{|\vec{r}-\vec{r}'|}\ \phi_j(\vec{r}) = \lambda_i\phi_i(\vec{r}). \tag{4.38}$$

Since the two terms in the j-sums cancel for $i = j$, Eq. (4.38) can be written

$$\left(\hat{H}_i + \hat{U}_i\right)\phi_i(\vec{r}_i) - \sum_{\substack{j=1\\ j\neq i}}^{N}\delta_{\sigma_i\sigma_j}\int \frac{\phi_j^*(\vec{r}')\phi_i(\vec{r}')d\vec{r}'}{|\vec{r}_i-\vec{r}'|}\ \phi_j(\vec{r}_i) = \lambda_i\phi_i(\vec{r}_i) \quad , \forall i, \tag{4.39}$$

with $\hat{U}_i$ being the Hartree potential of Eq. (4.13b). In this form, Eq. (4.39) constitute the Hartree-Fock equations. The normalized solutions ϕ_i are the HF orbitals which substituted in the Slater determinant in Eq. (4.18) yield the HF many-electron wave function.

Comparison of Eq. (4.39) with Eqs. (4.11) and (4.14) shows that the Hartree-Fock model reduces to the Hartree model if electron exchange is disregarded. As it includes electron exchange and satisfies the Pauli principle, the Slater determinant wave function used in the HF model is a significant improvement compared to the simple product wave function used in the Hartree model. However, the coupled integro-differential HF equations in Eq. (4.39) are impractical for many applications. In addition, the HF model still describes electron-electron interaction as happening between an electron and the averaged charge density of the remaining electrons while in fact electrons undergo pairwise correlation of movements due to their mutual Coulomb repulsion. To include this dynamic correlation, one would have to replace the single-determinant wave function in Eq. (4.18) with a linear combination of determinants leading to a multi-determinant wave function, and this would complicate matters even more. For this reason, historically many people tried to develop further the Thomas-Fermi concept of using electron density instead of wave functions when describing electron systems. For many years, this electron density approach was based on intuition rather than rigorous proof. This changed in 1964 when Hohenberg and Kohn (HK) [41] presented their two famous theorems which were to form the basic framework of the Density Functional Theory (DFT).

4.5 Hohenberg-Kohn Theorems

4.5.1 1st Hohenberg-Kohn Theorem (HK1)

In a system described by the Hamiltonian in Eq. (4.4), there is a one-to-one correspondence between the external potential $\hat{V}_{ext}$ and the ground state electron density $\rho_0(\vec{r})$.[6]

That $\hat{V}_{\text{ext}}$ determines $\rho_0(\vec{r})$ is rather obvious, as knowledge of $\hat{V}_{\text{ext}}$ along with the number of electrons N determines the Hamiltonian $\hat{H}$ which through the Schrödinger equation determines the ground state wave function $\Phi_0(\vec{r}_1, \ldots, \vec{r}_N)$ and thus the electron density $\rho_0(\vec{r})$ through Eq. (4.1).

It is the reverse statement that it interesting. If ρ_0, besides determining N through Eq. (4.2), also determines $\hat{V}_{\text{ext}}$, then, according to the above statement, $\rho_0(\vec{r})$ also determines Φ_0 and thus everything there is to know about the ground

[6] Note that $\hat{V}_{\text{ext}}$ is not restricted to a Coulomb potential as the one in Eq. (4.6b). Also, $\hat{V}_{\text{ext}}$ is only determined up to a trivial additive constant.

state[7]. In other words, if $\hat{V}_{\text{ext}}$ is uniquely determined from ρ_0, two different configurations cannot yield the same electron density, and the electron density will be sufficient for a unique description of the system. HK1 thus establishes the rigourousness of DFT.

For a non-degenerate ground state, the contradiction proof of HK1 is extremely simple: Assume the existence of two external potentials $\hat{V}_{\text{ext}}$ and $\hat{V}'_{\text{ext}}$ that differ by more than a constant but correspond to the same ground state electron density $\rho_0(\vec{r})$. Then $\hat{V}_{\text{ext}}$ and $\hat{V}'_{\text{ext}}$ would correspond to two different Hamiltonians $\hat{H}$ and $\hat{H}'$ with two different normalized ground state wave functions Φ_0 and Φ'_0. According to Eq. (A.1), and using Eq. (4.1), this would imply

$$\begin{aligned} E_0 &= \langle\Phi_0|\hat{H}|\Phi_0\rangle < \langle\Phi'_0|\hat{H}|\Phi'_0\rangle = \langle\Phi'_0|\hat{H}'|\Phi'_0\rangle + \langle\Phi'_0|\big(\hat{H}-\hat{H}'\big)|\Phi'_0\rangle \\ &= E'_0 + \langle\Phi'_0|\big(\hat{V}_{\text{ext}}-\hat{V}'_{\text{ext}}\big)|\Phi'_0\rangle = E'_0 + \int\rho_0(\vec{r})\Big[\hat{V}_{\text{ext}}(\vec{r})-\hat{V}'_{\text{ext}}(\vec{r})\Big]d\vec{r}, \quad (4.40a) \\ E'_0 &= \langle\Phi'_0|\hat{H}'|\Phi'_0\rangle < \langle\Phi_0|\hat{H}'|\Phi_0\rangle = \langle\Phi_0|\hat{H}|\Phi_0\rangle - \langle\Phi_0|\big(\hat{H}-\hat{H}'\big)|\Phi_0\rangle \\ &= E_0 - \langle\Phi_0|\big(\hat{V}_{\text{ext}}-\hat{V}'_{\text{ext}}\big)|\Phi_0\rangle = E_0 - \int\rho_0(\vec{r})\Big[\hat{V}_{\text{ext}}(\vec{r})-\hat{V}'_{\text{ext}}(\vec{r})\Big]d\vec{r}. \quad (4.40b) \end{aligned}$$

Adding Eqs. (4.40a) and (4.40b), one obtains

$$E_0 + E'_0 < E_0 + E'_0, \tag{4.41}$$

and the theorem is proved by contradiction. The theorem can be generalized to degenerate ground states.

4.5.2 2nd Hohenberg-Kohn Theorem (HK2)

The ground state electron density $\rho_0(\vec{r})$ can be found by applying the variational theorem to the energy functional[8] *$E[\rho]$, i.e.*

$$E[\rho] \leq E[\rho_0] = E_0$$

for any electron density that corresponds to some physical $\hat{V}_{ext}$[9] *and satisfies $\rho(\vec{r}) \geq 0$ and $\int\rho(\vec{r})d\vec{r} = N$* [10].

HK2 is actually a corollary of HK1, as any $\rho(\vec{r})$ according to HK1 corresponds to a wave function Φ which satisfies Eq. (A.1). Note that, in principle, the HK theorems only apply to the ground state electron density.

[7] The interpretation of the wave function as containing all information about a system of particles was first put forward by Max Born in 1928.

[8] Functionals are described in App. B.

[9] This restriction is known as $\hat{V}_{\text{ext}}$-representability.

[10] This restriction is known as N-representability.

As will be elaborated in the following, HK2 establishes a prescription for finding the ground state electron density ρ_0 of an electron system if the energy functional $E[\rho]$ is known.

Since, according to HK1, $\rho_0(\vec{r})$ determines all ground state properties including the electron kinetic energy and the electron-electron repulsion, one can write

$$\begin{aligned} E[\rho] &= T[\rho] + V_{\text{ext}}[\rho] + U_{\text{ee}}[\rho] \\ &= \int \hat{V}_{\text{ext}}(\vec{r})\ \rho(\vec{r})\ d\vec{r} + F^{\text{HK}}[\rho], \qquad (4.42a) \\ V_{\text{ext}}[\rho] &= \int \hat{V}_{\text{ext}}(\vec{r})\ \rho(\vec{r})\ d\vec{r}, \qquad (4.42b) \\ F^{\text{HK}}[\rho] &= T[\rho] + U_{\text{ee}}[\rho], \qquad (4.42c) \end{aligned}$$

where the HK functional $F^{\text{HK}}[\rho]$ is universal in the sense that its form is independent of the system under consideration.

Using Eq. (B.2), a Lagrange variation of $E[\rho]$ with respect to ρ yields

$$\begin{aligned} &\delta\Big(E[\rho] - \mu\Big(\int \rho(\vec{r})d\vec{r} - N\Big)\Big) = \\ &\delta\left(\int \hat{V}_{\text{ext}}(\vec{r})\ \rho(\vec{r})\ d\vec{r} + F^{\text{HK}}[\rho]\right) - \mu\ \delta\left(\int \rho(\vec{r})d\vec{r}\right) = \\ &\int \Big(\hat{V}_{\text{ext}}(\vec{r}) - \mu\Big)\,\delta\rho(\vec{r})\ d\vec{r} + \delta F^{\text{HK}}[\rho] = \\ &\int \left(\hat{V}_{\text{ext}}(\vec{r}) + \frac{\delta F^{\text{HK}}[\rho]}{\delta\rho} - \mu\right)\delta\rho(\vec{r})\ d\vec{r} = 0, \qquad (4.43) \end{aligned}$$

which has to be satisfied for all $\delta\rho$ and thus corresponds to[11]

$$\hat{V}_{\text{ext}}(\vec{r}) + \frac{\delta F^{\text{HK}}[\rho]}{\delta\rho} = \mu, \qquad (4.44)$$

in which μ has a physical interpretation as the chemical potential.

Insertion of an explicit expression for $F^{\text{HK}}[\rho]$ in Eq. (4.44) would lead to the ground state electron density ρ_0 of any system of electrons moving in an external potential $\hat{V}_{\text{ext}}$. The problem is, that such an expression has proved more than hard to come by. In fact, to this day the exact form of the energy functional is still not known. The HK theorems contain a prescription for finding the ground state electron density if the energy functional is known, but contain no prescription for constructing this energy functional. Isolating the classical Coulomb repulsion

[11] Eq. (4.44) can lead to solutions that are other kinds of extrema than minima. In that case, the ground state electron density ρ_0 is easily identified as the solution corresponding to the lowest energy.

part in the electron-electron interaction functional $U_{\rm ee}[\rho]$:

$$U_{\rm ee}[\rho] = U_{\rm cl}[\rho] + \Big(U_{\rm ee}[\rho] - U_{\rm cl}[\rho]\Big) \tag{4.45a}$$

$$, \quad U_{\rm cl}[\rho] = \frac{1}{2}\iint \frac{\rho(\vec{r})\ \rho(\vec{r}')}{|\vec{r}-\vec{r}'|}\ d\vec{r}\ d\vec{r}', \tag{4.45b}$$

the problem can be narrowed down to constructing a functional for the kinetic energy $T[\rho]$ and a functional for the non-classical part $U_{\rm ee}[\rho]-U_{\rm cl}[\rho]$ of the electron-electron interaction. Notice that $U_{\rm ee}[\rho] - U_{\rm cl}[\rho]$ also includes the correction for the self-interaction introduced in Eq. (4.45b).

4.5.3 The Thomas-Fermi and Thomas-Fermi-Dirac Models

The TF model briefly described in Sec. 4.2 constitutes the simplest way of obtaining approximate expressions for $T[\rho]$ and $U_{\rm ee}[\rho]-U_{\rm cl}[\rho]$. In the TF functional for electron-electron interaction, all non-classical terms are disregarded:

$$U_{\rm ee}^{\rm TF}[\rho] = U_{\rm cl}[\rho]. \tag{4.46}$$

The TF functional for kinetic energy $T^{\rm TF}[\rho]$ is the functional for independent electrons characterized by the free-electron wave functions

$$\phi_{\vec{k}}(\vec{r}) = \frac{1}{\sqrt{V}}\ e^{i\vec{k}\cdot\vec{r}}, \tag{4.47}$$

where $\vec{k}$ is the wave vector, and where V is the volume in which the electron moves. Using the three-dimensional equivalent of Eq. (3.35), one obtains

$$\begin{aligned} T^{\rm TF}[\rho] &= 2\sum_{\vec{k}}^{\rm occ}\int_V \phi_{\vec{k}}^*(\vec{r})\Big(-\frac{1}{2}\nabla^2\Big)\phi_{\vec{k}}(\vec{r})\ d\vec{r} \\ &= \frac{1}{V}\int_V \sum_{\vec{k}}^{\rm occ} k^2\ d\vec{r} = \frac{1}{8\pi^3}\int_V\int_{|\vec{k}|\le k_{\rm F}} k^2 d\vec{k}\ d\vec{r} = \frac{1}{2\pi^2}\int_V\int_{|\vec{k}|\le k_{\rm F}} k^4 dk\ d\vec{r} \\ &= \frac{1}{10\pi^2}\int_V k_{\rm F}^5(\vec{r})\ d\vec{r}\ \ , \ \ k_{\rm F}(\vec{r}) = \sqrt[3]{3\pi^2\rho(\vec{r})}, \\ &= \frac{3}{10}\sqrt[3]{9\pi^4}\int_V \rho^{\frac{5}{3}}(\vec{r})\ d\vec{r}\ \simeq\ 2.871\int_V \rho^{\frac{5}{3}}(\vec{r})\ d\vec{r}, \end{aligned} \tag{4.48}$$

where $k_{\rm F}$ is the Fermi wave number which has the property that, at absolute zero[12], all occupied modes are characterized by $|\vec{k}| \le k_{\rm F}$.

The more reasonable Thomas-Fermi-Dirac (TFD) model [42] from 1930 has

$$T^{\rm TFD}[\rho] = T^{\rm TF}[\rho], \tag{4.49}$$

[12] The correction at room temperature is negligible.

but adds to $U_{\rm cl}[\rho]$ the exchange energy of a uniform electron gas.

For many applications, the results obtained with TF, TFD or subsequent improvements have been far from encouraging. Far more successful was the method presented in 1965 by Kohn and Sham [43]. Since then, the KS method has been the main contributor when it comes to turning DFT into a practical tool for rigourous calculations.

4.6 Kohn-Sham Method

Instead of facing the difficulties of treating a system of mutually interacting electrons head on, the idea of Kohn and Sham (KS) is instead to treat an auxilliary electron system in which there is no electron-electron interaction, but in which the electron density is nonetheless exactly the same as in the true system. So the prominent contribution of KS was to construct an effective one-electron potential $V_{\rm eff}$ for which the eigenfunctions of

$$\begin{aligned} \hat{H}^{\rm KS} &= \sum_i \left(-\frac{1}{2}\nabla_i^2 + V_{\rm eff}(\vec{r}_i) \right) = \sum_i \hat{H}_i^{\rm KS} \\ &, \quad \hat{H}_i^{\rm KS} = -\frac{1}{2}\nabla_i^2 + \hat{V}_{\rm eff}(\vec{r}_i), \end{aligned} \tag{4.50}$$

correspond to the electron density of the true system:

$$\hat{H}_i^{\rm KS}|\psi_i\rangle = \epsilon_i|\psi_i\rangle, \tag{4.51a}$$

$$\rho(\vec{r}) = \sum_{i=1}^{N} n_i \left|\psi_i(\vec{r})\right|^2, \tag{4.51b}$$

in which n_i is the occupation number of the ith orbital.

In this independent-electron picture, the many-electron wave function is a Slater determinant as the one in Eq. (4.18). Notice that the KS method constitutes a sort of compromise between wave function based methods and strict DFT which is based on electron densities alone.

Instead of writing the energy functional as in Eq. (4.42a), the KS method has

$$E[\rho] = T_0[\rho] + V_{\rm ext}[\rho] + U_{\rm cl}[\rho] + E_{\rm xc}[\rho], \tag{4.52}$$

where the exchange-correlation functional

$$E_{\rm xc}[\rho] = \Big(T[\rho] - T_0[\rho] \Big) + \Big(U_{\rm ee}[\rho] - U_{\rm cl}[\rho] \Big) \tag{4.53}$$

contains the necessary corrections to the kinetic energy and the non-classical part of the electron-electron interaction. The latter consists of electron exchange, electron correlation, which is disregarded in the HF model, and the correction for the self-interaction associated with $U_{\rm cl}$. The functionals $T[\rho]$ and $U_{\rm ee}[\rho] - U_{\rm cl}[\rho]$, which are hard to come by, are thus concentrated in $E_{\rm xc}[\rho]$.

4.6.1 Effective Potential

In a system with independent electrons, one would have

$$E[\rho] = T_0[\rho] + V_{\text{eff}}[\rho]. \tag{4.54}$$

Comparison of Eqs. (4.52) and (4.54) thus yields

$$\begin{aligned} V_{\text{eff}}[\rho] &= V_{\text{ext}}[\rho] + U_{\text{cl}}[\rho] + E_{\text{xc}}[\rho] \\ &= \int \hat{V}_{\text{ext}}(\vec{r})\ \rho(\vec{r})\ d\vec{r} + \frac{1}{2}\int\int \frac{\rho(\vec{r})\ \rho(\vec{r}')}{|\vec{r}-\vec{r}'|}\ d\vec{r}\ d\vec{r}' + E_{\text{xc}}[\rho], \end{aligned} \tag{4.55}$$

where Eqs. (4.42b) and (4.45b) have been used.

Eq. (4.55) defines the functional for the effective potential $V_{\text{eff}}[\rho]$. The effective potential itself $\hat{V}_{\text{eff}}(\vec{r})$ is found by performing on Eq. (4.54) a Lagrange variation similar to the one performed in Eqs. (4.43) and (4.44). This leads to

$$\frac{\delta T_0[\rho]}{\delta\rho} + \frac{\delta V_{\text{eff}}[\rho]}{\delta\rho} = \mu. \tag{4.56}$$

Comparison with Eq. (4.44), which written in full corresponds to

$$\frac{\delta T[\rho]}{\delta\rho} + \frac{\delta U_{\text{ee}}[\rho]}{\delta\rho} + \hat{V}_{\text{ext}}(\vec{r}) = \mu, \tag{4.57}$$

shows that these two equations for $\rho(\vec{r})$ are identical for

$$T_0[\rho] \leftrightarrow T[\rho] \quad \wedge \quad \frac{\delta V_{\text{eff}}[\rho]}{\delta\rho} \leftrightarrow \frac{\delta U_{\text{ee}}[\rho]}{\delta\rho} + \hat{V}_{\text{ext}}(\vec{r}). \tag{4.58}$$

It can thus be concluded that independent electrons, for which $U_{\text{ee}} = 0$, moving in an effectice, "external" potential given by

$$\hat{V}_{\text{eff}}(\vec{r}) = \frac{\delta V_{\text{eff}}[\rho]}{\delta\rho}, \tag{4.59}$$

are characterized by the same chemical potential μ and the same electron density $\rho(\vec{r})$ as the electrons moving in the true system.

Inserting Eq. (4.55) in Eq. (4.59), one obtains

$$\hat{V}_{\text{eff}}(\vec{r}) = \hat{V}_{\text{ext}}(\vec{r}) + \hat{V}_{\text{H}}(\vec{r}) + \hat{V}_{\text{xc}}(\vec{r}), \tag{4.60a}$$

$$, \quad \hat{V}_{\text{H}}(\vec{r}) \equiv \int \frac{\rho(\vec{r}')}{|\vec{r}-\vec{r}'|}\ d\vec{r}', \tag{4.60b}$$

$$, \quad \hat{V}_{\text{xc}}(\vec{r}) \equiv \frac{\delta E_{\text{xc}}[\rho]}{\delta\rho}, \tag{4.60c}$$

where the factor of $\frac{1}{2}$ in the Hartree energy disappears because the derivation leading to the Hartree potential $\hat{V}_{\text{H}}$ yields two terms.

4.6.2 Energy Functional

As for an energy expression, according to Eqs. (4.50), (4.51a) and (4.60a), one has

$$\begin{aligned}\sum_i n_i\ \epsilon_i &= \sum_i n_i \left\langle \psi_i \right| -\frac{1}{2}\nabla_i^2 + \hat{V}_{\text{eff}}(\vec{r}_i) \left| \psi_i \right\rangle \\ &= T_0[\rho] + \int \hat{V}_{\text{eff}}(\vec{r})\ \rho(\vec{r})\ d\vec{r} \qquad (4.61) \\ &= T_0[\rho] + \int \hat{V}_{\text{ext}}(\vec{r})\ \rho(\vec{r})\ d\vec{r} + \iint \frac{\rho(\vec{r})\ \rho(\vec{r}')}{|\vec{r}-\vec{r}'|}\ d\vec{r}d\vec{r}' + \int \hat{V}_{\text{xc}}(\vec{r})\ \rho(\vec{r})\ d\vec{r}.\end{aligned}$$

Inserting in Eq. (4.54) $T_0[\rho]$ from Eq. (4.61) and $V_{\text{eff}}[\rho]$ from Eq. (4.55), one obtains[13]:

$$E[\rho] = \sum_i n_i\ \epsilon_i - \frac{1}{2}\iint \frac{\rho(\vec{r})\ \rho(\vec{r}')}{|\vec{r}-\vec{r}'|}\ d\vec{r}\ d\vec{r}' + E_{\text{xc}}[\rho] - \int \hat{V}_{\text{xc}}(\vec{r})\ \rho(\vec{r})\ d\vec{r}. \quad (4.62)$$

Eqs. (4.51), (4.60a) and (4.62) are known as the Kohn-Sham equations.

Eq. (4.62) shows that the one-electron KS energies ϵ_i require a substantial correction in order to yield the correct energy. In fact, besides yielding the correct electron density, the KS orbitals ψ_i are stricly speaking an unphysical abstraction, although an abstraction that in a highly efficient manner facilitates the treatment of large electron systems. The band structure in a periodic crystal is a plot of the ϵ_i, and the sum over ϵ_i in Eq. (4.62) is therefore known as the electron band structure energy:

$$E_{\text{el}}^{\text{BS}} = \sum_i n_i\ \epsilon_i. \qquad (4.63)$$

From a comparison of Eq. (4.51a) with the Hartree-Fock equations in Eq. (4.39) it is obvious that the KS equation is much easier to solve. The exchange term in the HF equations introduces a coupling that makes the HF equations different for different electrons. So besides being simpler, the KS equation is the same for all electrons. In addition, the KS method is in principle exact, whereas HF disregards electron correlation. In practice, it is not necessarily a question of HF or DFT. So-called hybrid DFT is based on functionals that are a mixture of HF exchange and DFT exchange-correlation.

As seen in connection with the Hartree model, the KS solution to a many-electron problem can be found by self-consistency in the following manner: A reasonable guess for the effective potential $\hat{V}_{\text{eff}}^{(0)}$ leads through Eqs. (4.51) to a first approximation for the KS orbitals $\psi_i^{(0)}$ and subsequently to a first approximation for the electron density $\rho^{(0)}$. Using $\rho^{(0)}$ in Eqs. (4.60) leads to an improved effective potential $\hat{V}_{\text{eff}}^{(1)}$, etc.

[13] Notice that, as opposed to e.g. Coulombic potentials, $E_{\text{xc}}[\rho] \neq \int \hat{V}_{\text{xc}}(\vec{r})\ \rho(\vec{r})\ d\vec{r}$.

4.6.3 Approximations to E_{xc}

The attainment of an exact solution to the KS equations requires an exact expression for the exchange-correlation functional $E_{\mathrm{xc}}[\rho]$. A such has still to be achieved, and the challenge within the KS approach can thus be boiled down to finding that approximation of $E_{\mathrm{xc}}[\rho]$ which is most appropriate for the problem at hand.

Local Density Approximation

The simplest of these approximations is the Local Density Approximation (LDA):

$$E_{\mathrm{xc}}^{\mathrm{LDA}}[\rho] = \int e_{\mathrm{xc}}\big(\rho(\vec{r})\big)\ \rho(\vec{r})\ d\vec{r}, \tag{4.64}$$

in which $e_{\mathrm{xc}}\big(\rho(\vec{r})\big)$ is the exchange-correlation energy per electron in a uniform electron gas of density ρ. Using Eq. (4.64) in Eq. (4.60c), one obtains

$$\hat{V}_{\mathrm{xc}}^{\mathrm{LDA}}(\vec{r}) = \frac{\delta E_{\mathrm{xc}}^{\mathrm{LDA}}[\rho]}{\delta\rho} = e_{\mathrm{xc}}\big(\rho(\vec{r})\big) + \rho(\vec{r})\frac{\partial e_{\mathrm{xc}}(\rho)}{\partial\rho}\bigg|_{\rho=\rho(\vec{r})}. \tag{4.65}$$

In general, LDA corresponds to the assumption that relations applicable to a macroscopic, uniform electron system are valid on a local scale in a system with varying electron density. This is a good approximation for slowly varying electron densities. Eq. (4.48), by the way, is also obtained under LDA, since the relation $k_{\mathrm{F}}(\vec{r}) = \sqrt[3]{3\pi^2\rho(\vec{r})}$ is applied locally even though it is derived for a uniform electron gas.

Local Spin Density Approximation

The Local Spin Density Approximation (LSDA) operates with seperate spin up and spin down electron densities:

$$E_{\mathrm{xc}}^{\mathrm{LSDA}}[\rho_\uparrow, \rho_\downarrow] = \int e_{\mathrm{xc}}\big(\rho_\uparrow(\vec{r}), \rho_\downarrow(\vec{r})\big)\ \rho(\vec{r})\ d\vec{r}, \tag{4.66}$$

which is necessary for a proper description of systems with unpaired electron spin.

Generalized Gradient Approximation

LDA refined to include density gradients is called the Generalized Gradient Approximation (GGA):

$$E_{\mathrm{xc}}^{\mathrm{GGA}}[\rho] = \int f\big(\rho(\vec{r}), |\nabla\rho(\vec{r})|\big)\ \rho(\vec{r})\ d\vec{r}, \tag{4.67}$$

where a proper choice of the function f can reduce the LDA-error by as much as an order of magnitude.

For historical reasons, $E_{\mathrm{xc}}[\rho]$ is sometimes partioned into an exchange and a correlation part:

$$E_{\mathrm{xc}}[\rho] = E_{\mathrm{x}}[\rho] + E_{\mathrm{c}}[\rho]. \tag{4.68}$$

4.7 Ab initio, Empirical and Semi-empirical Methods

A calculation is said to be "ab initio" or "from first principles" if it is free of any kind of parameters[14]. Both DFT in the Kohn-Sham formulation as well as the Hartree-Fock approach are examples of ab initio methods. To distinguish, ab initio methods based on wave functions are sometimes termed traditional ab initio.

There exist traditional ab initio methods which include the electron correlation that was disregarded in the HF model. Propably one of the better known among these is the MP2 (2nd order Møller-Plesset) method. MP2, and other methods like it, are very accurate but also computationally cumbersome for all but the smallest systems.

At the other end of the scale of computational methods are the empirical approaches which rely on simple, generic models based on parameters determined through experiments[15]. Empirical methods are computationally highly efficient, but have limited accuracy.

Semi-empirical methods, in which the parameters used are mainly calculated, serve as a compromise between ab initio and empirical approaches considering both computational efficiency and reliability. An example of a semi-empirical method is the Density Functional-based Tight-Binding approach presented in Chap. 5.

Appendices

A The Variational Theorem

For any Hamiltonian $\hat{H}$ representing a physical system, the energy expectation value E_Φ in any state $|\Phi\rangle$ is greater than or equal to the ground state energy E_0 of the system:

$$E_\Phi = \frac{\left\langle \Phi \left| \hat{H} \right| \Phi \right\rangle}{\langle \Phi | \Phi \rangle} \geq \frac{\left\langle \Phi_0 \left| \hat{H} \right| \Phi_0 \right\rangle}{\langle \Phi_0 | \Phi_0 \rangle} = E_0, \tag{A.1}$$

[14] The effective mass is an example of such a parameter.

[15] *Empeira* means "through experience" in greek.

and equality occurs if and only if $\Phi = \Phi_0$.

This last statement in the variational theorem provides a prescription for finding the ground state Φ_0 as the state in which the expectation value of the energy is minimal.

The differential δE_Φ, in this case with respect to Φ, is defined as that part of the difference $E_{\Phi+\delta\Phi} - E_\Phi$ which is linear in the small variation $\delta\Phi$. I.e. for normalized Φ:

$$\begin{aligned} E_{\Phi+\delta\Phi} - E_\Phi &= \left\langle \Phi + \delta\Phi \left| \hat{H} \right| \Phi + \delta\Phi \right\rangle - \left\langle \Phi \left| \hat{H} \right| \Phi \right\rangle \\ &= \left\langle \Phi \left| \hat{H} \right| \delta\Phi \right\rangle + \left\langle \delta\Phi \left| \hat{H} \right| \Phi \right\rangle + \left\langle \delta\Phi \left| \hat{H} \right| \delta\Phi \right\rangle \\ &\Downarrow \\ \delta E_\Phi &= \left\langle \Phi \left| \hat{H} \right| \delta\Phi \right\rangle + \left\langle \delta\Phi \left| \hat{H} \right| \Phi \right\rangle . \end{aligned} \tag{A.2}$$

The ground state Φ_0 can thus be found as the state for which

$$\delta E_\Phi = 0. \tag{A.3}$$

The proof of the variational theorem is very simple: Expanding the state Φ in the complete set of orthonormalized eigenfunctions Φ_i,

$$|\Phi\rangle = \sum_i c_i |\Phi_i\rangle \quad , \quad \hat{H}|\Phi_i\rangle = E_i|\Phi_i\rangle \quad , \quad \langle\Phi_i|\Phi_j\rangle = \delta_{ij}, \tag{A.4}$$

one has, since $E_0 \leq E_1 \leq E_2 \leq \cdots$,

$$E_\Phi = \frac{\sum_{i,j} c_i^* c_j \left\langle \Phi_i \left| \hat{H} \right| \Phi_j \right\rangle}{\sum_{i,j} c_i^* c_j \langle \Phi_i | \Phi_j \rangle} = \frac{\sum_i |c_i|^2 E_i}{\sum_i |c_i|^2} \geq E_0, \tag{A.5}$$

with equality for $c_i = c_0 \delta_{0i}$ only.

B Functionals

A functional is a mapping of a function into a number.

A simple example would be the functional for the number of electrons

$$N[\rho] = \int \rho(\vec{r}) d\vec{r}. \tag{B.1}$$

Another example is the energy functional $E[\rho]$ which yields the total energy of an electron system with electron density $\rho(\vec{r})$.

In a generalized version of the chain rule, the differential of a functional $F[f(x)]$ can be written

$$\delta F[f(x)] = \int \frac{\delta F[f(x)]}{\delta f(x)} \, \delta f(x) \, dx. \tag{B.2}$$

Chapter 5

Density Functional-based Tight-Binding

During the last decades, the Self-Consistent Density Functional Theory (SC-DFT) scheme presented in Chap. 4 has proved to be a very powerful ab initio computational tool with the range of practically solvable problems increasing concurrently with the appearance of more and more powerful computers. The superior predictability has a price, however, as the iterative nature of the scheme makes it computationally cumbersome.

The purpose of this chapter is to present a computationally more efficient semi-empirical alternative to SC-DFT. As shown in Chaps. 10 and 11, results obtained with this method are in reasonable agreement with experimental results as well as with results based on more sophisticated methods. The method in question is the non-SC parametrized Density Functional-based Tight-Binding (DFTB) approach presented by Porezag and co-workers [44, 45] in 1995. In that work, the model was successfully applied to the calculation of equilibrium configurations and phonon frequencies of a number of small carbohydrate molecules. As for the descriptions of electrons, the DFTB approach is based on LCAO expanded Kohn-Sham (KS) orbitals and thus combines the tight-binding (TB) approximation described in Sec. 2.2 with the KS method described in Sec. 4.6.

In this chapter, the DFTB approach is described in the context of finite molecules consisting of carbon and hydrogen, but use of the Bloch formalism presented in Chap. 2 leads to a straightforward generalization to periodic crystals, and a generalization to other types of atoms is also quite feasonable.

5.1 The Model

Within the Born-Oppenheimer approximation, the Hamiltonian for an isolated system of nuclei and electrons is given by

$$\hat{\mathcal{H}} = \hat{T}_{\text{nuc}} + V(\vec{R}), \tag{5.1}$$

where $\hat{T}_{\text{nuc}}$ is the kinetic energy operator of the N nuclei, where $\vec{R}$ is the 3N-dimensional coordinate vector, and where the nuclear potential

$$V(\vec{R}) = E_{\text{el}}^{\text{GS}}(\vec{R}) + \mathsf{V}_{\text{rep}}(\vec{R}) \tag{5.2}$$

consists of the electron ground state energy $E_{\text{el}}^{\text{GS}}$ and the nuclear repulsion potential V_{rep}.

In the KS picture, $E_{\text{el}}^{\text{GS}}$ is given by Eq. (4.62), and for atomic sites $\vec{R}_i$ and $\vec{R}_j$, V_{rep} is given by

$$\mathsf{V}_{\text{rep}}(\vec{R}) = \sum_{i<j} \frac{Z_i Z_j}{\left|\vec{R}_i - \vec{R}_j\right|}. \tag{5.3}$$

Within DFTB, however, the nuclear potential $V(\vec{R})$ is approximated by a sum over one-electron KS energies ϵ_m plus a sum over short-range repulsive two-body potentials V_{rep}^{ij}:

$$V(\vec{R}) \simeq \sum_m n_m \epsilon_m(\vec{R}) + \sum_{i<j} V_{\text{rep}}^{ij}\left(\left|\vec{R}_i - \vec{R}_j\right|\right), \tag{5.4}$$

with n_m being the occupation number of the mth orbital. As described in Ref. [44], the approximation in Eq. (5.4) has been applied successfully by a variety of authors in other connections than DFTB.

5.1.1 Electron Band Structure Energy

The first term in Eq. (5.4) is the electron band structure energy:

$$E_{\text{el}}^{\text{BS}}(\vec{R}) = \sum_m n_m \epsilon_m(\vec{R}). \tag{5.5}$$

The mth KS eigenvalue ϵ_m is a solution to the one-electron KS equation

$$\hat{H}\psi_m(\vec{r}) = \epsilon_m \psi_m(\vec{r}), \tag{5.6}$$

in which the one-electron Hamiltonian

$$\hat{H} = \hat{T}_{\text{el}} + \hat{V}_{\text{eff}}(\vec{r}) \tag{5.7}$$

consists of the one-electron kinetic energy operator $\hat{T}_{\text{el}}$ and the effective one-electron potential $\hat{V}_{\text{eff}}(\vec{r})$.

The KS orbitals ψ_m are LCAO-expanded in a basis consisting of localized, atom-centered wave functions ϕ_ν:

$$\psi_m(\vec{r}) = \sum_\nu m_\nu \phi_\nu(\vec{r} - \vec{R}^\nu), \tag{5.8}$$

in which $\vec{R}^{\nu}$ is the atomic site of ϕ_ν. The basis includes one basis function for each atomic valence orbital with the extra requirement that all subshells are completed. For hydrogen, the ν-sum is thus limited to an orbital with $1s$-symmetry while it for carbon includes one $2s$- and three $2p$-orbitals ($2p_x, 2p_y, 2p_z$).

As shown in Sec. 2.2, the energy is given as the solution to

$$\left(\overleftrightarrow{H} - \epsilon_m \overleftrightarrow{S}\right) \vec{m} = 0 \tag{5.9a}$$

$$, \quad H_{\mu\nu} = \left\langle \phi_\mu \left| \hat{H} \right| \phi_\nu \right\rangle \tag{5.9b}$$

$$, \quad S_{\mu\nu} = \langle \phi_\mu | \phi_\nu \rangle \,. \tag{5.9c}$$

Eqs. (5.9) constitute the standard non-orthogonal[1] TB matrix eigenvalue problem. Within DFTB, the matrix elements are calculated analytically.

It is known from experience that true atomic orbitals do not constitute a very efficient basis for large condensed system such as the polymers treated in this work. The long range tails of true atomic orbitals, e.g., lead to numerical difficulties without contributing much to the total energy. Within DFTB, therefore, the basis functions ϕ_ν are not atomic orbitals of any actual free atoms but are instead so-called pseudoatomic wave functions constructed in the manner described below.

Pseudoatomic Wave Functions

The pseudoatomic wave functions are constructed as the following linear combination of so-called Slater-type orbitals:

$$\phi_\nu(\vec{r}) = \sum_{n,\alpha} a_{n\alpha}\; r^{l_\nu + n}\; e^{-\alpha r}\; Y_{l_\nu m_\nu}\left(\frac{\vec{r}}{r}\right), \tag{5.10}$$

in which the $Y_{l_\nu m_\nu}$ are the spherical harmonics[2]. The pseudoatomic wave functions thus have the same s- and p-symmetry, etc. as the true atomic orbitals[3].

For $n = 0, 1, 2, 3$ and for 5 values of α in the range $0.5 \leq \alpha \leq Z$, where Z is the nuclear charge of the atom in question, Eq. (5.10) can be shown to be an sufficient basis for all atoms up to the third row in the periodic table of elements.

The pseudoatomic wave functions are the self-consistent solutions to the following generalized KS equation:

$$\hat{H}^{\text{psat}} \phi_\nu(\vec{r}) = \epsilon_\nu^{\text{psat}} \phi_\nu(\vec{r}), \tag{5.11}$$

[1] In orthogonal TB, the overlap matrix elements are set to zero.

[2] The spherical harmonics $Y_{l_\nu m_\nu}$ are the simultaneous eigenfunctions of the angular momentum operators $\hat{L}_z = \left(\vec{r} \times \frac{\hbar}{i}\nabla\right)_z = x\frac{\hbar}{i}\frac{\partial}{\partial y} - y\frac{\hbar}{i}\frac{\partial}{\partial x}$ and $\hat{\vec{L}}^2 = \hat{L}_x^2 + \hat{L}_y^2 + \hat{L}_z^2$. The Slater-type orbitals $r^{l_\nu+n}\; e^{-\alpha r}\; Y_{l_\nu m_\nu}\left(\frac{\vec{r}}{r}\right)$ enter in the analytic solutions to a single electron in the electrostatic Coulomb field of a fixed point charge. The hydrogen atom is an example of such a system.

[3] s- and p-orbitals correspond to $l = 0, m = 0$ and $l = 1, m = -1, 0, +1$, respectively.

with

$$\hat{H}^{\text{psat}} = \hat{T}_{\text{el}} + \hat{V}_{\text{nuc}}(\vec{r}) + \hat{V}_{\text{H}}\left(\rho^{\text{psat}}(\vec{r})\right) + \hat{V}_{\text{xc}}^{\text{LDA}}\left(\rho^{\text{psat}}(\vec{r})\right) + \left(\frac{r}{r_0}\right)^2 \tag{5.12a}$$

$$, \quad \hat{T}_{\text{el}} = -\frac{1}{2}\nabla^2, \tag{5.12b}$$

$$, \quad \hat{V}_{\text{nuc}}(\vec{r}) = -\frac{Z}{r}, \tag{5.12c}$$

$$, \quad \hat{V}_{\text{H}}\left(\rho^{\text{psat}}(\vec{r})\right) = \int \frac{\rho^{\text{psat}}(\vec{r}')}{|\vec{r} - \vec{r}'|}\, d\vec{r}', \tag{5.12d}$$

where $\hat{V}_{\text{nuc}}$ is the electrostatic nuclear potential of Eq. (4.6b), where $\hat{V}_{\text{H}}$ is the Hartree potential of Eq. (4.60b), and where the LDA exchange-correlation potential $\hat{V}_{\text{xc}}^{\text{LDA}}$ of Eq. (4.65) is expressed in terms of the Perdew and Zunger parametrization [46]. The term $\left(\frac{r}{r_0}\right)^2$ makes it energetically favourable for the wave functions to avoid areas far away from the nucleus and thus serves to compress the electron density compared with that in a free atom. By experience, this is known to improve band structure calculations within DFTB. The radius r_0 is set to 1.42Å for carbon and 0.69Å for hydrogen.

Effective One-electron Potential

The effective potential is approximated by a sum over spherically symmetric atom-centered potentials:

$$\hat{V}_{\text{eff}}(\vec{r}) \simeq \sum_i \hat{V}_i\left(\left|\vec{r} - \vec{R}_i\right|\right), \tag{5.13}$$

where $\hat{V}_i\left(\left|\vec{r} - \vec{R}_i\right|\right)$ is the potential due to a neutral pseudoatom at $\vec{R}_i$ when the pseudoatom is characterized by the compressed electron density but without including the compression term $\left(\frac{r}{r_0}\right)^2$ in $\hat{V}_i$. I.e.

$$\hat{V}_i\left(\left|\vec{r} - \vec{R}_i\right|\right) = \hat{V}_{\text{nuc}}^i(\vec{r}) + \hat{V}_{\text{H}}\left(\rho_i^{\text{com}}(\vec{r})\right) + \hat{V}_{\text{xc}}^{\text{LDA}}\left(\rho_i^{\text{com}}(\vec{r})\right) \tag{5.14a}$$

$$, \quad \hat{V}_{\text{nuc}}^i(\vec{r}) = -\frac{Z_i}{\left|\vec{r} - \vec{R}_i\right|} \tag{5.14b}$$

$$, \quad V_{\text{H}}\left(\rho_i^{\text{com}}(\vec{r})\right) = \int \frac{\rho_i^{\text{com}}(\vec{r}')}{|\vec{r} - \vec{r}'|}\, d\vec{r}' \tag{5.14c}$$

$$, \quad \rho_i^{\text{com}}(\vec{r}) = \sum_\nu n_\nu |\phi_\nu(\vec{r})|^2, \tag{5.14d}$$

where the ϕ_ν are the compressed pseudoatomic wave functions of Eq. (5.11).

Hamilton and Overlap Matrix Elements

In the two-centre approximation[4], the Hamilton and overlap matrix elements of Eqs. (5.9) are given by

$$H_{\mu\nu} \simeq \begin{cases} \epsilon_\mu^{\text{free atom}} & \text{for } \mu = \nu \\ \langle \phi_\mu | \hat{T}_{\text{el}} + \hat{V}_\mu + \hat{V}_\nu | \phi_\nu \rangle & \text{for } \vec{R}^\mu \neq \vec{R}^\nu \\ 0 & \text{otherwise} \end{cases} , \tag{5.15a}$$

$$S_{\mu\nu} = \begin{cases} 1 & \text{for } \mu = \nu \\ \langle \phi_\mu | \phi_\nu \rangle & \text{for } \vec{R}^\mu \neq \vec{R}^\nu \\ 0 & \text{otherwise} \end{cases} , \tag{5.15b}$$

where $\hat{V}_\mu$ is the potential in Eq. (5.14a) centrered on $\vec{R}^\mu$, and where $\epsilon_\mu^{\text{free atom}}$ ensures the right atomic limit for large interatomic distances.

Resolving p-orbitals ϕ_μ^p in $p\sigma$-orbitals $\phi_\mu^{p\sigma}$ and $p\pi$-orbitals $\phi_\mu^{p\pi}$ with symmetry axes along and perpendicular to the line of sight $\vec{R}^\mu - \vec{R}^\nu$, respectively, symmetry considerations allow $\langle \phi_\mu | \hat{T}_{\text{el}} + \hat{V}_\mu + \hat{V}_\nu | \phi_\nu \rangle$ and $\langle \phi_\mu | \phi_\nu \rangle$ to be written as linear combinations of the following so-called Slater-Koster integrals [47] that depend on interatomic distance $r = |\vec{R}^\mu - \vec{R}^\nu|$ only:

$$H_{ss\sigma}(r) = \langle \phi_\mu^s | \hat{T}_{\text{el}} + \hat{V}_\mu + \hat{V}_\nu | \phi_\nu^s \rangle, \tag{5.16a}$$
$$H_{sp\sigma}(r) = \langle \phi_\mu^s | \hat{T}_{\text{el}} + \hat{V}_\mu + \hat{V}_\nu | \phi_\nu^{p\sigma} \rangle, \tag{5.16b}$$
$$H_{pp\sigma}(r) = \langle \phi_\mu^{p\sigma} | \hat{T}_{\text{el}} + \hat{V}_\mu + \hat{V}_\nu | \phi_\nu^{p\sigma} \rangle, \tag{5.16c}$$
$$H_{pp\pi}(r) = \langle \phi_\mu^{p\pi} | \hat{T}_{\text{el}} + \hat{V}_\mu + \hat{V}_\nu | \phi_\nu^{p\pi} \rangle, \tag{5.16d}$$
$$S_{ss\sigma}(r) = \langle \phi_\mu^s | \phi_\nu^s \rangle, \tag{5.16e}$$
$$S_{sp\sigma}(r) = \langle \phi_\mu^s | \phi_\nu^{p\sigma} \rangle, \tag{5.16f}$$
$$S_{pp\sigma}(r) = \langle \phi_\mu^{p\sigma} | \phi_\nu^{p\sigma} \rangle, \tag{5.16g}$$
$$S_{pp\pi}(r) = \langle \phi_\mu^{p\pi} | \phi_\nu^{p\pi} \rangle. \tag{5.16h}$$

As an example, for ϕ_μ being an s-orbital on one atom and ϕ_ν being a p_x-orbital on another atom, Fig. 5.1 shows that

$$\begin{aligned} X_{sp_x} &= \cos\eta_x \; X_{sp\sigma}(r) + \cos\left(\eta_x + \frac{\pi}{2}\right) X_{sp\pi}(r) \quad , \quad X \in \{H, S\}, \\ &= l X_{sp\sigma}(r) \quad , \quad l = \cos\eta_x. \end{aligned} \tag{5.17}$$

In this manner, the different types of matrix elements can be written as the

[4] In the two-centre approximation, the potential in a Hamilton matrix element only includes contributions centrered on one of the sites of the two wave functions in question.

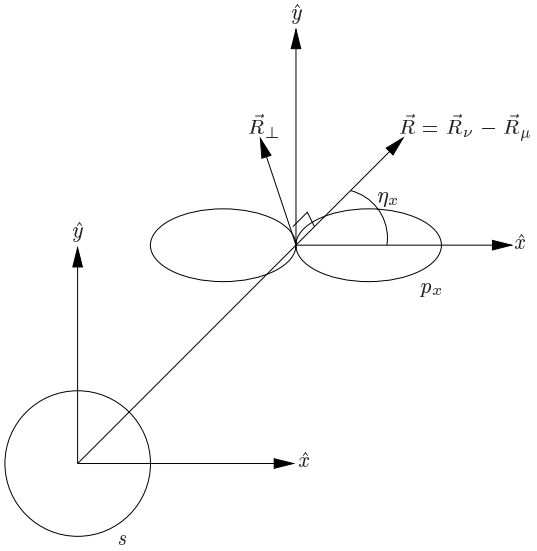

Figure 5.1: Calculation of the matrix element between an s- and a p_x-orbital on different atoms. The p_x-orbital is written as the sum of its projections on $\vec{R}$ and $\vec{R}_\perp$ which is perpendicular to $\vec{R}$ and lies in the plane spanned by $\vec{R}$ and the unit vector $\hat{x}$.

following linear combinations of Slater-Koster integrals:

$$
\begin{aligned}
X_{ss} &= X_{ss\sigma}(r), && \text{(5.18a)}\\
X_{sp_x} &= lX_{sp\sigma}(r), && \text{(5.18b)}\\
X_{sp_y} &= mX_{sp\sigma}(r) \quad , \quad m = \cos\eta_y, && \text{(5.18c)}\\
X_{sp_z} &= nX_{sp\sigma}(r) \quad , \quad n = \cos\eta_z, && \text{(5.18d)}\\
X_{p_xs} &= -lX_{sp\sigma}(r), && \text{(5.18e)}\\
X_{p_xp_x} &= l^2X_{pp\sigma}(r) + (1-l^2)H_{pp\pi}(r), && \text{(5.18f)}\\
X_{p_xp_y} &= lmX_{pp\sigma}(r) - lmH_{pp\pi}(r), && \text{(5.18g)}\\
X_{p_xp_z} &= lnX_{pp\sigma}(r) - lnH_{pp\pi}(r), && \text{(5.18h)}\\
X_{p_ys} &= -mX_{sp\sigma}(r), && \text{(5.18i)}\\
X_{p_yp_x} &= lmX_{pp\sigma}(r) - lmH_{pp\pi}(r), && \text{(5.18j)}\\
X_{p_yp_y} &= m^2X_{pp\sigma}(r) + (1-m^2)H_{pp\pi}(r), && \text{(5.18k)}\\
X_{p_yp_z} &= mnX_{pp\sigma}(r) - mnH_{pp\pi}(r), && \text{(5.18l)}\\
X_{p_zs} &= -nX_{sp\sigma}(r), && \text{(5.18m)}\\
X_{p_zp_x} &= lnX_{pp\sigma}(r) - lnH_{pp\pi}(r), && \text{(5.18n)}\\
X_{p_zp_y} &= mnX_{pp\sigma}(r) - mnH_{pp\pi}(r), && \text{(5.18o)}\\
X_{p_zp_z} &= n^2X_{pp\sigma}(r) + (1-n^2)H_{pp\pi}(r). && \text{(5.18p)}
\end{aligned}
$$

The Slater-Koster integrals are calculated analytically using the formula pre-

sented in Ref. [48] and subsequently parametrized with respect to Chebyshev polynomials T_j:

$$X(r) = \sum_{j=1}^{10} c_j T_{j-1}(y) - \frac{c_1}{2} \tag{5.19a}$$

$$, \quad T_j(y) = \cos\Big(j \cdot \arccos(y)\Big) \tag{5.19b}$$

$$, \quad y = \frac{r - \frac{b+a}{2}}{\frac{b-a}{2}}, \tag{5.19c}$$

where the interatomic distance r is defined on the interval $[a, b]$. In TABLE 1 of Ref. [44], which contains $c_1, \ldots, c_{10}$ and $[a, b]$ for the 14 different[5] Slater-Koster integrals, there occur the following errors: The parameters for $S^{\mathrm{CC}}_{pp\sigma}$ and $S^{\mathrm{CC}}_{pp\pi}$ should be interchanged, the parameters for $H^{\mathrm{CH}}_{ss\sigma}$ and $S^{\mathrm{CH}}_{ss\sigma}$ have the wrong sign, and the interval endpoint b for the $S^{\mathrm{HH}}_{ss\sigma}$ curve should be 6.0Bohr rather than 6.5Bohr.

5.1.2 Short-range Repulsive Two-body Potential

The second term in Eq. (5.4), the short-range repulsive two-body potential

$$V_{\mathrm{rep}}(\vec{R}) = \sum_{i<j} V^{ij}_{\mathrm{rep}}\big(|\vec{R}_i - \vec{R}_j|\big), \tag{5.20}$$

is seen to be the difference between the nuclear potential V and the electron band structure energy $E^{\mathrm{BS}}_{\mathrm{el}}$. The short-range repulsive two-body potential V_{rep} is therefore found by fitting Eq. (5.20) to

$$V_{\mathrm{rep}}(\vec{R}) = V^{\text{SC-LDA}}(\vec{R}) - E^{\mathrm{BS}}_{\mathrm{el}}(\vec{R}), \tag{5.21}$$

where $V^{\text{SC-LDA}}$ is obtained through a self-consistent LDA calculation.

For HH- and CH-interactions, the fit is performed for the coresponding diatomic molecules H_2 and CH, but due to energy level crossings in the C_2-molecule, graphite and diamond have been used for fitting the CC-interaction for interatomic distances exceeding 1.4Å.

V_{rep} is written as

$$V_{\mathrm{rep}}(R) = \begin{cases} \sum_{n=2}^{5} d_n (R_{\mathrm{c}} - R)^n & \text{for } R < R_{\mathrm{c}} \\ 0 & \text{otherwise} \end{cases}, \tag{5.22}$$

such that the fit has 5 degrees of freedom in the form of d_2, d_3, d_4, d_5 and the cut-off radius R_{c}.

The three different types of repulsive two-body potentials[6] are also parametrized with respect to Chebyshev polynomials.

[5] $H^{\mathrm{CC}}_{ss\sigma}, H^{\mathrm{CC}}_{sp\sigma}, H^{\mathrm{CC}}_{pp\sigma}, H^{\mathrm{CC}}_{pp\pi}, H^{\mathrm{CH}}_{ss\sigma}, H^{\mathrm{CH}}_{sp\sigma}, H^{\mathrm{HH}}_{ss\sigma}$ and correspondingly for the overlap elements.
[6] $V^{\mathrm{CC}}_{\mathrm{rep}}, V^{\mathrm{CH}}_{\mathrm{rep}}, V^{\mathrm{HH}}_{\mathrm{rep}}$.

Chapter 6

Phonons

This chapter contains a description of phonon dynamics in a periodic crystal. Sec. 6.1 deals with phonon dispersion while Sec. 6.2 contains a derivation of the infrared absorption spectrum. Sec. 6.3 describes the phenomenon of Raman scattering while Sec. 6.4 shows how to distinguish between infrared active and Raman active phonon modes.

6.1 Phonon Dispersion

Consider a system of N atoms with 3N-dimensional atomic configuration

$$\vec{R} = \begin{pmatrix} x_1 \\ y_1 \\ z_1 \\ \vdots \\ x_{\mathrm{N}} \\ y_{\mathrm{N}} \\ z_{\mathrm{N}} \end{pmatrix}. \tag{6.1}$$

According to Eq. (5.1), the Hamiltonian of the system is given by

$$\hat{H} = \hat{T}_{\mathrm{nuc}} + V(\vec{R}), \tag{6.2}$$

with

$$\hat{T}_{\mathrm{nuc}} = -\frac{\hbar^2}{2} \sum_{j=1}^{3\mathrm{N}} \frac{1}{M_j} \frac{\partial^2}{\partial R_j^2}, \tag{6.3}$$

where M_j is the nuclear mass of the atom to which the jth degree of freedom belongs.

A harmonic approximation of the nuclear potential yields

$$V(\vec{R}) \simeq V(\vec{R}^0) + \frac{1}{2}\sum_{j,l=1}^{3\mathrm{N}} C_{jl}\Delta R_j \Delta R_l, \tag{6.4}$$

where $\vec{R}^0$ is the equilibrium configuration for which $V(\vec{R})$ is a minimum, where $\Delta R_j = (R_j - R_j^0)$ is the displacement of the jth degree of freedom, and where

$$C_{jl} = \left.\frac{\partial^2 V}{\partial R_j \partial R_l}\right|_{\vec{R}^0} \tag{6.5}$$

is the force constant matrix[1]. Since all atomic forces are zero in the equilibrium configuration, the first-order term vanishes in Eq. (6.4)[2].

Introducing the normal mode vectors $\vec{X}_i$ and corresponding normal mode coordinates Q_i:

$$\left(\overleftrightarrow{C} - \omega_i^2 \overleftrightarrow{M}\right)\vec{X}_i = 0 \quad , \quad i \in \{1, \ldots, 3\mathrm{N}\}, \tag{6.6a}$$

$$\vec{R} - \vec{R}^0 = \sum_{i=1}^{3\mathrm{N}} Q_i \vec{X}_i, \tag{6.6b}$$

$$\vec{X}_i^{\mathrm{T}} \overleftrightarrow{M} \vec{X}_j = \delta_{ij}, \tag{6.6c}$$

$$, \quad \overleftrightarrow{M} = \begin{bmatrix} M_1 & 0 & 0 & 0 & 0 & \cdots & \cdots & \cdots & 0 \\ 0 & M_1 & 0 & 0 & 0 & \cdots & \cdots & \cdots & 0 \\ 0 & 0 & M_1 & 0 & 0 & \cdots & \cdots & \cdots & 0 \\ 0 & 0 & 0 & M_2 & 0 & \cdots & \cdots & \cdots & 0 \\ 0 & \cdots & \cdots & \cdots & \ddots & \cdots & \cdots & \cdots & 0 \\ 0 & \cdots & \cdots & \cdots & 0 & M_{\mathrm{N}-1} & 0 & 0 & 0 \\ 0 & \cdots & \cdots & \cdots & 0 & 0 & M_{\mathrm{N}} & 0 & 0 \\ 0 & \cdots & \cdots & \cdots & 0 & 0 & 0 & M_{\mathrm{N}} & 0 \\ 0 & \cdots & \cdots & \cdots & 0 & 0 & 0 & 0 & M_{\mathrm{N}} \end{bmatrix}, \tag{6.6d}$$

where $^{\mathrm{T}}$ denotes taking the transpose, the Hamiltonian can be separated and thereby seen to represent a system of 3N decoupled harmonic oscillators with frequencies $\omega_i = 2\pi\nu_i$ (see the appendix):

$$\hat{H} = \sum_{i=1}^{3\mathrm{N}} \hat{H}_i \tag{6.7a}$$

$$, \quad \hat{H}_i = -\frac{\hbar^2}{2}\frac{\partial^2}{\partial Q_i^2} + \frac{1}{2}\omega_i^2 Q_i^2. \tag{6.7b}$$

[1] Also known as the Hessian matrix.

[2] Apart from a sign, the force components are the first-order derivatives of the potential.

As can be seen from Eq. (6.6b), the introduction of normal modes corresponds to an expansion of the displacement $\vec{R}-\vec{R}^0$ in a basis consisting of the normal mode vectors $\vec{X}_i$. The $\vec{X}_i$ thus indicate the direction of movement of the N atoms in connection with the ith vibrational mode, while Q_i and ω_i express the amplitude and frequency of the vibration, respectively.

Due to the separability of the Hamiltonian, the solution to the energy eigenvalue equation

$$\hat{H}\psi_n(\vec{Q}) = E_n\psi_n(\vec{Q}) \tag{6.8}$$

satisfies

$$\psi_n(\vec{Q}) = \prod_{i=1}^{3N}\psi_{n_i}(Q_i) \tag{6.9a}$$

$$, \quad \hat{H}_i\psi_{n_i}(Q_i) = \left(n_i+\frac{1}{2}\right)\hbar\omega_i\ \psi_{n_i}(Q_i) \quad , \quad n_i = 0,1,2,\ldots \tag{6.9b}$$

$$, \quad E_n = \sum_{i=1}^{3N}\left(n_i+\frac{1}{2}\right)\hbar\omega_i. \tag{6.9c}$$

Due to the energy quantization of the harmonic oscillators, it is convenient to describe the vibrations through the concept of bosonic pseudoparticles known as phonons[3]. A phonon associated with the ith vibrational mode carries the energy $\hbar\omega_i$, and n_i thus indicates the number of phonons in the ith vibrational mode.

The phonon frequencies ω_i can be found as the solutions to the generalized matrix eigenvalue problem in Eq. (6.6a) which can be orthogonalized as

$$\left(\overleftrightarrow{D}-\omega_i^2\overleftrightarrow{I}\right)\vec{X}_i' = 0, \tag{6.10}$$

where

$$\overleftrightarrow{M}^{-\frac{1}{2}}\vec{X}_i' = \vec{X}_i, \tag{6.11a}$$

$$, \quad \left(\overleftrightarrow{M}^{-\frac{1}{2}}\right)_{ij} = \frac{1}{\sqrt{M_{ij}}}, \tag{6.11b}$$

and where

$$\overleftrightarrow{D} = \overleftrightarrow{M}^{-\frac{1}{2}}\ \overleftrightarrow{C}\ \overleftrightarrow{M}^{-\frac{1}{2}} \tag{6.12}$$

is the dynamical matrix.

Analogous to the matrix eigenvalue problem derived in Chap. 2 for the electron energy bands, in a periodic crystal with N atoms in the unit cell, Eq. (6.10) can be written as the following $3N$-dimensional matrix eigenvalue equation:

$$\left(\overleftrightarrow{D}(\vec{q})-\omega_i^2(\vec{q})\overleftrightarrow{I}\right)\vec{X}_i'(\vec{q}) = 0 \quad , \quad i\in\{1,\ldots,3N\}, \tag{6.13}$$

[3]This is quite analogous to the concept of photons. *Photo* and *phono* are derived from the greek words for "light" and "sound", respectively.

where $\vec{q}$ is the phonon momentum[4], and where

$$\overleftrightarrow{D}(\vec{q}) = \sum_n \overleftrightarrow{D}^{n0} e^{i\vec{q}\cdot(\vec{R}_n - \vec{R}_0)} \tag{6.14}$$

is the Fourier transform of the dynamical matrices $\overleftrightarrow{D}^{n0}$ between the nth and zeroth unit cells[5] which are characterized by $\vec{R}_n$ and $\vec{R}_0$, respectively. In Eq. (6.14), the contributions to the dynamical matrix from atoms in different unit cells are "folded" into a dynamical matrix $\overleftrightarrow{D}(\vec{q})$ of reduced dimensions $3N$. In this way, the dimension of the matrix eigenvalue problem is reduced from 3N to $3N$.

The ith solution to Eq. (6.13) yields the phonon dispersion curve or phonon spectrum $\omega_i(\vec{q})$ of the ith phonon mode. Allowing for degeneration, there are thus seen to be $3N$ different phonon modes.

6.2 Infrared Absorption Spectrum

The absorption spectrum $\overleftrightarrow{\alpha}$ relates to the imaginary part $\overleftrightarrow{\chi}''$ of the susceptibility tensor:

$$\alpha_{ab}(\omega) \propto \omega \chi''_{ab}(\omega) \quad , \quad a, b \in \{x, y, z\}. \tag{6.15}$$

For conjugated polymers, the electron contributions to $\overleftrightarrow{\chi}''$ are mainly in the visible range whereas the vibronic contributions are in the infrared (IR) range. The IR absorption spectrum is therefore mainly determined by the vibronic susceptibility $\overleftrightarrow{\chi}^{\text{vib}}$. In the dipole approximation (see Sec. 3.2.1), where the absorbed photons are assumed to carry a negligible momentum, momentum conservation requires $\overleftrightarrow{\chi}^{\text{vib}}$ to depend on zone center ($q = 0$) phonon modes only.

Analogous to Eq. (3.33), one has

$$\chi^{\text{vib}}_{ab}(\omega) \propto \sum_n d^a_{n0} d^b_{n0} \frac{E_{n0}}{E^2_{n0} - \hbar^2\Omega^2} \quad , \quad \Omega = \omega + i\hbar, \tag{6.16}$$

where d^a_{n0} and E_{n0} are the a-component of the electric dipole matrix element and energy difference, respectively, between the zone center ground state $\psi_0(\vec{Q})$ and nth vibronic state $\psi_n(\vec{Q})$:

$$\vec{d}_{n0} = \int \psi^*_n(\vec{Q})\ \vec{d}(\vec{Q})\ \psi_0(\vec{Q})\ d\vec{Q}, \tag{6.17a}$$

$$E_{n0} = E_n - E_0 = \sum_{i=1}^{3N} n_i \hbar\omega_i, \tag{6.17b}$$

[4] The phonon momentum $\vec{q}$ enters in the phase difference between vibrational displacements in different unit cells. For $\vec{q} = 0$, all identical atoms in different unit cells vibrate in phase.

[5] The two degrees of freedom R_j and R_l in Eq. (6.5) correspond to atoms in the nth and zeroth unit cells.

where $\vec{Q}$ is the $3N$-dimensional vector of normal coordinates and $\vec{d}(\vec{Q})$ is the electric dipole moment of a unit cell, and where $q = 0$ is implied.

Expanding $\vec{d}(\vec{Q})$ to the first order in $\vec{Q}$ around the equilibrium yields

$$\vec{d}(\vec{Q}) \;\simeq\; \vec{d}^{\,0} + \vec{\nabla}_{\vec{Q}}\vec{d}\big|_{\vec{R}^0} \cdot \vec{Q}, \tag{6.18}$$

where $\vec{d}^{\,0} = \vec{d}(\vec{R}^0)$ is the permanent dipole moment.

Inserting Eq. (6.18) in Eq. (6.17a), one has

$$\vec{d}_{n0} \;=\; \vec{d}^{\,0} \int \psi_n^*(\vec{Q})\; \psi_0(\vec{Q})\; d\vec{Q} \;+\; \vec{\nabla}_{\vec{Q}}\vec{d}\big|_{\vec{R}^0} \cdot \int \psi_n^*(\vec{Q})\; \vec{Q}\; \psi_0(\vec{Q})\; d\vec{Q}. \tag{6.19}$$

According to Eq. (6.9a), one has

$$\int \psi_n^*(\vec{Q})\; \psi_0(\vec{Q})\; d\vec{Q} = 0 \tag{6.20}$$

due to orthogonality unless $n_i = 0\ \forall i$.

The permanent dipole moment is thus seen not to contribute to the dipole matrix element, and Eq. (6.19) yields

$$\vec{d}_{n0} = \sum_{j=1}^{3N} \left[\frac{\partial \vec{d}}{\partial Q_j}\bigg|_{\vec{R}^0} \int \psi_{n_j}^*(Q_j)\; Q_j\; \psi_0(Q_j)\; dQ_j \prod_{i \neq j} \int \psi_{n_i}^*(Q_i)\; \psi_0(Q_i)\; dQ_i \right]. \tag{6.21}$$

Due to the orthogonality and the selection rule for harmonic oscillator transitions, Eq. (6.21) yields

$$\vec{d}_{n0} = \sum_{j=1}^{3N} \left[\frac{\partial \vec{d}}{\partial Q_j}\bigg|_{\vec{R}^0} \delta_{n_j,1} \int \psi_{n_j}^*(Q_j)\; Q_j\; \psi_0(Q_j)\; dQ_j \prod_{i \neq j} \delta_{n_i,0} \int \psi_{n_i}^*(Q_i)\; \psi_0(Q_i)\; dQ_i \right]. \tag{6.22}$$

$\vec{d}_{n0}$ is thus zero unless the nth vibrational state for some κ satisfies

$$(n_i = 0\ \forall i \neq \kappa) \;\wedge\; (n_\kappa = 1). \tag{6.23}$$

The transitions contributing to the absorption spectrum are thus those in which a single phonon is created.

Since

$$\int \psi_1^*(Q_\kappa)\; Q_\kappa\; \psi_0(Q_\kappa)\; dQ_\kappa = \sqrt{\frac{\hbar}{2\omega_\kappa}}, \tag{6.24}$$

one has

$$\vec{d}_{n0} = \sqrt{\frac{\hbar}{2\omega_\kappa}} \frac{\partial \vec{d}}{\partial Q_\kappa}\bigg|_{\vec{R}^0}, \tag{6.25}$$

and by insertion in Eq. (6.16)

$$\chi_{ab}^{\mathrm{vib}}(\omega) \propto \sum_{\kappa=1}^{3N} \left.\frac{\partial d^a}{\partial Q_\kappa}\right|_{\vec{R}^0} \left.\frac{\partial d^b}{\partial Q_\kappa}\right|_{\vec{R}^0} \frac{1}{\hbar^2\omega_\kappa^2 - \hbar^2\Omega^2}, \tag{6.26}$$

where d^a is the a-component of $\vec{d}(\vec{Q})$, and where $\omega_\kappa = \omega_\kappa(q=0)$.

Finding the imaginary part of Eq. (6.26) for $\gamma \ll \omega$, one finally obtains

$$\alpha_{ab}(\omega) \propto \omega \sum_{\kappa=1}^{3N} \left.\frac{\partial d^a}{\partial Q_\kappa}\right|_{\vec{R}^0} \left.\frac{\partial d^b}{\partial Q_\kappa}\right|_{\vec{R}^0} \frac{2\hbar\omega\hbar\gamma}{(\hbar^2\omega_\kappa^2 - \hbar^2\omega^2)^2 + (2\hbar\omega\hbar\gamma)^2}, \tag{6.27}$$

where $q = 0$ is implied.

6.2.1 Derivative of the Electric Dipole Moment

In this subsection, expressions are found for the electric dipole moment derivatives $\frac{\partial d^a}{\partial Q_\kappa}|_{\vec{R}^0}$ in the context of a one-dimensional periodic crystal.

The electric dipole moment $\vec{d}$ consists of a nuclear contribution $\vec{d}_{\mathrm{nuc}}$ and an electron contribution $\vec{d}_{\mathrm{el}}$:

$$\vec{d} = \vec{d}_{\mathrm{nuc}} + \vec{d}_{\mathrm{el}}. \tag{6.28}$$

Nuclear Contribution

The nuclear contribution is given by

$$\vec{d}_{\mathrm{nuc}} = e \sum_{p=1}^{N} Z_p \vec{R}_p, \tag{6.29}$$

where $Z_p e$ is the charge of the pth nucleus in the unit cell, and where $\vec{R}_p$ is the coordinate vector of the nucleus with respect to an arbitrary origo[6].

Since from Eq. (6.6b)

$$\vec{R} = \vec{R}^0 + \overleftrightarrow{X}\vec{Q}, \tag{6.30}$$

one has

$$\vec{R}_p = \vec{R}_p^0 + \sum_{m=1}^{3N} \begin{pmatrix} X_{3p-2,m}Q_m \\ X_{3p-1,m}Q_m \\ X_{3p,m}Q_m \end{pmatrix}, \tag{6.31}$$

and thus

$$\left.\frac{\partial d_{\mathrm{nuc}}^a}{\partial Q_\kappa}\right|_{\vec{R}^0} = e \sum_{p=1}^{N} Z_p X_{3(p-1)+a,\kappa}, \tag{6.32}$$

with $\overleftrightarrow{X} = \overleftrightarrow{X}(q=0)$, and with the convention $x \leftrightarrow 1, y \leftrightarrow 2, z \leftrightarrow 3$ for the values of a.

[6] For charge-neutral systems, the electric dipole moment is independent of the choice of origo.

Electron Contribution

In the Born-Oppenheimer approximation (see Sec. 4.1), where the electrons are assumed to be in the ground state, the electron contribution is given by

$$\vec{d}_{\rm el} = -\frac{2e}{N_{\rm uc}} \sum_{{\rm v},k} \langle {\rm v}k|\, \vec{r}\, |{\rm v}k\rangle\,, \tag{6.33}$$

where $N_{\rm uc}$ is the number of unit cells, where $|{\rm v}k\rangle$ is the eigenstate of an electron in the v'th valence band with wave number k, and where the factor of 2 occurs due to spin degeneration.

In a LCAO-expansion as the one in Eq. (2.28a), one has

$$|{\rm v}k\rangle = \frac{1}{\sqrt{N}_{\rm uc}} \sum_{\nu} \sum_{n}^{N_{\rm uc}} \sum_{p}^{N} {\rm v}_{\nu p}(k) e^{iknl} \left|\nu \vec{R}_{np}\right\rangle, \tag{6.34}$$

where l is the length of the unit cell, and $|\nu \vec{R}_{np}\rangle$ is an atomic orbital centrered on

$$\vec{R}_{np} = nl\hat{x} + \vec{R}_p, \tag{6.35}$$

which is the site of the pth atom in the nth unit cell.

Inserting Eq. (6.34) in Eq. (6.33), one obtains

$$\vec{d}_{\rm el} = \frac{-2e}{N_{\rm uc}^2} \sum_{{\rm v},k} \sum_{\nu,\nu'} \sum_{n,n'}^{N_{\rm uc}} \sum_{p,p'}^{N} {\rm v}^*_{\nu' p'}(k)\ {\rm v}_{\nu p}(k)\ e^{ik(n-n')l} \left\langle \nu' \vec{R}_{n'p'} \right| \vec{r}\, \left| \nu \vec{R}_{np} \right\rangle. \tag{6.36}$$

The dipole matrix element between the atomic orbitals can be rewritten

$$\begin{aligned} \left\langle \nu' \vec{R}_{n'p'} \right| \vec{r}\, \left| \nu \vec{R}_{np} \right\rangle &= \left\langle \nu' \vec{R}_{n'p'} \right| \vec{r} - \frac{\vec{R}_{n'p'} + \vec{R}_{np}}{2} \left| \nu \vec{R}_{np} \right\rangle \\ &\quad + \frac{\vec{R}_{n'p'} + \vec{R}_{np}}{2} \left\langle \nu' \vec{R}_{n'p'} \middle| \nu \vec{R}_{np} \right\rangle. \end{aligned} \tag{6.37}$$

Assuming that only on-site contributions are significant, Eq. (6.37) yields

$$\begin{aligned} \left\langle \nu' \vec{R}_{n'p'} \right| \vec{r}\, \left| \nu \vec{R}_{np} \right\rangle &\simeq \delta_{nn'}\delta_{pp'} \left\langle \nu' \vec{R}_{np} \right| \vec{r} - \vec{R}_{np} \left| \nu \vec{R}_{np} \right\rangle \\ &\quad + \delta_{nn'}\delta_{pp'} \vec{R}_{np} \left\langle \nu' \vec{R}_{np} \middle| \nu \vec{R}_{np} \right\rangle \\ &= \delta_{\nu\nu'}\delta_{nn'}\delta_{pp'} \vec{R}_{np} \end{aligned} \tag{6.38}$$

due to the symmetry[7] of the orthonormal atomic orbitals.

[7] All three cartesian components in $\vec{r} - \vec{R}_{np}$ change signs when inverted with $\vec{R}_{np}$ as the point of inversion, and, accordingly, $\vec{r} - \vec{R}_{np}$ is said to have odd parity with respect to $\vec{R}_{np}$. Similarly, functions which are invariant to such an inversion are said to have even parity. For $\left\langle \nu' \vec{R}_{np} \right| \vec{r} - \vec{R}_{np} \left| \nu \vec{R}_{np} \right\rangle$ to be non-zero, $|\nu \vec{R}_{np}\rangle$ and $|\nu' \vec{R}_{np}\rangle$ must have different parities in all three dimensions, and such atomic orbitals do not exist. Therefore, $\left\langle \nu' \vec{R}_{np} \right| \vec{r} - \vec{R}_{np} \left| \nu \vec{R}_{np} \right\rangle = 0$.

Inserting Eq. (6.38) in Eq. (6.36), one obtains

$$\vec{d}_{\mathrm{el}} = \frac{-2e}{N_{\mathrm{uc}}} \sum_{\mathrm{v},k,\nu} \sum_{p=1}^{N} |\mathrm{v}_{\nu p}(k)|^2 \vec{R}_{np}. \tag{6.39}$$

The derivative of Eq. (6.39) with respect to Q_κ may be taken quite easily if one makes the bold assumption that the electron localization propabilities remain unchanged under a change in the atomic configuration:

$$\left.\frac{\partial \mathrm{v}_{\nu p}(k)}{\partial Q_\kappa}\right|_{\vec{R}^0} = 0. \tag{6.40}$$

In this case, use of Eqs. (6.35) and (6.31) yields

$$\left.\frac{\partial d^a_{\mathrm{el}}}{\partial Q_\kappa}\right|_{\vec{R}^0} \simeq \frac{-2e}{N_{\mathrm{uc}}} \sum_{\mathrm{v},k,\nu} \sum_{p=1}^{N} |\mathrm{v}_{\nu p}(k)|^2 X_{3(p-1)+a,\kappa}. \tag{6.41}$$

Combining Eqs. (6.32) and (6.41), one finally obtains

$$\left.\frac{\partial d^a}{\partial Q_\kappa}\right|_{\vec{R}^0} = e \sum_{p=1}^{N} \left(Z_p - \frac{2}{N_{\mathrm{uc}}} \sum_{\mathrm{v},k,\nu} |\mathrm{v}_{\nu p}(k)|^2 \right) X_{3(p-1)+a,\kappa}, \tag{6.42}$$

with $\overleftrightarrow{X} = \overleftrightarrow{X}(q=0)$, with $\mathrm{v}_{\nu p}(k)$ evaluated for the equilibrium configuration, and with the convention $x \leftrightarrow 1, y \leftrightarrow 2, z \leftrightarrow 3$ for the values of a.

Equation (6.42) is thus valid only when a change in the atomic configuration results in a negligible electron charge transfer between atomic sites. The impacts of this assumption will be discussed in Chapter 10.

6.3 Raman Scattering

Photons can scatter off an atom or a molecule either elastically or inelastically. Elastic scattering, which is also known as Rayleigh scattering, implies that the energy $\hbar\omega$ and frequency ω of the photon is preserved in the scattering proces[8]. In inelastic scattering, which is known as Raman scattering or the Raman effect, the frequency of the photon undergoes a Raman shift. Raman scattering thus involves a change in either the vibrational, rotational or electron energy of the scatterer.

In a film consisting of conjugated polymer molecules, inter-chain interaction will hinder rotations, so for photon energies in the IR range, vibrational Raman scattering will be the dominant Raman effect. In the following, therefore, Raman

[8] It is the highly wavelength dependent nature of Rayleigh scattering of sun light from air molecules and aerosol particles that gives the sky its blue colour.

scattering will imply a change in the vibrational energy of the crystal or, in other words, to a change in the number of phonons. If the Raman scattering involves the creation of a phonon, the scattered photon frequency ω_{scat} is smaller than the incident frequency ω_{inc} by an amount matching the energy ω_{phon} of one of the phonon modes. This proces is called a Stokes proces. The opposite proces, in which a phonon is destroyed, is called an anti-Stokes proces. Both processes are depicted in Fig. 6.1. At room temperature, the thermal population of phonons is small, and Stokes scattering will be the dominant proces. As the photon momentum is much smaller than the phonon momentum, the phonon modes affected by Raman scattering will predominantly be zone-centre modes.

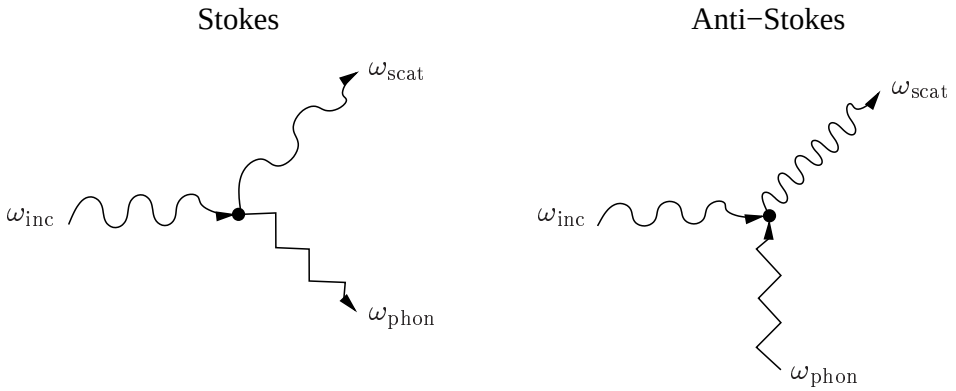

Figure 6.1: Left: Stokes Raman scattering involving the creation of a phonon and a lowering of the photon frequency ($\omega_{\text{scat}} = \omega_{\text{inc}} - \omega_{\text{phon}}$). Right: Anti-Stokes Raman scattering involving the destruction of a phonon and an increase in the photon frequency ($\omega_{\text{scat}} = \omega_{\text{inc}} + \omega_{\text{phon}}$).

Stokes and anti-Stokes scattering can be described as the two-stage processes shown in Fig. 6.2: After absorbing the incident photon, the molecule is excited to an intermediate, virtual state from which it almost instantaneously relaxes into a different vibrational state under the emission of the scattered photon.

Just like IR absorption spectroscopy, Raman spectroscopy makes it possible to characterize vibrations in molecules by measuring the absorption and transmission of light.

6.4 Infrared Active and Raman Active Modes

The following argument shows that in inversion-symmetrical molecules, such as the conjugated polymers treated in this work, the phonon modes are either IR active or Raman active. I.e., the phonon modes that can be excited through the absorption of photons in the IR frequency range do not take part in Raman scattering of photons and vice versa.

As mentioned in Sec. 6.3 and shown in Fig. 6.2, Raman scattering involves

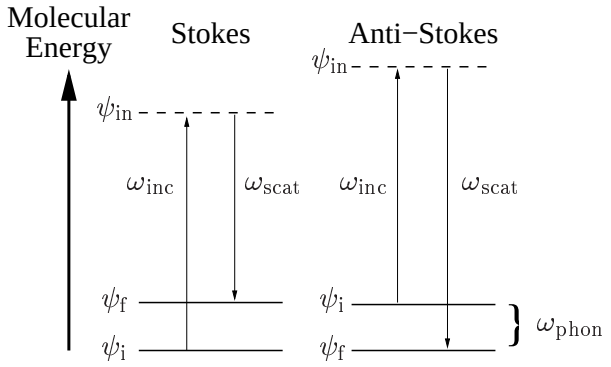

Figure 6.2: Energy level diagrams for Stokes Raman scattering (left) and anti-Stokes Raman scattering (right).

two transitions from an initial vibrational state ψ_i via an intermediate, virtual state ψ_in to a final vibrational state ψ_f, whereas IR absorption only involves one transition from an initial to a final state. An IR absorption process thus requires a non-zero dipole transition matrix element $\langle \psi_\mathrm{i} | \vec{r} | \psi_\mathrm{f} \rangle \neq 0$, whereas Raman scattering requires $\langle \psi_\mathrm{i} | \vec{r} | \psi_\mathrm{in} \rangle \neq 0$ and $\langle \psi_\mathrm{in} | \vec{r} | \psi_\mathrm{f} \rangle \neq 0$. In a material with inversion symmetry, the eigenfunctions can be chosen with definite parity around the point of inversion[9]. For IR absorption, therefore, one has due to the odd parity of $\vec{r}$ that $\mathrm{par}(\psi_\mathrm{i}) \neq \mathrm{par}(\psi_\mathrm{f})$, whereas Raman scattering corresponds to $\mathrm{par}(\psi_\mathrm{i}) \neq \mathrm{par}(\psi_\mathrm{in}) \neq \mathrm{par}(\psi_\mathrm{f})$ which is equivalent to $\mathrm{par}(\psi_\mathrm{i}) = \mathrm{par}(\psi_\mathrm{f})$. The vibrational transition from ψ_i to ψ_f can thus either be involved in IR absorption or in Raman scattering.

Equation (6.27) shows that the IR active modes are characterized by $\frac{\partial \vec{d}}{\partial Q_i} \neq 0$. Since the conjugated polymers treated in this work are inversion-symmetrical in their equilibrium configurations, their equilibrium dipole moments are zero. The Raman active modes with $\frac{\partial \vec{d}}{\partial Q_i} = 0$ are thus the modes that preserve this inversion symmetry. The Raman active modes are therefore termed $\mathrm{A_g}$, where g stands for "gerade", the german word for even, while the IR active modes are termed $\mathrm{B_u}$ with "ungerade" being the german word for odd.

While Eq. (6.27) shows the IR absorption intensity to be proportional to the squared normal coordinate derivative of the electric dipole moment, the Raman intensity can be shown to be proportional to the squared normal coordinate derivative of the susceptibility[10].

[9] Choosing the point of inversion as origo, one has $V(\vec{r}) = V(-\vec{r})$. Therefore, since $\psi(-\vec{r})$ and $\psi(\vec{r})$ are thus seen to be degenerate eigenfunctions, so are the even and odd eigenfunctions $\psi_\mathrm{e}(\vec{r}) = \frac{1}{2}[\psi(\vec{r}) + \psi(-\vec{r})]$ and $\psi_\mathrm{o}(\vec{r}) = \frac{1}{2}[\psi(\vec{r}) - \psi(-\vec{r})]$.

[10] For a single molecule, the relevant physical quantity is the polarizability which is defined as the intermediary between an electric field and its induced electric dipole moment. According to Chap. 3, the polarizability is thus the microscopic counterpart of the susceptibility.

Appendix

A Separation of the Hamiltonian

Inserting Eqs. (6.3) and (6.4) in Eq. (6.2), one has

$$\begin{aligned}\hat{H} &= \hat{T}_{\rm nuc} + V(\vec{R}) \\ &= -\frac{\hbar^2}{2}\sum_{j=1}^{3\rm N}\frac{1}{M_j}\frac{\partial^2}{\partial R_j^2} + V(\vec{R}^0) + \frac{1}{2}\sum_{j,l=1}^{3\rm N} C_{jl}\Delta R_j \Delta R_l. \end{aligned} \tag{A.1}$$

Since, using Eqs. (6.6c) and (6.6b) one has

$$\left(\overleftrightarrow{X}^{\rm T}\overleftrightarrow{M}^{\frac{1}{2}}\right)\left(\overleftrightarrow{M}^{\frac{1}{2}}\overleftrightarrow{X}\right) = \overleftrightarrow{X}^{\rm T}\overleftrightarrow{M}\overleftrightarrow{X} = \overleftrightarrow{I} \;\Rightarrow\; \overleftrightarrow{X}^{\rm T}\overleftrightarrow{M}^{\frac{1}{2}} = \left(\overleftrightarrow{M}^{\frac{1}{2}}\overleftrightarrow{X}\right)^{-1}, \tag{A.2a}$$

$$\begin{aligned}\overleftrightarrow{M}^{\frac{1}{2}}\left(\vec{R}-\vec{R}^0\right) &= \overleftrightarrow{M}^{\frac{1}{2}}\overleftrightarrow{X}\vec{Q}, \\ \vec{Q} &= \left(\overleftrightarrow{M}^{\frac{1}{2}}\overleftrightarrow{X}\right)^{-1}\overleftrightarrow{M}^{\frac{1}{2}}\left(\vec{R}-\vec{R}^0\right), \\ Q_i &= \sum_j \left(\overleftrightarrow{M}^{\frac{1}{2}}\overleftrightarrow{X}\right)^{-1}_{ij}\sqrt{M_j}\Delta R_j, \end{aligned} \tag{A.2b}$$

$$\begin{aligned}\frac{\partial Q_i}{\partial R_j} &= \left(\overleftrightarrow{M}^{\frac{1}{2}}\overleftrightarrow{X}\right)^{-1}_{ij}\sqrt{M_j} = \left(\overleftrightarrow{X}^{\rm T}\overleftrightarrow{M}^{\frac{1}{2}}\right)_{ij}\sqrt{M_j} \\ &= \sum_k X_{ki}\sqrt{M_k}\delta_{kj}\sqrt{M_j} = M_j X_{ji}\ , \end{aligned} \tag{A.2c}$$

$$\frac{\partial}{\partial R_j} = \sum_i \frac{\partial Q_i}{\partial R_j}\frac{\partial}{\partial Q_i} = \sum_i M_j X_{ji}\frac{\partial}{\partial Q_i}, \tag{A.2d}$$

$$\frac{\partial^2}{\partial R_j^2} = \sum_{i,l} M_j^2 X_{ji}X_{jl}\frac{\partial^2}{\partial Q_i \partial Q_l}, \tag{A.2e}$$

one obtains the following for the nuclear kinetic energy written in normal mode coordinates:

$$\begin{aligned}-\frac{\hbar^2}{2}\sum_{j=1}^{3\rm N}\frac{1}{M_j}\frac{\partial^2}{\partial R_j^2} &= -\frac{\hbar^2}{2}\sum_{j,i,l=1}^{3\rm N} M_j X_{ji}X_{jl}\frac{\partial^2}{\partial Q_i\partial Q_l} = -\frac{\hbar^2}{2}\sum_{i,l=1}^{3\rm N}\delta_{il}\frac{\partial^2}{\partial Q_i\partial Q_l} \\ &= -\frac{\hbar^2}{2}\sum_{i=1}^{3\rm N}\frac{\partial^2}{\partial Q_i^2}. \end{aligned} \tag{A.3}$$

Concerning the nuclear potential, one has from Eq. (6.6b) that

$$\Delta R_j = \sum_i Q_i X_{ji}, \tag{A.4}$$

and from Eq. (6.6a) that

$$\overleftrightarrow{C}\overleftrightarrow{X} = \overleftrightarrow{M}\overleftrightarrow{X}\overleftrightarrow{\omega^2}, \tag{A.5}$$

where $\overleftrightarrow{\omega^2}$ is the diagonal matrix of squared phonon frequencies ω_i^2.

Therefore

$$\begin{aligned}
\frac{1}{2}\sum_{j,l=1}^{3N} C_{jl}\Delta R_j \Delta R_l &= \frac{1}{2}\sum_{j,l} C_{jl}\sum_i Q_i X_{ji}\sum_k Q_k X_{lk} \\
&= \frac{1}{2}\sum_j \left(\overleftrightarrow{C}\overleftrightarrow{X}\vec{Q}\right)_j \sum_i Q_i X_{ji} \\
&= \frac{1}{2}\sum_j \left(\overleftrightarrow{M}\overleftrightarrow{X}\overleftrightarrow{\omega^2}\vec{Q}\right)_j \sum_i Q_i X_{ji} \\
&= \frac{1}{2}\sum_{j,k,l} M_j \delta_{jl} X_{lk}\omega_k^2 Q_k \sum_i Q_i X_{ji} \\
&= \frac{1}{2}\sum_{i,j,k} M_j X_{jk} X_{ji}\omega_k^2 Q_k Q_i = \frac{1}{2}\sum_{i,k}\delta_{ik}\omega_k^2 Q_k Q_i \\
&= \frac{1}{2}\sum_{i=1}^{3N}\omega_i^2 Q_i^2.
\end{aligned} \tag{A.6}$$

Inserting Eqs. (A.3) and (A.6) in Eq. (A.1) and choosing $V(\vec{R}^0)$ as the zero point for the potential energy, one obtains Eqs. (6.7).

Chapter 7

Polarons

7.1 The Question of Polaron Formation

In an inorganic semiconductor crystal, the excitation of a valence electron is normally described as a transition from the valence band (VB) to the conduction band (CB), and vice versa for the opposite process of recombination. Similarly, the injection or removal of an electron is described, respectively, by placing an electron in the CB (reduction) or by placing a hole in the VB (oxidation). This means that in inorganic semiconductor crystals, the creation of excess charges is described in terms of the already existing band structure without considering any new energy levels[1]. This assumption of the energy bands being the same whether they are occupied by an electron or not is known as the rigid band approximation (RBA). Since the band structure is a result of the periodicity of the crystal, the RBA implies that the deformation introduced by the excess charge is negligible or, equivalently, that the excess charge is completely delocalized over the in principle infinitely large crystal. The validity of the RBA is given by the strength of the coupling between an electron and the surrounding lattice. If this electron-phonon coupling is appreciable, an excess charge will deform the lattice around it, and the RBA is invalid.

Organic compounds are generally known to display a relatively large electron-phonon coupling, and in an organic molecule, the equilibrium geometry in an ionized state is in general substantially different from that in the ground state. For an organic semiconductor crystal like the polymer chains treated in this work, therefore, the question is whether the localization of an excess elementary charge is energetically favourable or not.

[1] In the case of doping, where electron-donating (n-type doping) or electron-accepting (p-type doping) impurity atoms are introduced, the donor or acceptor energy levels are typically close enough to the CB or VB, respectively, for all of the excess charges to be released into the bands due to thermal excitation. Even in this case, therefore, a description purely based on the band structure will often suffice for a first approximation.

Localization of an excess elementary charge corresponds to the formation of a polaron which is a self-localized, charged lattice deformation. Such a deformation will cause two localized polaron energy levels to split-off from the continuum band structure and move into the band gap, and this has a significant impact on the electrical and optical properties of the crystal: The excess charge will be transported as a polaron, which implies dragging the lattice deformation and concomitant polaron levels along, and the in-gap polaron levels will lead to optical subgap transitions.

If, on the other hand, the excess charge is delocalized, the excess charge per unit cell is zero, and the carrier is instead added to the band structure leading to unfilled bands and band-like, or metallic-like, charge conduction.

The question of polaron formation or not is thus seen to be a matter of importance, whether it arises in connection with the addition of excess charges through doping, or in connection with solar cells or light emitting diodes in which excess charges are created by photoexcitation or injected from electrodes, respectively.

7.1.1 Polaron Binding Energy

A polaron formed upon injection of an electron or a hole is called an electron polaron and a hole polaron, respectively.

The formation of an electron polaron is energetically favourable if the elastic energy needed to deform the lattice is smaller than the concomitant increase in electron affinity[2]. The in that case positive energy won by deforming the lattice and forming the polaron is called the polaron binding energy. The hole polaron binding energy is the decrease in ionization energy[3] minus the elastic deformation energy.

7.1.2 Bipolarons

Injection of two like elementary charges can lead to charge delocalization, the creation of two separate polarons, or to the creation of one strong, localized deformation called a bipolaron. In a material that favours polaron formation, bipolarons are favoured over polarons if the net energy gained by the increased deformation is larger than the Coulomb repulsion energy between the like charges. The bipolaron binding energy is defined in the same way as for polarons.

[2]The electron affinity is the energy won when the crystal receives an electron, i.e. the energy of the neutral crystal plus the energy of a free electron minus the energy of the negatively charged crystal.

[3]The ionization energy is the energy needed to remove an electron from the crystal.

7.2 Characteristics of Polarons and Bipolarons

Fig. 7.1 shows schematically the energy levels and their occupation, the induced subgap transitions and the charge and spin for electron and hole polarons and bipolarons. For symmetrical VB and CB, there are only three distinct transition energies in the polaron case. Notice that the energy levels of the bipolarons, which correspond to the largest deformation, have moved the furthest into the band gap. Also notice that charge conduction by bipolarons is an example of spinless charge conduction. In fact, it was the 1980 discovery of spinless charge conduction in polyacetylene [49] and poly(*para*-phenylene) [50] that challenged the until then dominating assumption of metallic-like conduction in doped conjugated polymers.

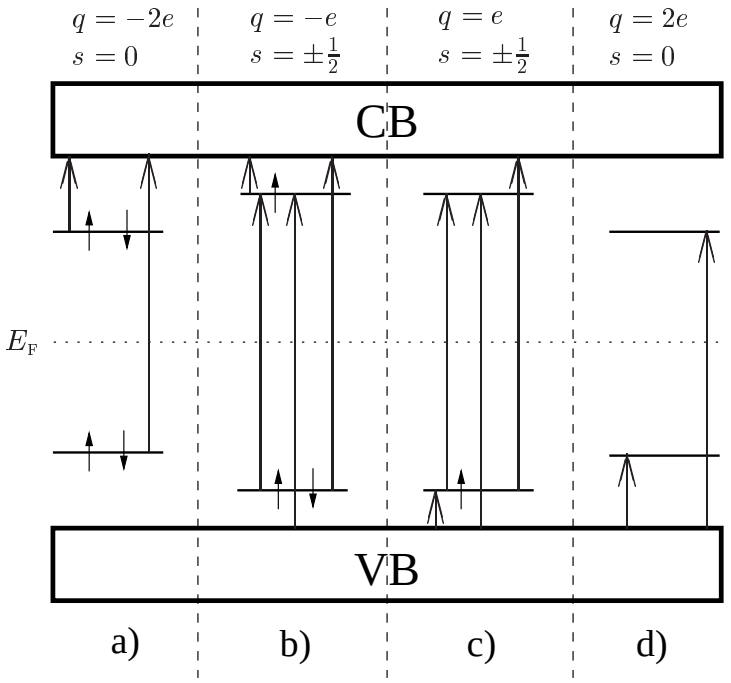

Figure 7.1: Energy levels and their occupation, induced subgap transitions and the charge q and spin s for a) electron bipolaron, b) electron polaron, c) hole polaron, and d) hole bipolaron. E_F is the Fermi energy.

7.3 Solitons

Due to its degenerate ground state, *trans*-polyacetylene (tPA) displays a speciel kind of spinless conduction that is due to so-called solitons [5].

One of the two ground states is shown in Fig. 10.1 and the other is obtained by interchanging the single and double bonds. The two different ground states

thus correspond to two different bond alternation domains. As shown in Fig. 7.2, a soliton is a domain wall separating two different domains[4]. From one side of the soliton, the double and single bonds become gradually longer and shorter, respectively, and at the center of the soliton, the bond length alternation is zero.

In a tPA chain characterized by one of the ground state configurations, solitons can only be created or destroyed in pairs (a so-called soliton-antisoliton pair), but single solitons can arise as isomerization defects is connection with cis- to trans-isomerization, and solitons will also necessarily arise in tPA segments containing an odd number of carbon atoms. Due to the degeneracy of the ground states, the soliton is in principle free to move along the chain, and the word "soliton" derives from the fact that the soliton preserves its shape as it propagates.

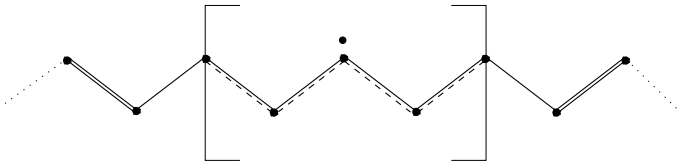

Figure 7.2: A neutral soliton on a *trans*-polyacetylene chain. The dot marks the center of the soliton, and the square brackets mark its extent which in reality is about 7 unit cells.

Due to the degeneracy of the ground states, the Coulomb repulsion makes tPA bipolarons unstable with respect to the creation of two charged solitons. In tPA, therefore, the predominant spinless charge conduction mechanism is due to solitons and not bipolarons. However, injection of one electron or hole will still lead to the creation of a polaron corresponding to a bound soliton-antisoliton pair with one soliton charged and the other one neutral. In this connection, the two polaron energy levels correspond to the bonding and anti-bonding combinations of the two mid-gap soliton levels.

The deformation associated with a soliton corresponds to the creation of a localized mid-gap electron energy level, and Fig. 7.3 shows the occupation of this soliton level for the three diffent types of solitons. Notice the reversed spin-charge relation which is the hallmark of a soliton. As in the case of polarons, soliton formation induces optical subgap transitions.

Note that while the existence of solitons requires degenerate ground states, polarons and bipolarons are generic.

[4] A soliton is also called a bond alternation defect or a phase kink in the conjugation sequence.

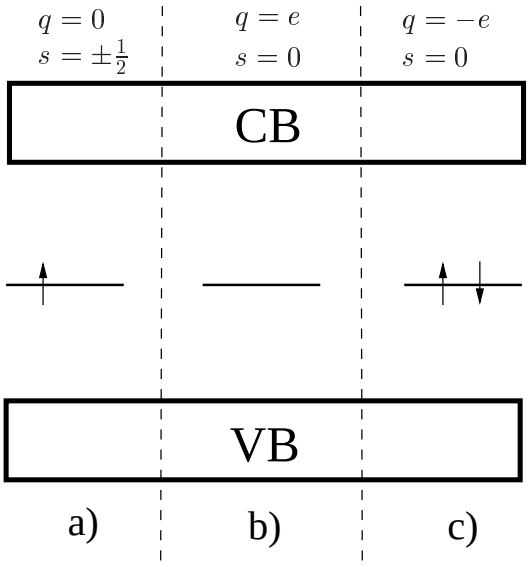

Figure 7.3: The occupation of the soliton energy level along with the charge q and spin s in case of a) a neutral soliton, b) a positively charged soliton, and c) a negatively charged soliton.

Part III

Linear Optical and Electro-optic Susceptibility

Chapter 8

Linear Optical Susceptibility

Pioneering the field of calculating the optical properties of conjugated polymers, in 1977 Cojan et al. [16] derived an analytic expression for the long-axis optical susceptibility of polyene chains, such as *trans*-polyacetylene (tPA). Later, Baeriswyl et al. [18] found an analytic expression for the imaginary part of the dielectric tensor of tPA, and Neumann and von Baltz [25] found an analytic expression for the real and imaginary parts of the long-axis dielectric function of tPA. In all three cases, the treated chains were parallel and infinite, and damping was not included.

To this date, no analytic expressions for the various susceptibilities associated with poly(*para*-phenylene) (PPP) have been derived. Such analytic expressions would expectedly increase the understanding of the optical properties of PPP and might ultimately serve to improve the application of PPP, e.g. in connection with polymer-based light emitting diodes, solar cells or photodetecting devices.

The purpose of this chapter is firstly to derive analytic closed-form expressions including damping for the complex linear optical susceptibilities of pristine, infinite, parallel and non-interacting tPA and PPP chains. For tPA the complete linear optical susceptibility tensor is derived, and for PPP the complex long-axis linear optical susceptibility and the imaginary part of the short-axis linear optical susceptibility are derived. Secondly, the purpose is to obtain through comparison a general expression for the complex long-axis linear optical susceptibility applicable to all conjugated polymers. The inclusion of damping, the calculations for PPP, and the comparison of the long-axis susceptibilities of an acetylene- and a phenyl-based polymer make the present results more general than the previous results in this field.

The analytic susceptibility expressions are obtained in the free-carrier dipole approximation using an orthogonal, nearest neighbour tight-binding model based on carbon π-electrons only. All excitonic and polaronic effects are disregarded. Polarons are described in Chap. 7 and treated in Chap. 11.

The results presented in this chapter have been published in Ref. [1].

8.1 The Model

The conjugated polymers are treated as planar molecules lying in the xy-plane with the polymer chain being oriented along the x-axis. The x- and y-axes are accordingly called the long-axis and short-axis, respectively. In such planar conjugated polymers, three of the four valence electrons of the carbon atoms form sp^2-hybridized bonds with the three neighbouring atoms in the xy-plane, while the fourth electron forms a delocalized π-orbital with p_z-symmetry. As the excitation energy is smaller for the π-electrons than for the sp^2-electrons, the π-electrons will be the main contributors to the low-photon-energy part of the optical susceptibility. Furthermore, since, due to symmetry, the π-orbitals couple to other π-orbitals only, the π-electrons can be treated seperately.

8.1.1 Band Structure

The π-band states are characterized by a band number a and a crystal wave number k and are therefore written $|ak\rangle$. In a tight-binding treatment applicable to the energy range in the vicinity of the band gap, the π-band states are expanded in the atomic $2p_z$-orbitals. Using the one-dimensional equivalents of Eqs. (2.28a) and (2.22) one has

$$\begin{aligned} |ak\rangle &= \frac{1}{\sqrt{N_{\mathrm{uc}}}} \sum_{n,p}^{N_{\mathrm{uc}},P} a_p(k) e^{iknl} |pn\rangle \qquad (8.1) \\ &, \quad k = \frac{2\pi}{N_{\mathrm{uc}} l} u \quad , \quad u \in \{0, 1, \ldots, N_{\mathrm{uc}} - 1\}, \end{aligned}$$

where l is the lattice constant, $|pn\rangle$ is the $2p_z$-orbital centered at the pth carbon atom in the nth unit cell, N_{uc} is the number of unit cells, and P is the number of atoms in the unit cell.

Inserting Eq. (8.1) in the energy eigenvalue equation

$$\hat{H}|ak\rangle = E_a(k)|ak\rangle \qquad (8.2)$$

and applying the atomic orbital $\langle qm|$ from the left yields

$$\sum_{n,p} e^{iknl} \left[\left\langle qm \left| \hat{H} \right| pn \right\rangle - E_a(k) \left\langle qm \middle| pn \right\rangle \right] a_p(k) = 0. \qquad (8.3)$$

Eq. (8.2) is thus seen to be equivalent to a $p \times p$-matrix eigenvalue problem.

In this chapter, wavefunction overlap will be disregarded[1]:

$$\langle qm|pn\rangle = \delta_{pq}\delta_{mn}, \qquad (8.4)$$

and only Hamilton matrix elements $\langle qm|\hat{H}|pn\rangle$ between nearest neighbours will be considered.

[1] According to Ref. [19], the correction to the optical susceptibility due to such overlaps is significant only for photon energies much greater than the band gap.

8.1.2 Electric Dipole Matrix Element

The x- and y-components of the electric dipole matrix element between valence and conduction bands v and c are given by

$$d^x_{\rm cv} = -e\langle {\rm c}k|x|{\rm v}k\rangle, \tag{8.5a}$$
$$d^y_{\rm cv} = -e\langle {\rm c}k|y|{\rm v}k\rangle, \tag{8.5b}$$

where $e > 0$ is the elementary charge.

As linear combinations of $2p_z$-orbitals, all valence and conduction band states $|{\rm v}k\rangle$ and $|{\rm c}k\rangle$ have odd parity in z, and therefore

$$d^z_{\rm cv} = 0. \tag{8.6}$$

Long-axis Electric Dipole Matrix Element

Using Eq. (8.2), the long-axis electric dipole matrix element can be written

$$\begin{aligned} d^x_{\rm cv}(k) &= -e\frac{\left\langle {\rm c}k\left|\hat{H}x - x\hat{H}\right|{\rm v}k\right\rangle}{E_{\rm c}(k) - E_{\rm v}(k)} \\ &= \frac{-e}{E_{\rm cv}(k)N_{\rm uc}}\sum_{n,p,m,q} {\rm c}^*_q(k){\rm v}_p(k)e^{ik(n-m)l}\left\langle qm\left|\hat{H}x - x\hat{H}\right|pn\right\rangle, \end{aligned} \tag{8.7}$$

where $E_{\rm cv} = E_{\rm c} - E_{\rm v}$ is the excitation energy.

The matrix element $\langle qm|x\hat{H}|pn\rangle$ is found by inserting the completeness relation $\sum_{n,p}|pn\rangle\langle pn| = 1$ between x and $\hat{H}$ and using the fact that for x_{qm} being the x-coordinate of the qth atom in the mth unit cell, due to symmetry one has

$$\left\langle qm\left|x - \frac{x_{qm} + x_{q'm'}}{2}\right|q'm'\right\rangle = 0. \tag{8.8}$$

In this manner, one finds

$$\begin{aligned} \left\langle qm\left|x\hat{H}\right|pn\right\rangle &= \sum_{m',q'}\langle qm|\,x\,|q'm'\rangle\left\langle q'm'\left|\hat{H}\right|pn\right\rangle \\ &= \sum_{m',q'}\frac{x_{qm} + x_{q'm'}}{2}\langle qm|q'm'\rangle\left\langle q'm'\left|\hat{H}\right|pn\right\rangle \\ &= x_{qm}\left\langle qm\left|\hat{H}\right|pn\right\rangle, \end{aligned} \tag{8.9a}$$

$$\left\langle qm\left|\hat{H}x\right|pn\right\rangle = x_{pn}\left\langle qm\left|\hat{H}\right|pn\right\rangle. \tag{8.9b}$$

Inserting Eqs. (8.9) in Eq. (8.7), one obtains

$$\begin{aligned} d^x_{\rm cv}(k) &= \frac{-e}{E_{\rm cv}(k)N_{\rm uc}}\sum_{n,p,m,q}{\rm c}^*_q(k){\rm v}_p(k)e^{ik(n-m)l}(x_{pn} - x_{qm})\left\langle qm\left|\hat{H}\right|pn\right\rangle \\ &= \frac{-e}{E_{\rm cv}(k)}\sum_{n,p,q}{\rm c}^*_q(k){\rm v}_p(k)e^{iknl}(x_{pn} - x_{q0})\left\langle q0\left|\hat{H}\right|pn\right\rangle, \end{aligned} \tag{8.10}$$

where it has been used that with periodic boundary conditions, all $N_{\rm uc}$ unit cells are identical.

Short-axis Electric Dipole Matrix Element

$d^y_{\rm cv}(k)$ is obtained by replacing x with y in Eq. (8.10).

8.1.3 Linear Optical Susceptibility

Since $d^z_{\rm cv} = 0$, the linear optical susceptibility tensor is given by

$$\overleftrightarrow{\chi}^{(1)}(\omega) = \begin{bmatrix} \chi^{(1)}_{xx} & \chi^{(1)}_{xy} & 0 \\ \chi^{(1)}_{yx} & \chi^{(1)}_{yy} & 0 \\ 0 & 0 & 0 \end{bmatrix}, \tag{8.11}$$

where, for this case of real electric dipole matrix elements, the components are given by Eq. (3.36):

$$\chi^{(1)}_{ij}(\omega) \;=\; \frac{2}{\pi\varepsilon_0 A}\sum_{\rm c,v}\int_{-\frac{\pi}{l}}^{\frac{\pi}{l}} d^i_{\rm cv}(k)d^j_{\rm cv}(k)\frac{E_{\rm cv}(k)}{E^2_{\rm cv}(k)-\hbar^2\Omega^2}\,dk. \tag{8.12}$$

8.2 *Trans*-polyacetylene

The *trans*-polyacetylene (tPA) chain is shown in Fig. 8.1 with the bond lengths obtained from Ref. [23].

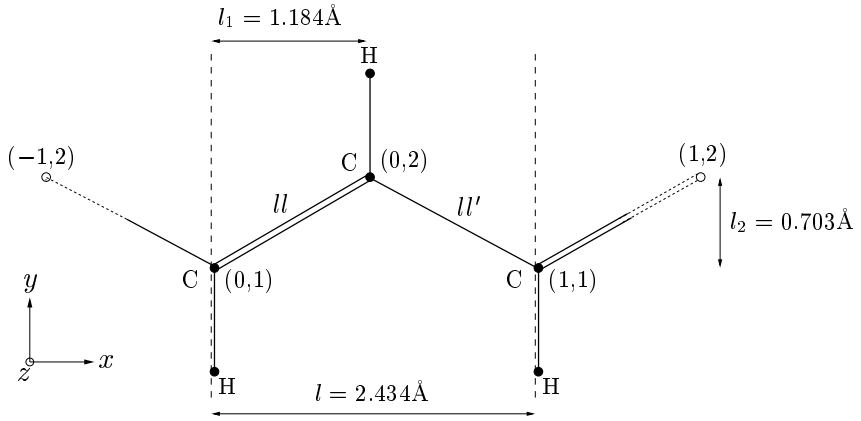

Figure 8.1: The *trans*-polyacetylene chain. The coordinates (n, p) indicate carbon atom p in the nth unit cell. The bond lengths are $ll = 1.377$Å and $ll' = 1.434$Å.

8.2.1 Band Structure

For tPA, Eq. (8.3) corresponds to the following matrix eigenvalue problem:

$$\begin{bmatrix} -E(k) & e^{-ikl}\beta' + \beta \\ \beta + e^{ikl}\beta' & -E(k) \end{bmatrix} \begin{pmatrix} a_1(k) \\ a_2(k) \end{pmatrix} = \begin{pmatrix} 0 \\ 0 \end{pmatrix}, \tag{8.13}$$

where β and β' are the Hamilton matrix elements along ll and ll', respectively, and where the energy of a carbon $2p_z$-orbital is chosen as the zero point of the energy $\left(\langle pn|\hat{H}|pn\rangle \equiv 0\right)$.

Nontrivial solutions to Eq. (8.13) are found for

$$\begin{vmatrix} -E(k) & e^{-ikl}\beta' + \beta \\ \beta + e^{ikl}\beta' & -E(k) \end{vmatrix} = 0, \tag{8.14}$$

corresponding to

$$E_{\mathrm{c}}(k) = +\sqrt{\beta^2 + \beta'^2 + 2\beta\beta'\cos(kl)}, \tag{8.15a}$$

$$E_{\mathrm{v}}(k) = -\sqrt{\beta^2 + \beta'^2 + 2\beta\beta'\cos(kl)}, \tag{8.15b}$$

and

$$E_{\mathrm{cv}}(k) = E_{\mathrm{c}}(k) - E_{\mathrm{v}}(k) = 2\sqrt{\beta^2 + \beta'^2 + 2\beta\beta'\cos(kl)}. \tag{8.16}$$

The π-electron band structure is shown in Fig. 8.2.

Inserting $E_{\mathrm{c}}(k)$ and $E_{\mathrm{v}}(k)$ in Eq. (8.13) and solving for the eigenvector $\vec{a}(k)$, one obtains

$$\vec{\mathrm{c}}(k) = \begin{pmatrix} \frac{1}{\sqrt{2}} \\ \frac{W}{\sqrt{2}} \end{pmatrix}, \quad \vec{\mathrm{v}}(k) = \begin{pmatrix} \frac{1}{\sqrt{2}} \\ -\frac{W}{\sqrt{2}} \end{pmatrix}, \quad W = \frac{E_{\mathrm{c}}}{e^{-ikl}\beta' + \beta}. \tag{8.17}$$

8.2.2 Electric Dipole Matrix Element

Long-axis Electric Dipole Matrix Element

Inserting Eq. (8.17) in Eq. (8.10), summing over nearest neighbours, and making the approximation $l_1 \simeq l/2$ yields

$$\begin{aligned} d^x_{\mathrm{cv}}(k) &= \frac{-e}{E_{\mathrm{cv}}(k)} \sum_{n,p,q} \mathrm{c}^*_q(k)\mathrm{v}_p(k)e^{iknl}\left[nl + (p-q)l_1\right] \left\langle q0 \left| \hat{H} \right| pn \right\rangle \\ &= \frac{-e}{E_{\mathrm{cv}}(k)} \frac{1}{2}\Big[(l-l_1)\beta'\left(e^{ikl}W^* + e^{-ikl}W\right) - l_1\beta\left(W^* + W\right)\Big] \\ &= \frac{-2e}{E^2_{\mathrm{cv}}(k)}\Big[(l-l_1)\beta'^2 - l_1\beta^2 + (l-2l_1)\beta'\beta\cos(kl)\Big] \\ &\simeq \frac{-el}{E^2_{\mathrm{cv}}(k)}\left(\beta'^2 - \beta^2\right). \end{aligned} \tag{8.18}$$

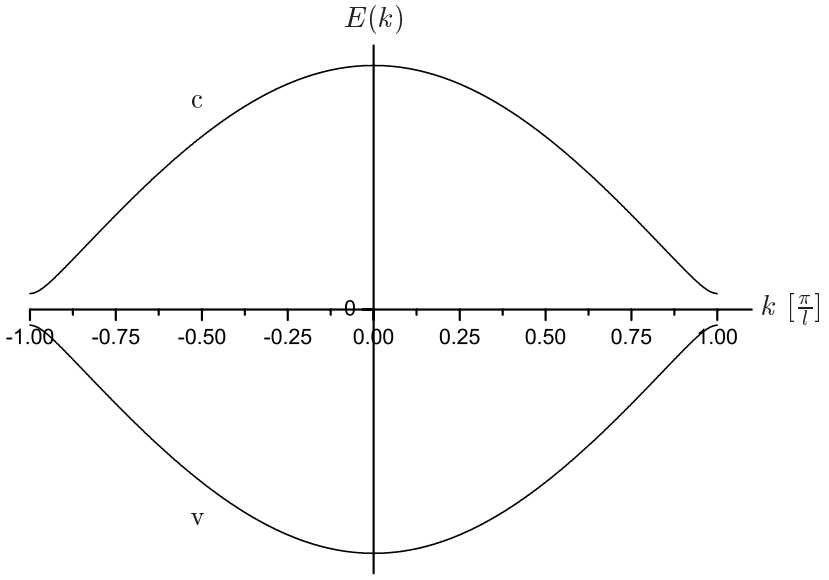

Figure 8.2: The π-electron band structure of *trans*-polyacetylene.

In connection with Eq. (8.18) it should be noted that tPA is degenerate in the sense that Fig. 8.1 might just as well have been flipped 180° about the y-axis. This would lead to the transformation $\beta \to \beta'$ and thus to a change of sign in Eq. (8.18).

Introducing the band gap

$$E_{\mathrm{g}} = E_{\mathrm{cv}}\left(\frac{\pi}{l}\right) = 2|\beta - \beta'| \tag{8.19}$$

and the π-band width

$$E_0 = E_{\mathrm{cv}}(0) = 2|\beta + \beta'|, \tag{8.20}$$

Eq. (8.18) yields

$$d^x_{\mathrm{cv}}(k) = \frac{el E_{\mathrm{g}} E_0}{4E^2_{\mathrm{cv}}(k)}. \tag{8.21}$$

A plot of $|d^x_{\mathrm{cv}}(k)|^2$ is shown in Fig. 8.3.

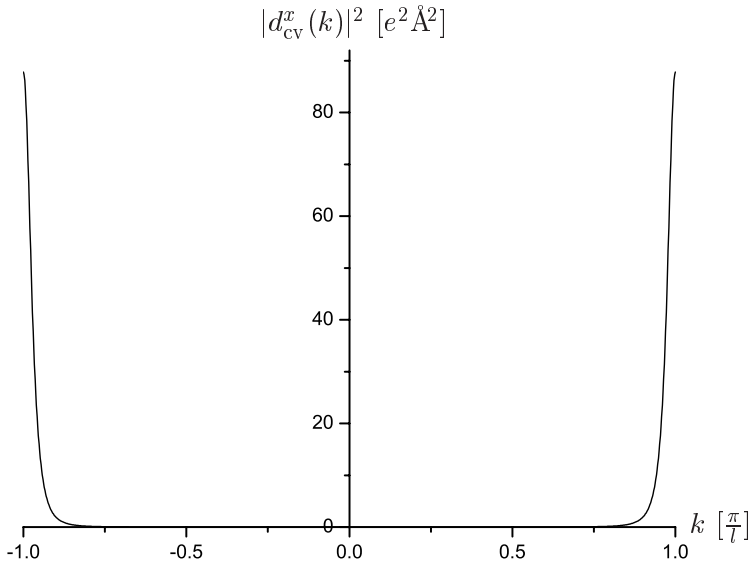

Figure 8.3: The absolute square of the long-axis electric dipole matrix element of *trans*-polyacetylene.

Short-axis Electric Dipole Matrix Element

One obtains

$$\begin{aligned} d^y_{\rm cv}(k) &= \frac{-e}{E_{\rm cv}(k)} \sum_{n,p,q} {\rm c}^*_q(k) {\rm v}_p(k) e^{iknl} \left[(p-q)l_2\right] \left\langle q0 \left| \hat{H} \right| pn \right\rangle \\ &= \frac{2el_2}{E^2_{\rm cv}(k)} \Big[\beta'^2 + \beta^2 + 2\beta'\beta\cos(kl)\Big] \\ &= \frac{el_2}{2}. \end{aligned} \tag{8.22}$$

8.2.3 Linear Optical Susceptibility

Long-axis Linear Optical Susceptibility

Inserting Eq. (8.21) in Eq. (8.12), one has

$$\chi^{(1)}_{xx,{\rm tPA}}(\omega) = \frac{e^2 l^2 E_{\rm g}^2 E_0^2}{4\pi\varepsilon_0 A} \int_0^{\pi/l} \frac{1}{E^3_{\rm cv}(k)} \left(\frac{1}{E^2_{\rm cv}(k) - \hbar^2\Omega^2} \right) dk. \tag{8.23}$$

Since, from Eq. (8.16) one has

$$k = \frac{1}{l} \arccos\left(\frac{E^2_{\rm cv}(k) - 4\beta^2 - 4\beta'^2}{8\beta\beta'} \right) \tag{8.24}$$

and thus

$$dk = \frac{dk}{dE_{\rm cv}^2}\frac{dE_{\rm cv}^2}{dE_{\rm cv}}dE_{\rm cv} = -\frac{2}{l}\frac{E_{\rm cv}}{\sqrt{\left(8\beta\beta'\right)^2 - \left(E_{\rm cv}^2 - 4\beta^2 - 4\beta'^2\right)^2}}\,dE_{\rm cv}$$
$$= -\frac{2}{l}\frac{E_{\rm cv}}{\sqrt{(E_{\rm cv}^2 - E_{\rm g}^2)(E_0^2 - E_{\rm cv}^2)}}\,dE_{\rm cv}, \qquad (8.25)$$

Eq. (8.23) can be written as the following integral over $E_{\rm cv}$:

$$\chi^{(1)}_{xx,{\rm tPA}}(\omega) = \frac{e^2 l E_{\rm g}^2 E_0^2}{2\pi\varepsilon_0 A}\int_{E_{\rm g}}^{E_0}\frac{1}{E_{\rm cv}^2(E_{\rm cv}^2 - \hbar^2\Omega^2)}\frac{dE_{\rm cv}}{\sqrt{(E_{\rm cv}^2 - E_{\rm g}^2)(E_0^2 - E_{\rm cv}^2)}}. \qquad (8.26)$$

Evaluating Eq. (8.26) as shown in App. A, one obtains the following result for the long-axis linear optical susceptibility of *trans*-polyacetylene:

$$\chi^{(1)}_{xx,{\rm tPA}}(\omega) = \frac{e^2 l}{2\pi\varepsilon_0 A}\frac{E_0^2}{E_{\rm g}\hbar^2\Omega^2}\left[\frac{E_{\rm g}^2}{E_{\rm g}^2 - \hbar^2\Omega^2}\,\Pi\left(\frac{E_{\rm g}^2 - E_0^2}{E_{\rm g}^2 - \hbar^2\Omega^2}, \frac{E_{\rm g}^2 - E_0^2}{E_{\rm g}^2}\right) - \Pi\left(\frac{E_{\rm g}^2 - E_0^2}{E_{\rm g}^2}, \frac{E_{\rm g}^2 - E_0^2}{E_{\rm g}^2}\right)\right], \qquad (8.27)$$

where $\Pi(n,k)$ is the Complete Elliptic Integral of the Third Kind. In this work, the MATHEMATICA definition of elliptic integrals has been adopted and reproduced in Eq. (A.3), and MATHEMATICA has been used to evaluate the various expressions. It has been verified by numerical integration that Eqs. (8.27) and (8.26) are in agreement.

The result of Eq. (8.27) is the equivalent of equation 4.4 in Ref. [25] with the present result generalized to include damping.

Plots in the vicinity of the band gap of the real part $\chi^{(1)'}_{xx,{\rm tPA}}(\omega)$ and imaginary part $\chi^{(1)''}_{xx,{\rm tPA}}(\omega)$ of Eq. (8.27) are shown in Fig. 8.4. The band gap $E_{\rm g}$ and the π-band width E_0 are set to their experimental values $E_{\rm g} = 1.9eV$[2] and $E_0 = 12.8eV$ [22] corresponding to $\beta = -3.7eV$ and $\beta' = -2.7eV$. The damping parameter $\hbar\gamma = 0.2eV$ is obtained by fitting to the experimental curves in Ref. [22]. According to Ref. [6], the cross sectional area of tPA is $A = 15.5\text{Å}^2$. In addition to the band gap resonance shown in Fig. 8.4, there is a weak resonance around E_0 also.

[2]This band gap corresponds to a wavelength of $653nm$ which is the wavelength of visible light in the red part of the spectrum.

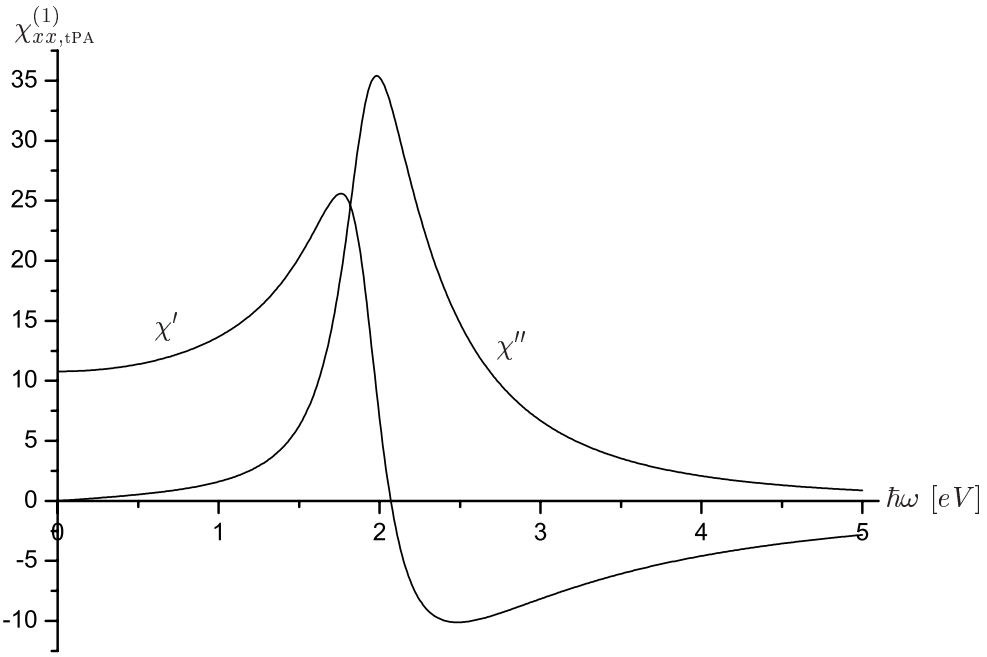

Figure 8.4: The real part χ' and imaginary part χ'' of the long-axis linear optical susceptibility of *trans*-polyacetylene for $E_\mathrm{g} = 1.9eV$, $E_0 = 12.8eV$, $\hbar\gamma = 0.2eV$, and $A = 15.5\text{Å}^2$.

Approximate Linear Optical Susceptibility Expression For $\hbar\omega \ll E_0$, Eq. (8.26) can be approximated as

$$\chi^{(1)}_{xx,\mathrm{tPA}}(\omega) \simeq \frac{e^2 l E_\mathrm{g}^2 E_0}{2\pi\varepsilon_0 A} \int_{E_\mathrm{g}}^{\infty} \frac{1}{E_\mathrm{cv}^2 (E_\mathrm{cv}^2 - \hbar^2\Omega^2)} \frac{dE_\mathrm{cv}}{\sqrt{E_\mathrm{cv}^2 - E_\mathrm{g}^2}} \tag{8.28}$$

leading to

$$\chi^{(1)}_{xx,\mathrm{tPA}}(\omega) \simeq \frac{e^2 l E_\mathrm{g}^2 E_0}{2\pi\varepsilon_0 A \hbar^2\Omega^2} \left[\frac{\arcsin\left(\frac{\hbar\Omega}{E_\mathrm{g}}\right)}{\hbar\Omega\sqrt{E_\mathrm{g}^2 - \hbar^2\Omega^2}} - \frac{1}{E_\mathrm{g}^2} \right]. \tag{8.29}$$

As an evaluation of this approximation, Fig. 8.5 shows a plot of Eq. (8.29) together with a plot of Eq. (8.27). The approximation is seen to be excellent in the vicinity of the band gap.

Notice that comparison of Eqs. (8.27) and (8.29) yields

$$\Pi\left(\frac{E_\mathrm{g}^2 - E_0^2}{E_\mathrm{g}^2 - \hbar^2\Omega^2}, \frac{E_\mathrm{g}^2 - E_0^2}{E_\mathrm{g}^2}\right) \simeq \frac{E_\mathrm{g}}{E_0} \frac{\sqrt{E_\mathrm{g}^2 - \hbar^2\Omega^2}}{\hbar\Omega} \arcsin\left(\frac{\hbar\Omega}{E_\mathrm{g}}\right) \quad , \ \hbar\omega \ll E_0, \tag{8.30a}$$

$$\Pi\left(\frac{E_\mathrm{g}^2 - E_0^2}{E_\mathrm{g}^2}, \frac{E_\mathrm{g}^2 - E_0^2}{E_\mathrm{g}^2}\right) \simeq \frac{E_\mathrm{g}}{E_0}. \tag{8.30b}$$

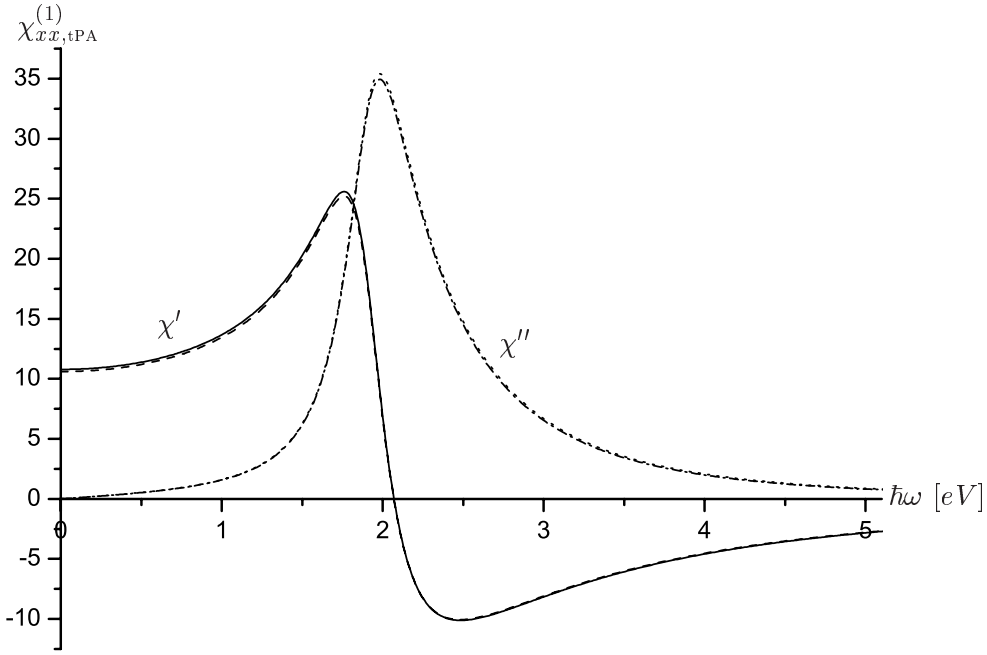

Figure 8.5: A comparison of Eqs. (8.29) and (8.27) with parameters as in Fig. 8.4.

Effective Mass Approximation In the effective mass approximation (EMA), the band structure is given by the following parabolic expansion in the vicinity of the band gap:

$$E_{\mathrm{cv}}(k) \simeq E_{\mathrm{g}} + \frac{\hbar^2 k'^2}{2\mu} \quad , \quad k' = k - \frac{\pi}{l}, \tag{8.31}$$

where μ is the reduced mass given by

$$\begin{aligned} \mu &\equiv \frac{\hbar^2}{\left.\frac{d^2 E_{\mathrm{cv}}(k)}{dk^2}\right|_{k=\frac{\pi}{l}}} \\ &= 4\frac{\hbar^2}{l^2}\frac{E_{\mathrm{g}}}{E_0^2 - E_{\mathrm{g}}^2} \\ &\simeq 0.06 m_0, \end{aligned} \tag{8.32}$$

where $m_0 = 9.109 \cdot 10^{-31} kg$ is the electron rest mass.

Writing the electric dipole matrix element in terms of the momentum matrix

element $p^x_{\rm cv}(k)$, one has

$$\begin{aligned} d^x_{\rm cv}(k) &= \frac{-e}{E_{\rm cv}(k)} \left\langle {\rm c}k \left| \left(\hat{H}x - x\hat{H} \right) \right| {\rm v}k \right\rangle \\ &= \frac{e\hbar^2}{2m_0 E_{\rm cv}(k)} \left\langle {\rm c}k \left| \left(\frac{\partial^2}{\partial x^2}x - x\frac{\partial^2}{\partial x^2} \right) \right| {\rm v}k \right\rangle \\ &= \frac{ie\hbar}{m_0 E_{\rm cv}(k)} \left\langle {\rm c}k \left| \frac{\hbar}{i}\frac{\partial}{\partial x} \right| {\rm v}k \right\rangle \\ &= \frac{ie\hbar}{m_0 E_{\rm cv}(k)} p^x_{\rm cv}(k). \end{aligned} \tag{8.33}$$

In the constant momentum matrix element approximation (CMMEA), one assumes that $p^x_{\rm cv}(k)$ is constant and equal to its value at the band gap:

$$\begin{aligned} p^x_{\rm cv}(k) \simeq p^x_{\rm cv}\left(\frac{\pi}{l}\right) &= \frac{m_0 E_{\rm cv}\left(\frac{\pi}{l}\right)}{ie\hbar}\, d^x_{\rm cv}\left(\frac{\pi}{l}\right) \\ &= \frac{m_0 l}{4i\hbar} E_0. \end{aligned} \tag{8.34}$$

From Fig. 8.6, which shows a plot of $|p^x_{\rm cv}(k)|^2$ together with $|p^x_{\rm cv}(\pi/l)|^2$, it can be seen that the CMMEA is a significant approximation.

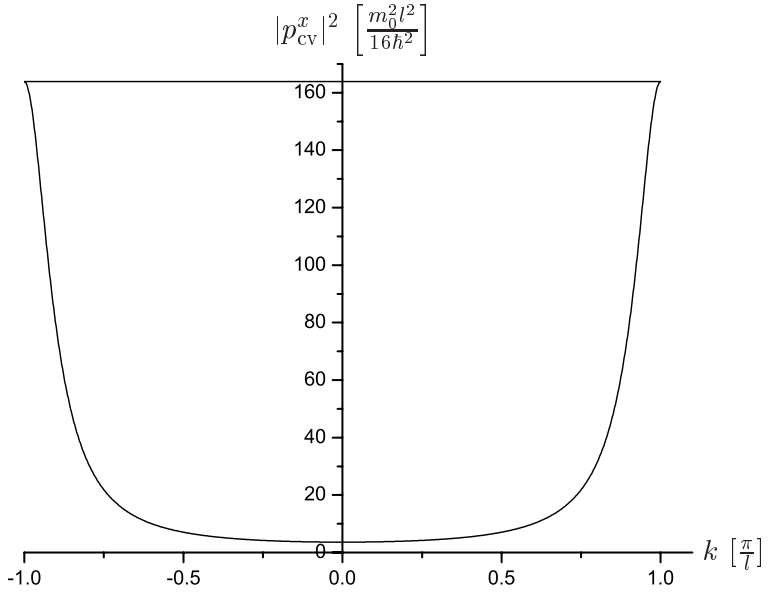

Figure 8.6: The absolute square of the long-axis momentum matrix element of *trans*-polyacetylene together with the constant used in the CMMEA.

As shown in App. B, the EM-CMMEA linear optical susceptibility $\tilde{\chi}^{(1)}_{xx,{\rm tPA}}(\omega)$

is given by

$$\tilde{\chi}^{(1)}_{xx,\mathrm{tPA}}(\omega) \;=\; \frac{e^2 l^2 \sqrt{2\mu}}{16\hbar\varepsilon_0 A}\frac{E_0^2}{\hbar^2\Omega^2}\left[\frac{1}{\sqrt{E_\mathrm{g}+\hbar\Omega}}+\frac{1}{\sqrt{E_\mathrm{g}-\hbar\Omega}}-\frac{2}{\sqrt{E_\mathrm{g}}}\right], \quad (8.35)$$

which is in agreement with Ref. [51].

Fig. 8.7 shows a plot of the EM-CMMEA linear optical susceptibility $\tilde{\chi}^{(1)}_{xx,\mathrm{tPA}}(\omega)$ together with $\chi^{(1)}_{xx,\mathrm{tPA}}(\omega)$. Inspection of Fig. 8.7 shows that $\chi^{(1)}_{xx,\mathrm{tPA}}(\omega)$ approaches

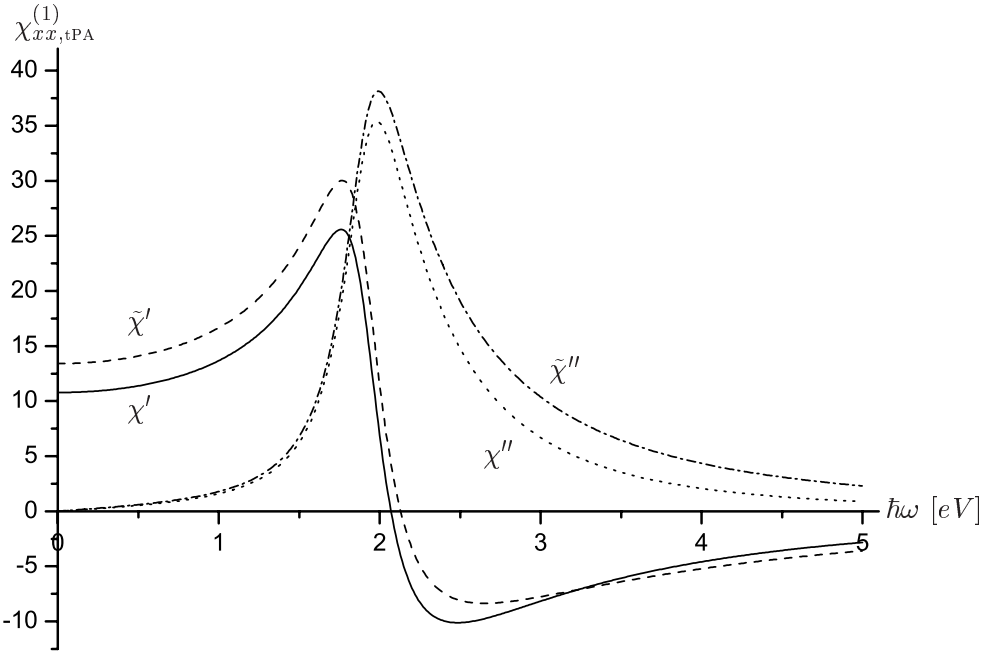

Figure 8.7: The EM-CMMEA linear optical susceptibility $\tilde{\chi}$ together with the ordinary linear optical susceptibility χ of *trans*-polyacetylene for $E_g = 1.9eV$, $E_0 = 12.8eV$, $\hbar\gamma = 0.2eV$, and $A = 15.5\text{Å}^2$.

zero faster than $\tilde{\chi}^{(1)}_{xx,\mathrm{tPA}}(\omega)$. This is due to the fact that in CMMEA, the factor $1/E^2_{\mathrm{cv}}(k) \sim 1/\hbar^2\omega^2$ in the electric dipole matrix element is treated as a constant.

Zero Band Gap Limit The tPA chain is distorted in the sense that there is a bond length alternation $ll \neq ll'$ leading to $\beta \neq \beta'$. As can be seen from Eq. (8.19), this so-called Peierls distortion introduces a band gap E_g in the band structure making tPA a semiconductor. This section treats the more or less hypothetical case of an undistorted and thus metallic tPA chain.

In the limit $E_{\rm g} \to 0$, Eq. (8.27) yields

$$\begin{aligned}
\lim_{E_{\rm g}\to 0}\chi^{(1)}_{xx,{\rm tPA}} &= \frac{e^2 l}{2\pi\varepsilon_0 A}\frac{E_0^2}{\hbar^2\Omega^2}\lim_{E_{\rm g}\to 0}\left[\int_0^1 \frac{-\frac{E_{\rm g}}{\hbar^2\Omega^2}dx}{\left(1-\frac{E_0^2}{\hbar^2\Omega^2}x^2\right)\sqrt{(1-x^2)\left(1+\frac{E_0^2}{E_{\rm g}^2}x^2\right)}}\right.\\
&\qquad\left. - \int_0^1 \frac{\frac{1}{E_{\rm g}}dx}{\left(1+\frac{E_0^2}{E_{\rm g}^2}x^2\right)^{3/2}\sqrt{1-x^2}}\right]\\
&= \frac{e^2 l}{2\pi\varepsilon_0 A}\frac{E_0^2}{\hbar^2\Omega^2}\lim_{E_{\rm g}\to 0}\left[\frac{-E_0}{2\hbar^2\Omega^2}\int_{-1}^1 \frac{\frac{E_{\rm g}^2}{E_0^2}}{\left(\frac{E_{\rm g}^2}{E_0^2}+x^2\right)^{3/2}}\frac{\left(\frac{E_{\rm g}^2}{E_0^2}+x^2\right)dx}{\left(1-\frac{E_0^2}{\hbar^2\Omega^2}x^2\right)\sqrt{1-x^2}}\right.\\
&\qquad\left. - \frac{1}{2E_0}\int_{-1}^1 \frac{\frac{E_{\rm g}^2}{E_0^2}}{\left(\frac{E_{\rm g}^2}{E_0^2}+x^2\right)^{3/2}}\frac{dx}{\sqrt{1-x^2}}\right]\\
&= -\frac{e^2 l}{2\pi\varepsilon_0 A}\frac{E_0}{\hbar^2\Omega^2}, \qquad (8.36)
\end{aligned}$$

since

$$\lim_{E_{\rm g}\to 0}\frac{\frac{E_{\rm g}^2}{E_0^2}}{\left(\frac{E_{\rm g}^2}{E_0^2}+x^2\right)^{3/2}} = 2\delta(x), \qquad (8.37)$$

where $\delta(x)$ is the Dirac delta function.

A plot of the linear optical susceptibility of tPA in the zero band gap limit is shown in Fig. 8.8. The figure shows that the present result is well-behaved in the metallic limit.

At this point it may be noted that Eq. (8.36) is in accordance with the Drude theory of metals [52] according to which

$$\chi^{(1)}_{xx}(\omega) = -\frac{\rho e^2}{\varepsilon_0\Omega^2\langle m^*\rangle}, \qquad (8.38)$$

where $\rho = \frac{2}{Al}$ is the π-electron density, and where

$$\begin{aligned}
\langle m^*\rangle &= \frac{\hbar^2}{\frac{l}{2\pi}\int_{-\pi/l}^{\pi/l}\frac{d^2E_{\rm v}(k)}{dk^2}dk}\quad,\quad E_{\rm v} = -\frac{E_0}{2}\cos\left(\frac{kl}{2}\right),\\
&= \frac{4\pi\hbar^2}{E_0 l^2} \qquad (8.39)
\end{aligned}$$

is an effective mass averaged over all valence states.

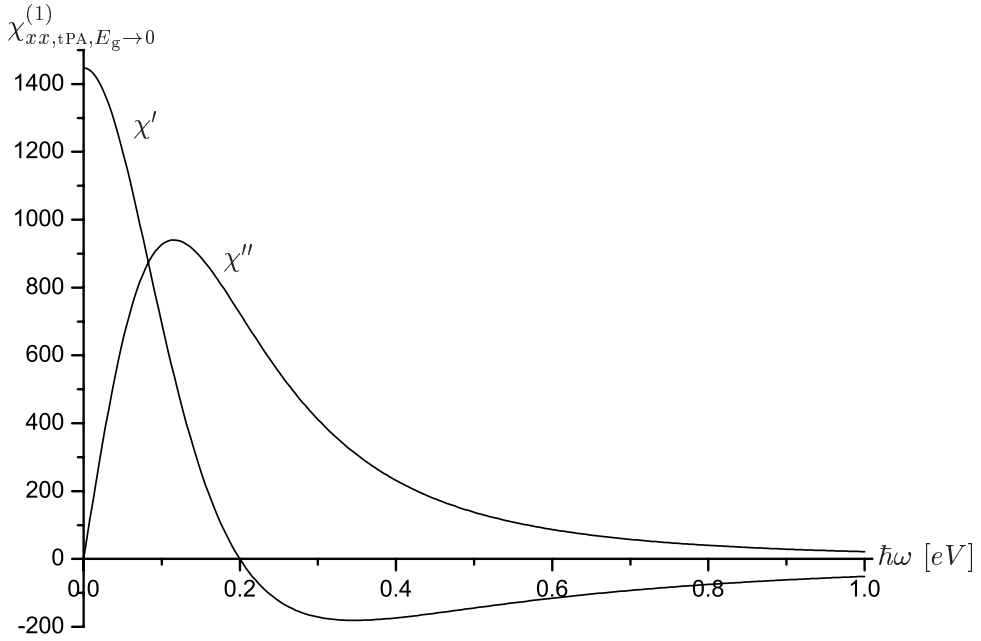

Figure 8.8: The real part χ' and imaginary part χ'' of the linear optical susceptibility of *trans*-polyacetylene in the limit $E_\mathrm{g} \to 0$ for $E_0 = 12.8eV$, $\hbar\gamma = 0.2eV$, and $A = 15.5\text{Å}^2$.

Short-axis Linear Optical Susceptibility

As shown in App. C, the following result is obtained for the short-axis linear optical susceptibility of *trans*-polyacetylene:

$$\chi^{(1)}_{yy,\mathrm{tPA}}(\omega) = \frac{2e^2 l_2^2}{\pi\varepsilon_0 lA}\frac{1}{E_\mathrm{g}}\left[\frac{\hbar^2\Omega^2}{E_\mathrm{g}^2-\hbar^2\Omega^2}\,\Pi\left(\frac{E_\mathrm{g}^2-E_0^2}{E_\mathrm{g}^2-\hbar^2\Omega^2},\frac{E_\mathrm{g}^2-E_0^2}{E_\mathrm{g}^2}\right)+F\left(\frac{E_\mathrm{g}^2-E_0^2}{E_\mathrm{g}^2}\right)\right], \tag{8.40}$$

where $F(k)$ is the Complete Elliptic Integral of the First Kind. A plot of $\chi^{(1)}_{yy,\mathrm{tPA}}(\omega)$ is shown in Fig. 8.9.

Off-diagonal Linear Optical Susceptibility

As shown in App. D, one obtains

$$\begin{aligned}\chi^{(1)}_{xy,\mathrm{tPA}}(\omega) &= \chi^{(1)}_{yx,\mathrm{tPA}}(\omega)\\ &= \frac{\pm l_2 e^2}{\pi\varepsilon_0 A}\frac{E_0}{E_\mathrm{g}^2-\hbar^2\Omega^2}\,\Pi\left(\frac{E_\mathrm{g}^2-E_0^2}{E_\mathrm{g}^2-\hbar^2\Omega^2},\frac{E_\mathrm{g}^2-E_0^2}{E_\mathrm{g}^2}\right),\end{aligned} \tag{8.41}$$

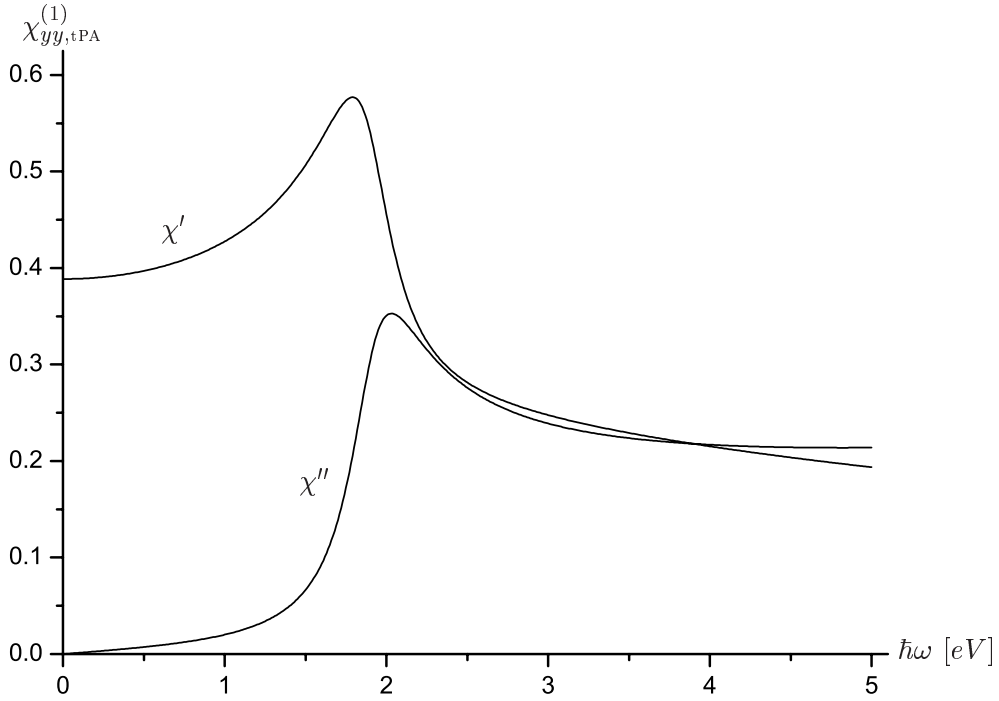

Figure 8.9: The real part χ' and imaginary part χ'' of the short-axis linear optical susceptibility of *trans*-polyacetylene for $E_{\mathrm{g}} = 1.9eV$, $E_0 = 12.8eV$, $\hbar\gamma = 0.2eV$, and $A = 15.5\text{Å}^2$.

where the different signs apply to the two degenerate states mentioned in the comment following Eq. (8.18) with the plus sign applying to the configuration of Fig. 8.1. A plot of $\chi^{(1)}{}_{xy,\mathrm{tPA}}(\omega)$ is shown in Fig. 8.10.

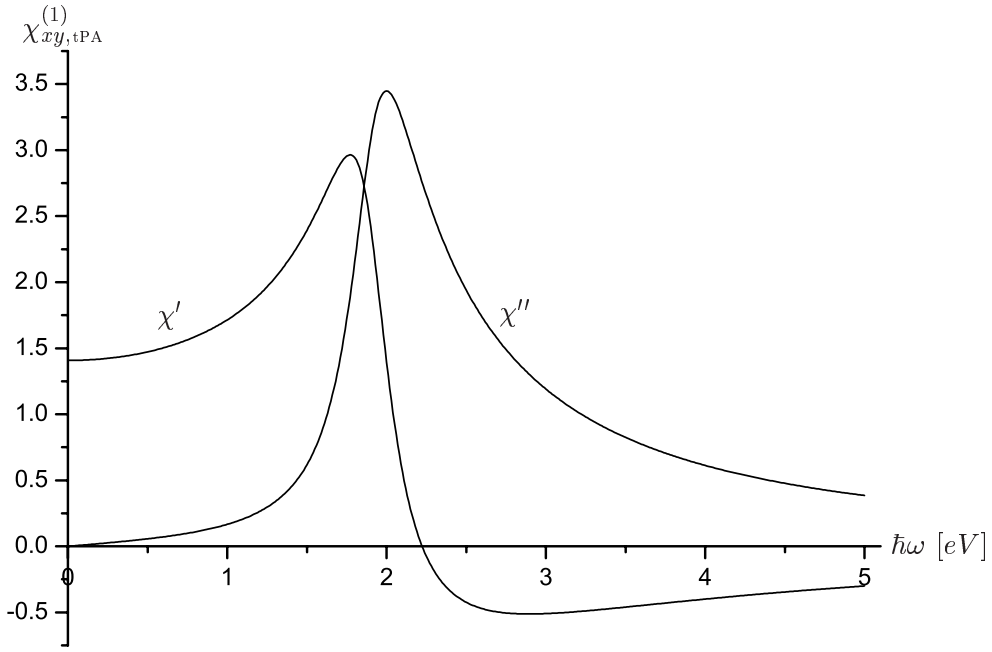

Figure 8.10: The real part χ' and imaginary part χ'' of the off-diagonal linear optical susceptibility of *trans*-polyacetylene for $E_{\mathrm{g}} = 1.9eV$, $E_0 = 12.8eV$, $\hbar\gamma = 0.2eV$ and $A = 15.5\text{Å}^2$.

Note that the following relation applies [18]:

$$\chi^{(1)''}_{xy,\mathrm{tPA}}(\omega) = \pm\sqrt{\chi^{(1)''}_{xx,\mathrm{tPA}}(\omega)\ \chi^{(1)''}_{yy,\mathrm{tPA}}(\omega)}. \tag{8.42}$$

8.3 Poly(*para*-phenylene)

The poly(*para*-phenylene) (PPP) chain is shown in Fig. 8.11 with structure parameters from Ref. [31]. Note that adjacent phenyl rings in an isolated PPP chain are twisted approximately 26° with respect to each other [31]. In this work, this torsion is disregarded, and the PPP chain is treated as a planar molecule with π-orbitals coupling to other π-orbitals only, since this assumption simplifies the derivations considerably.

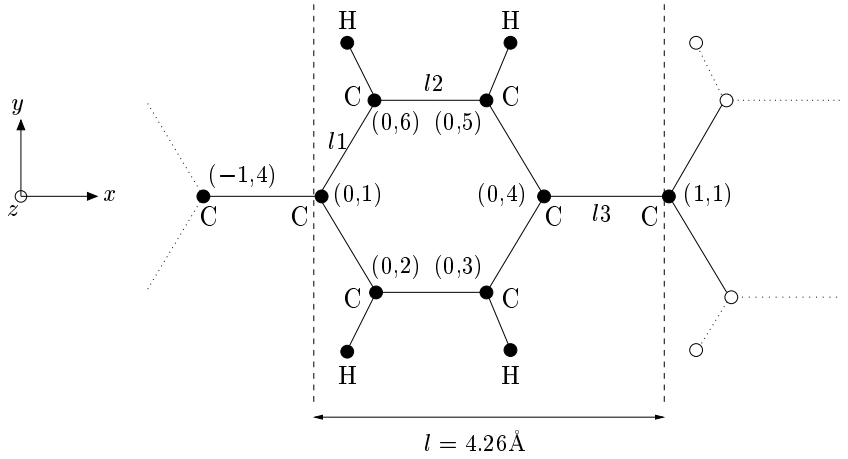

Figure 8.11: The poly(*para*-phenylene) chain. The coordinates (n, p) indicate carbon atom p in the nth unit cell. Bond lengths are $l_1 = 1.407$Å, $l_2 = 1.388$Å, and $l_3 = 1.465$Å, and angles are $\angle 123 = 121°$ and $\angle 612 = 118°$.

8.3.1 Band Structure

Using the same value β for all Hamilton matrix elements, one obtains

$$\begin{bmatrix} -E(k) & \beta & 0 & e^{-ikl}\beta & 0 & \beta \\ \beta & -E(k) & \beta & 0 & 0 & 0 \\ 0 & \beta & -E(k) & \beta & 0 & 0 \\ e^{ikl}\beta & 0 & \beta & -E(k) & \beta & 0 \\ 0 & 0 & 0 & \beta & -E(k) & \beta \\ \beta & 0 & 0 & 0 & \beta & -E(k) \end{bmatrix} \begin{pmatrix} a_1(k) \\ a_2(k) \\ a_3(k) \\ a_4(k) \\ a_5(k) \\ a_6(k) \end{pmatrix} = \begin{pmatrix} 0 \\ 0 \\ 0 \\ 0 \\ 0 \\ 0 \end{pmatrix}. \quad (8.43)$$

Since the xz-plane is a plane of symmetry for the PPP chain, all eigenstates can be chosen with definite parity in y. The 6×6-matrix eigenvalue problem of Eq. (8.43) can therefore be decomposed into two smaller eigenvalue problems for which the eigenstates have even and odd parity in y, respectively.

Eigenstates of Even Parity

For eigenstates of even parity, one has the following eigenvector components:

$$a_1,\ a_2 = a_6,\ a_3 = a_5,\ a_4, \quad (8.44)$$

which leads to the following matrix eigenvalue problem:

$$\begin{bmatrix} -E(k) & 2\beta & 0 & e^{-ikl}\beta \\ \beta & -E(k) & \beta & 0 \\ 0 & \beta & -E(k) & \beta \\ e^{ikl}\beta & 0 & 2\beta & -E(k) \end{bmatrix} \begin{pmatrix} a_1(k) \\ a_2(k) \\ a_3(k) \\ a_4(k) \end{pmatrix} = \begin{pmatrix} 0 \\ 0 \\ 0 \\ 0 \end{pmatrix}. \quad (8.45)$$

Eq. (8.45) has the following four nontrivial solutions:

$$E(k) = \pm|\beta|\sqrt{3 \pm \sqrt{8}\cos\left(\frac{kl}{2}\right)}, \tag{8.46}$$

with corresponding eigenvectors

$$\vec{a}_{\rm e}(k) = \frac{1}{2}\begin{pmatrix} \frac{(\varrho^2-1)e^{-ikl}+2}{\varrho^3-3\varrho} \\ \frac{1+e^{-ikl}}{\varrho^2-3} \\ \frac{\varrho^2-2+e^{-ikl}}{\varrho^3-3\varrho} \\ 1 \\ \frac{\varrho^2-2+e^{-ikl}}{\varrho^3-3\varrho} \\ \frac{1+e^{-ikl}}{\varrho^2-3} \end{pmatrix} \tag{8.47a}$$

$$, \quad \varrho = \frac{E(k)}{|\beta|} \tag{8.47b}$$

Note that Eq. (8.47a) shows that

$$c_1 = -v_1 \ , \ c_2 = v_2 \ , \ c_3 = -v_3. \tag{8.48}$$

Eigenstates of Odd Parity

In this case, one has

$$a_1 = a_4 = 0, \ a_2 = -a_6, \ a_3 = -a_5 \tag{8.49}$$

and thus

$$\begin{bmatrix} -E(k) & \beta \\ \beta & -E(k) \end{bmatrix}\begin{pmatrix} a_2(k) \\ a_3(k) \end{pmatrix} = \begin{pmatrix} 0 \\ 0 \end{pmatrix}, \tag{8.50}$$

which has the two nontrivial solutions

$$E(k) = \pm|\beta| \tag{8.51}$$

with corresponding eigenvectors

$$\vec{c}_{\rm o}(k) = \frac{1}{2}\begin{pmatrix} 0 \\ 1 \\ -1 \\ 0 \\ 1 \\ -1 \end{pmatrix}, \tag{8.52a}$$

$$\vec{\rm v}_{\rm o}(k) = \frac{1}{2}\begin{pmatrix} 0 \\ 1 \\ 1 \\ 0 \\ -1 \\ -1 \end{pmatrix}. \tag{8.52b}$$

The π-electron band structure is shown in Fig. 8.12.

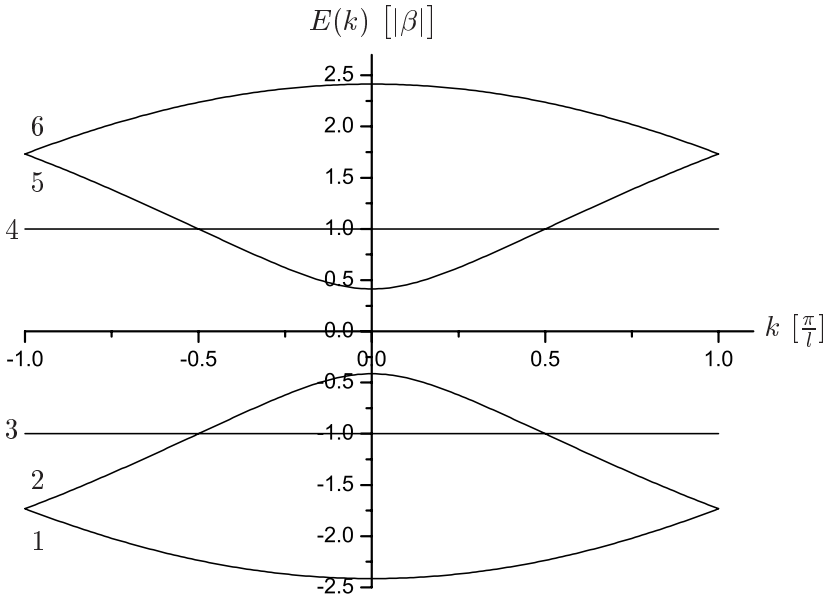

Figure 8.12: The π-electron band structure of poly(*para*-phenylene) with the bands numbered from 1 to 6. The bands 1,2,5,6 and 3,4 correspond to eigenstates with even and odd parity in y, respectively.

8.3.2 Electric Dipole Matrix Element

Long-axis Electric Dipole Matrix Element

Making the approximation

$$\angle 123 \simeq \angle 612 \simeq 120^\circ, \tag{8.53a}$$

$$l_1 \simeq l_2 \simeq l_3 \simeq l/3 = 1.42\text{Å}, \tag{8.53b}$$

Eq. (8.10) yields

$$d^x_{\rm cv}(k) = \frac{e|\beta|l}{3E_{\rm cv}}\left[c_1^*\left(-v_4e^{-ikl}+\frac{v_2}{2}+\frac{v_6}{2}\right)+c_2^*\left(-\frac{v_1}{2}+v_3\right)+c_3^*\left(-v_2+\frac{v_4}{2}\right)\right.$$
$$\left.+\,c_4^*\left(-\frac{v_3}{2}-\frac{v_5}{2}+v_1e^{ikl}\right)+c_5^*\left(-v_6+\frac{v_4}{2}\right)+c_6^*\left(-\frac{v_1}{2}+v_5\right)\right]. \tag{8.54}$$

Inspection of Eq. (8.54) shows that $d^x_{\rm cv}(k)$ is zero for transitions between states of different parity[3]. Furthermore, a more careful inspection shows that $d^x_{\rm cv}(k)$ is

[3]The dipole operator x is an even function in y, so when $\langle$c| and |v$\rangle$ have different parity in y, $\langle \text{c}|x|\text{v}\rangle = 0$.

also zero for the transitions $1 \to 5$ and $2 \to 6$. The only transitions contributing to the linear optical susceptibility are thus

$$1 \to 6 \quad , \quad 2 \to 5 \quad , \quad 3 \to 4, \tag{8.55}$$

where $1 \to 6$ and $2 \to 5$ are even-even transitions and $3 \to 4$ is an odd-odd transition.

Even-even Transitions Using Eqs. (8.44) and (8.48) in Eq. (8.54), one obtains

$$\begin{aligned} d^x_{\mathrm{cv,ee}}(k) &= \frac{-e|\beta|l}{3E_{\mathrm{cv}}} \frac{1+\cos(kl)}{\varrho_{\mathrm{c}}^3 - 3\varrho_{\mathrm{c}}} \\ &= \frac{-el}{24} \frac{\varrho_{\mathrm{c}}^2 - 3}{\varrho_{\mathrm{c}}^2} \qquad (8.56a) \\ &, \quad \varrho_{\mathrm{c}} = \frac{E_{\mathrm{c}}(k)}{|\beta|}. \qquad (8.56b) \end{aligned}$$

Plots of $|d^x_{61}(k)|^2$ and $|d^x_{52}(k)|^2$ are shown in Figs. 8.13 and 8.14, respectively.

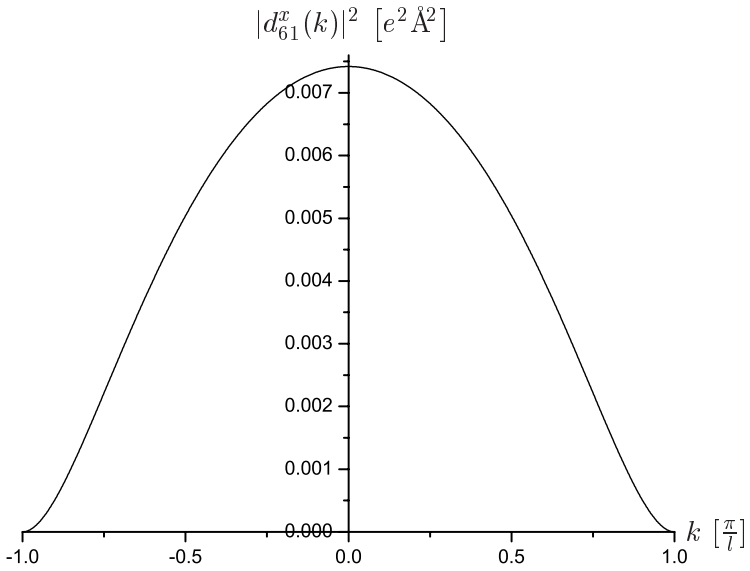

Figure 8.13: The absolute square of the long-axis electric dipole matrix element of the $1 \to 6$-transition in poly(*para*-phenylene).

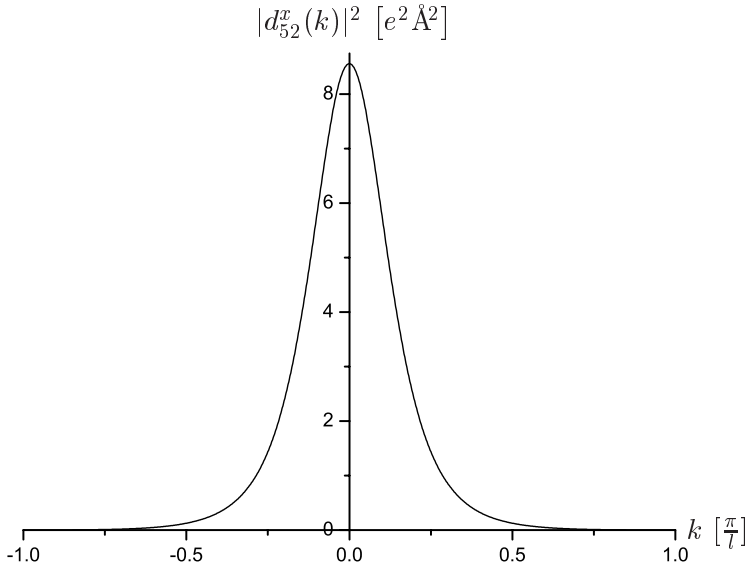

Figure 8.14: The absolute square of the long-axis electric dipole matrix element of the $2 \to 5$-transition in poly(*para*-phenylene).

Odd-odd Transitions Using Eqs. (8.52) in Eq. (8.54), one obtains

$$\begin{aligned} d^x_{\mathrm{cv,oo}}(k) &= \frac{e|\beta|l}{3E_{\mathrm{cv}}} \\ &= \frac{el}{6}. \end{aligned} \tag{8.57}$$

Short-axis Electric Dipole Matrix Element

The y-part of Eq. (8.10) yields

$$\begin{aligned} d^y_{\mathrm{cv}}(k) = \frac{\sqrt{3}e|\beta|l}{6E_{\mathrm{cv}}} \Big[& c^*_1(-v_2+v_6) + c^*_2(v_1) + c^*_3(v_4) \\ & + c^*_4(-v_3+v_5) + c^*_5(-v_4) + c^*_6(-v_1) \Big], \end{aligned} \tag{8.58}$$

which shows that the contributing transitions are

$$1 \to 4 \quad , \quad 2 \to 4 \quad , \quad 3 \to 5 \quad , \quad 3 \to 6, \tag{8.59}$$

where $1 \to 4$, $2 \to 4$ and $3 \to 5$, $3 \to 6$ are even-odd and odd-even transitions, respectively[4].

[4] $\langle \mathrm{c}|y|\mathrm{v}\rangle = 0$ unless $\langle \mathrm{c}|$ and $|\mathrm{v}\rangle$ have different parity in y

Even-odd Transitions Inserting Eq. (8.52a) in Eq. (8.58) and using Eq. (8.47a), one has

$$\begin{aligned} |d^y_{\mathrm{cv,oe}}(k)|^2 &= \frac{e^2\beta^2 l^2}{12E^2_{\mathrm{cv}}}|v_1 - v_4|^2 \\ &= \frac{e^2\beta^2 l^2}{12E^2_{\mathrm{cv}}}\frac{(\varrho_v+1)^2(\varrho_v^2-2\varrho_v-1)}{-8\varrho_v} \\ &= \frac{e^2 l^2}{96}\frac{(\varrho_v+1)^2(\varrho_v^2-2\varrho_v-1)}{-\varrho_v(1-\varrho_v)^2} \\ &= \frac{e^2 l^2}{96}\left[2\frac{(\varrho_v+1)^2}{\varrho_v(\varrho_v-1)^2} - \frac{(\varrho_v+1)^2}{\varrho_v}\right]. \end{aligned} \tag{8.60}$$

Odd-even Transitions Inserting Eq. (8.52b) in Eq. (8.58), one has

$$\begin{aligned} |d^y_{\mathrm{cv,eo}}(k)|^2 &= \frac{e^2\beta^2 l^2}{12E^2_{\mathrm{cv}}}|-c_1^* - c_4^*|^2 \\ &= \frac{e^2 l^2}{96}\left[\frac{(1-\varrho_{\mathrm{c}})^2}{\varrho_{\mathrm{c}}} - 2\frac{(1-\varrho_{\mathrm{c}})^2}{\varrho_{\mathrm{c}}(1+\varrho_{\mathrm{c}})^2}\right]. \end{aligned} \tag{8.61}$$

Fig. (8.15) shows plots of $|d^y_{\mathrm{cv}}(k)|^2$.

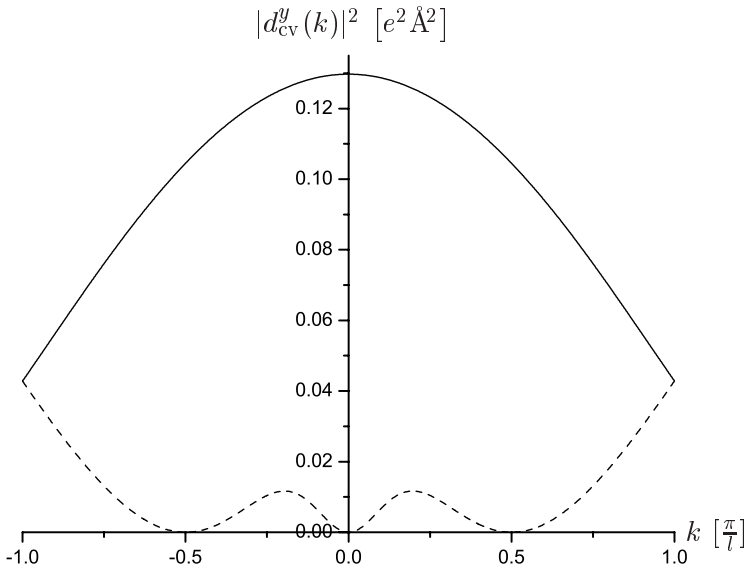

Figure 8.15: The absolute square of the short-axis electric dipole matrix element of poly(*para*-phenylene). The solid line shows $|d^y_{41}(k)|^2 = |d^y_{63}(k)|^2$, and the broken line shows $|d^y_{42}(k)|^2 = |d^y_{53}(k)|^2$.

8.3.3 Linear Optical Susceptibility

Long-axis Linear Optical Susceptibility

Inserting Eqs. (8.56a) and (8.57) in Eq. (8.12), one has

$$\chi^{(1)}_{xx,\mathrm{PPP}} = \frac{e^2|\beta|l^2}{72\pi\varepsilon_0 A}\int_0^{\pi/l}\left[\left(\frac{\varrho_6^2-3}{\varrho_6^2}\right)^2\frac{\varrho_6}{4\beta^2\varrho_6^2-\hbar^2\Omega^2}+\left(\frac{\varrho_5^2-3}{\varrho_5^2}\right)^2\frac{\varrho_5}{4\beta^2\varrho_5^2-\hbar^2\Omega^2}\right]dk + \frac{e^2 l}{9\varepsilon_0 A}\frac{2|\beta|}{4\beta^2-\hbar^2\Omega^2}. \tag{8.62}$$

Introducing the normalized band gap ϱ_g and normalized π-band width ϱ_0:

$$\varrho_\mathrm{g} = E_\mathrm{g}/|\beta| = 2\sqrt{3-\sqrt{8}}, \tag{8.63a}$$

$$\varrho_0 = E_0/|\beta| = 2\sqrt{3+\sqrt{8}}, \tag{8.63b}$$

and evaluating as shown in App. E, one obtains the following for the long-axis linear optical susceptibility of poly(*para*-phenylene):

$$\chi^{(1)}_{xx,\mathrm{PPP}}(\omega) = \frac{e^2 l}{4\pi\varepsilon_0 A}\frac{E_0^2}{E_\mathrm{g}\hbar^2\Omega^2}\left[\frac{\hbar^2\Omega^2}{9E_0^2}\,F\left(\frac{E_\mathrm{g}^2-E_0^2}{E_\mathrm{g}^2}\right) + \frac{\left(E_\mathrm{g}-\frac{\hbar^2\Omega^2}{3E_0}\right)^2}{E_\mathrm{g}^2-\hbar^2\Omega^2}\,\Pi\left(\frac{E_\mathrm{g}^2-E_0^2}{E_\mathrm{g}^2-\hbar^2\Omega^2},\frac{E_\mathrm{g}^2-E_0^2}{E_\mathrm{g}^2}\right) - \Pi\left(\frac{E_\mathrm{g}^2-E_0^2}{E_\mathrm{g}^2},\frac{E_\mathrm{g}^2-E_0^2}{E_\mathrm{g}^2}\right)\right] + \frac{e^2 l}{9\varepsilon_0 A}\frac{2|\beta|}{4\beta^2-\hbar^2\Omega^2}, \tag{8.64}$$

which can be approximated using Eqs. (8.30).

Plots of $\chi^{(1)'}_{xx,\mathrm{PPP}}(\omega)$ and $\chi^{(1)''}_{xx,\mathrm{PPP}}(\omega)$ are shown in Fig. 8.16. The band gap is set to its experimental value of $E_\mathrm{g} = 2.9eV$[5] [22] corresponding to $\beta = -3.5eV$ and $E_0 = 16.9eV$, and by fit to the experimental curves of Ref. [22], the damping parameter is set to $\hbar\gamma = 0.03eV$. The cross sectional area is $A = 21.5\text{Å}^2$ [30].

Short-axis Linear Optical Susceptibility

As shown in App. F, one obtains the following approximate expression for the imaginary part of the short-axis linear optical susceptibility of poly(*para*-phenylene):

[5] This band gap corresponds to a wavelength of $428nm$ which is the wavelength of visible light in the blue part of the spectrum.

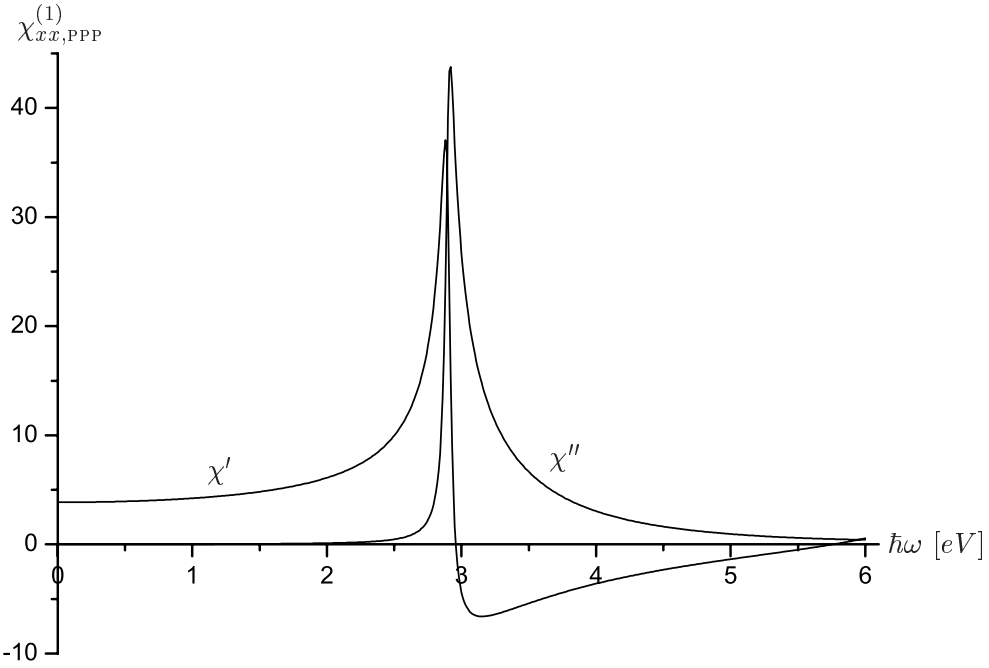

Figure 8.16: The real part χ' and imaginary part χ'' of the long-axis linear optical susceptibility of poly(*para*-phenylene) for $E_{\mathrm{g}} = 2.9eV$, $\hbar\gamma = 0.03eV$, and $A = 21.5\text{Å}^2$.

$$\chi^{(1)''}_{yy,\mathrm{PPP}}(\omega) \simeq \frac{e^2|\beta|l}{3\pi\varepsilon_0 A}\frac{\left(1-z^2\right)^2-2(1-z)^2}{z(1+z)}\,\mathrm{Im}\Bigg\{$$
$$\frac{1}{\hbar\Omega}\Bigg[\frac{4\left(|\beta|-\hbar\Omega\right)^2}{E_\mathrm{g}\left(E_\mathrm{g}^2-4\left(|\beta|-\hbar\Omega\right)^2\right)}\,\Pi\Bigg(\frac{E_\mathrm{g}^2-E_0^2}{E_\mathrm{g}^2-4\left(|\beta|-\hbar\Omega\right)^2},\frac{E_\mathrm{g}^2-E_0^2}{E_\mathrm{g}^2}\Bigg)$$
$$-\pi\frac{|\beta|-\hbar\Omega}{\sqrt{E_0^2-4\left(|\beta|-\hbar\Omega\right)^2}\sqrt{E_\mathrm{g}^2-4\left(|\beta|-\hbar\Omega\right)^2}}$$
$$-\frac{4\left(|\beta|+\hbar\Omega\right)^2}{E_\mathrm{g}\left(E_\mathrm{g}^2-4\left(|\beta|+\hbar\Omega\right)^2\right)}\,\Pi\Bigg(\frac{E_\mathrm{g}^2-E_0^2}{E_\mathrm{g}^2-4\left(|\beta|+\hbar\Omega\right)^2},\frac{E_\mathrm{g}^2-E_0^2}{E_\mathrm{g}^2}\Bigg)$$
$$-\pi\frac{\left(|\beta|+\hbar\Omega\right)\sqrt{E_\mathrm{g}^2+4\left(|\beta|+\hbar\Omega\right)^2}}{\sqrt{E_0^2-4\left(|\beta|+\hbar\Omega\right)^2}\left(E_\mathrm{g}^2-4\left(|\beta|+\hbar\Omega\right)^2\right)^{3/2}}\Bigg]\Bigg\}$$
$$,\quad z=\begin{cases}\frac{\varrho_\mathrm{g}}{2} & \text{for } \hbar\omega<|\beta|\left(1+\frac{\varrho_\mathrm{g}}{2}\right)\\ \frac{\hbar\omega-|\beta|}{|\beta|} & \text{for } |\beta|\left(1+\frac{\varrho_\mathrm{g}}{2}\right)\le\hbar\omega\le|\beta|\left(1+\frac{\varrho_0}{2}\right)\\ \frac{\varrho_0}{2} & \text{for } \hbar\omega>|\beta|\left(1+\frac{\varrho_0}{2}\right)\end{cases}. \qquad (8.65)$$

Fig. 8.17 shows a plot of Eq. (8.65) together with a numerical evaluation of Eq. (F.1). The figure shows a resonance at $\hbar\omega\approx|\beta|(1+\varrho_\mathrm{g}/2)\simeq 4.95eV$ which corresponds to the $2\rightarrow 4$- and $3\rightarrow 5$-transitions. Another resonance lies at $\hbar\omega\approx|\beta|(1+\varrho_0/2)\simeq 11.95eV$ corresponding to the $1\rightarrow 4$- and $3\rightarrow 6$-transitions.

8.4 Comparison

A significant advantage of the closed-form analytic expressions in Eqs. (8.27) and (8.64), e.g. over the expressions in Eqs. (8.26) and (8.62), is that certain similarities are readily identified. Hence, comparison of Eqs. (8.27) and (8.64) shows that the E_g- and E_0-dependence of the Π-function parameters is identical. Furthermore, for photon energies well below $3E_0$, the factors preceding the Π-integrals are approximately identical. The differences between the two expressions are a factor of 2 and two additional terms in the PPP-expression. As for the additional term containing the F-integral, the preceding factor is approximately zero for $\hbar\omega\ll 3E_0$, and the odd-transition contribution is significant for photon energies in the vicinity of $2|\beta|=7eV$ only. The factor of 2 in favour of tPA has the following origin: According to Eqs. (8.15) and (8.46), the cosine arguments of the tPA- and PPP-expressions for $E(k)$ are kl and $\frac{kl}{2}$, respectively, which yields a factor of 2 in favour of PPP in the density-of-states $\frac{dk}{dE}$. Furthermore, comparison of Eqs. (8.21) and (8.56a) yields a factor of 4 in favour of tPA in the expressions

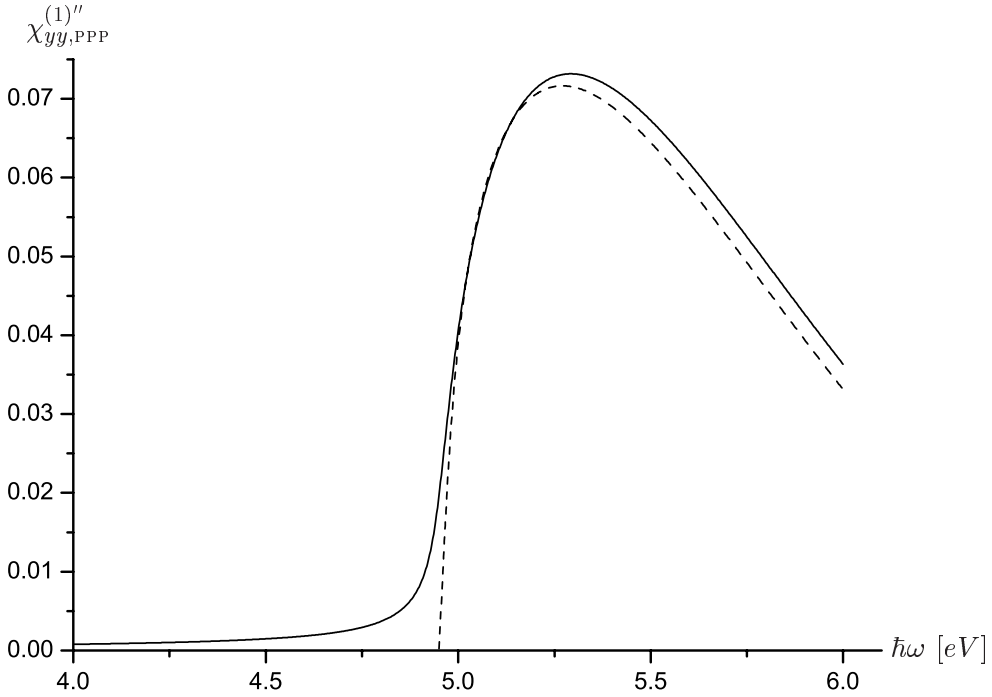

Figure 8.17: The full line shows a numerical evaluation of Eq. (F.1), while the dashed line shows the approximate result in Eq. (8.65).

for $|d^x_{\rm cv}|^2$:

$$d^x_{cv,\rm tPA} = \frac{el}{4}\frac{E_{\rm g}E_0}{E^2_{\rm cv}}, \tag{8.66a}$$

$$d^x_{cv,\rm PPP} = \frac{-el}{24}\frac{E^2_{\rm cv}-12\beta^2}{E^2_{\rm cv}} = \frac{-el}{24}\frac{E^2_{\rm cv}-3E_{\rm g}E_0}{E^2_{\rm cv}} \simeq \frac{el}{8}\frac{E_{\rm g}E_0}{E^2_{\rm cv}} \quad , \quad \hbar\omega \ll E_0. \tag{8.66b}$$

8.5 Conclusion

In this chapter, the linear optical susceptibility tensor of *trans*-polyacetylene and the long-axis linear optical susceptibility as well as the imaginary part of the short-axis linear optical susceptibility of poly(*para*-phenylene) have been derived. Even though the structures of these two conjugated polymers are widely different, remarkably similar results have been obtained. Hence, the present work suggests that for photon energies in the vicinity of the band gap, the long-axis linear optical susceptibility of a general conjugated polymer can be written

$$\chi^{(1)}_{xx,\rm CP}(\omega) = K\frac{e^2 l}{\pi\varepsilon_0 A}\frac{E_0^2}{E_{\rm g}\hbar^2\Omega^2}\left[\frac{E_{\rm g}^2}{E_{\rm g}^2-\hbar^2\Omega^2}\,\Pi\left(\frac{E_{\rm g}^2-E_0^2}{E_{\rm g}^2-\hbar^2\Omega^2},\frac{E_{\rm g}^2-E_0^2}{E_{\rm g}^2}\right) - \Pi\left(\frac{E_{\rm g}^2-E_0^2}{E_{\rm g}^2},\frac{E_{\rm g}^2-E_0^2}{E_{\rm g}^2}\right)\right] \quad , \quad \hbar\Omega = \hbar\omega + i\hbar\gamma, \tag{8.67}$$

where γ is the damping parameter, and where $E_{\rm g}$, E_0, A, l and K are material dependent constants. The band gap $E_{\rm g}$ and the π-band width E_0 characterize the band structure, the cross sectional area A and the lattice constant l characterize the size of the unit cell, and K is given by the density-of-states and the size of the long-axis electric dipole matrix element. For *trans*-polyacetylene and poly(*para*-phenylene), $K^{\rm tPA} = \frac{1}{2}$ and $K^{\rm PPP} = \frac{1}{4}$.

It is hoped that the distinct way in which Eq. (8.67) depends on the above-mentioned parameters serves to clarify the influence of these parameters on the optical properties of conjugated polymers.

Appendices

A Long-axis Linear Optical Susceptibility of tPA

Introducing the following shorthand notation:

$$a^2 = E_0^2 - E_\mathrm{g}^2, \tag{A.1a}$$

$$x^2 = \frac{E_\mathrm{cv}^2 - E_\mathrm{g}^2}{E_0^2 - E_\mathrm{g}^2}, \tag{A.1b}$$

$$S = \frac{e^2 l E_0^2 E_\mathrm{g}^2}{2\pi\varepsilon_0 A}, \tag{A.1c}$$

one has the following for Eq. (8.26):

$$\begin{aligned}
\chi^{(1)}_{xx,\mathrm{tPA}} &= S\int_0^1 \frac{1}{a^2x^2+E_\mathrm{g}^2}\frac{1}{a^2x^2+E_\mathrm{g}^2-\hbar^2\Omega^2}\frac{1}{\sqrt{a^2x^2(a^2-a^2x^2)}}\frac{a^2x}{\sqrt{E_\mathrm{g}^2+a^2x^2}}dx \\
&= S\int_0^1 \frac{1}{a^2x^2+E_\mathrm{g}^2}\frac{1}{a^2x^2+E_\mathrm{g}^2-\hbar^2\Omega^2}\frac{dx}{\sqrt{(1-x^2)(E_\mathrm{g}^2+a^2x^2)}} \\
&= \frac{S}{E_\mathrm{g}}\int_0^1 \left(\frac{\frac{1}{E_\mathrm{g}^2\hbar^2\Omega^2-\hbar^4\Omega^4}}{1+\frac{a^2}{E_\mathrm{g}^2-\hbar^2\Omega^2}x^2} - \frac{\frac{1}{E_\mathrm{g}^2\hbar^2\Omega^2}}{1+\frac{a^2}{E_\mathrm{g}^2}x^2}\right)\frac{dx}{\sqrt{(1-x^2)(1+\frac{a^2}{E_\mathrm{g}^2}x^2)}}.
\end{aligned} \tag{A.2}$$

Eq. (A.2) is a sum of two Complete Elliptic Integrals of the Third Kind $\Pi(n,k)$ defined by

$$\Pi(n,k) \equiv \int_0^1 \frac{1}{(1-nx^2)\sqrt{(1-x^2)(1-kx^2)}}dx, \tag{A.3}$$

and Eq. (A.2) can thus be written

$$\begin{aligned}
\chi^{(1)}_{xx,\mathrm{tPA}}(\omega) &= \frac{S}{E_\mathrm{g}^3\hbar^2\Omega^2 - E_\mathrm{g}\hbar^4\Omega^4}\,\Pi\!\left(-\frac{a^2}{E_\mathrm{g}^2-\hbar^2\Omega^2}, -\frac{a^2}{E_\mathrm{g}^2}\right) \\
&\quad - \frac{S}{E_\mathrm{g}^3\hbar^2\Omega^2}\,\Pi\!\left(-\frac{a^2}{E_\mathrm{g}^2}, -\frac{a^2}{E_\mathrm{g}^2}\right).
\end{aligned} \tag{A.4}$$

With a and S written in full, one obtains Eq. (8.27).

B EM-CMMEA Linear Optical Susceptibility of tPA

Using Eqs. (8.31), (8.33) and (8.34) in Eq. (8.12), one obtains

$$\begin{aligned}\tilde{\chi}^{(1)}_{xx,\mathrm{tPA}}(\omega) &= \frac{e^2l^2E_0^2}{4\pi\varepsilon_0 A}\int_0^\infty \frac{1}{E_\mathrm{g}+\frac{\hbar^2k'^2}{2\mu}}\frac{dk'}{(E_\mathrm{g}+\frac{\hbar^2k'^2}{2\mu})^2-\hbar^2\Omega^2} \\ &= \frac{e^2l^2\sqrt{2\mu}E_0^2}{8\pi\hbar\varepsilon_0 A}\int_0^\infty \frac{1}{E_\mathrm{g}+x}\frac{1}{(E_\mathrm{g}+x)^2-\hbar^2\Omega^2}\frac{dx}{\sqrt{x}} \quad , \quad x=\frac{\hbar^2k'^2}{2\mu} \\ &= \frac{e^2l^2\sqrt{2\mu}E_0^2}{16\pi\hbar\varepsilon_0 A\hbar^2\Omega^2}\int_0^\infty \left[\frac{1/\sqrt{x}}{x+E_\mathrm{g}+\hbar\Omega}+\frac{1/\sqrt{x}}{x+E_\mathrm{g}-\hbar\Omega}-\frac{2/\sqrt{x}}{x+E_\mathrm{g}}\right]dx,\end{aligned} \tag{B.1}$$

which integrates to Eq. (8.35).

C Short-axis Linear Optical Susceptibility of tPA

Inserting Eq. (8.22) in Eq. (8.12) and using the shorthands in Eqs. (A.1a) and (A.1b), one obtains

$$\begin{aligned}\chi^{(1)}_{yy,\mathrm{tPA}}(\omega) &= \frac{2e^2l_2^2}{\pi\varepsilon_0 lA}\int_0^1 \frac{1}{E_\mathrm{g}^2-\hbar^2\Omega^2+a^2x^2}\frac{\sqrt{E_\mathrm{g}^2+a^2x^2}}{\sqrt{1-x^2}}dx \\ &= S\int_0^1 \frac{1}{E_\mathrm{g}^2-\hbar^2\Omega^2+a^2x^2}\frac{E_\mathrm{g}^2+a^2x^2}{\sqrt{(1-x^2)(E_\mathrm{g}^2+a^2x^2)}}dx \quad , \quad S=\frac{2e^2l_2^2}{\pi\varepsilon_0 lA} \\ &= S\frac{E_\mathrm{g}}{E_\mathrm{g}^2-\hbar^2\Omega^2}\int_0^1 \frac{1}{1+\frac{a^2}{E_\mathrm{g}^2-\hbar^2\Omega^2}x^2}\frac{1}{\sqrt{(1-x^2)\left(1+\frac{a^2}{E_\mathrm{g}^2}x^2\right)}}dx \\ &\quad + \frac{S}{E_\mathrm{g}}\int_0^1 \frac{1}{1+\frac{a^2}{E_\mathrm{g}^2-\hbar^2\Omega^2}x^2}\frac{\left(1+\frac{a^2}{E_\mathrm{g}^2-\hbar^2\Omega^2}x^2\right)-1}{\sqrt{(1-x^2)\left(1+\frac{a^2}{E_\mathrm{g}^2}x^2\right)}}dx \\ &= S\frac{E_\mathrm{g}}{E_\mathrm{g}^2-\hbar^2\Omega^2}\,\Pi\!\left(-\frac{a^2}{E_\mathrm{g}^2-\hbar^2\Omega^2},-\frac{a^2}{E_\mathrm{g}^2}\right) \\ &\quad + \frac{S}{E_\mathrm{g}}\left[F\left(-\frac{a^2}{E_\mathrm{g}^2}\right)-\Pi\!\left(-\frac{a^2}{E_\mathrm{g}^2-\hbar^2\Omega^2},-\frac{a^2}{E_\mathrm{g}^2}\right)\right],\end{aligned} \tag{C.1}$$

where F is the Complete Elliptic Integral of the First Kind:

$$F(k)\equiv\int_0^1\frac{1}{\sqrt{(1-x^2)(1-kx^2)}}dx. \tag{C.2}$$

Writing Eq. (C.1) in full, one obtains Eq. (8.40).

D Off-diagonal Linear Optical Susceptibility of tPA

Inserting Eqs. (8.21) and (8.22) in Eq. (8.12) and using Eqs. (A.1a) and (A.1b), one has

$$\begin{aligned}\chi^{(1)}_{xy,\mathrm{tPA}}(\omega) &= \chi^{(1)}_{yx,\mathrm{tPA}}(\omega) \\ &= \frac{l_2 e^2 E_\mathrm{g} E_0}{\pi\varepsilon_0 A}\int_0^1 \frac{dx}{(E_\mathrm{g}^2-\hbar^2\Omega^2+a^2x^2)\sqrt{(1-x^2)(E_\mathrm{g}^2+a^2x^2)}} \end{aligned} \tag{D.1}$$

and thus Eq. (8.41).

E Long-axis Linear Optical Susceptibility of PPP

Evaluation of the first two terms in Eq. (8.62) yields

$$\begin{aligned}\chi^{(1)}_{xx,\mathrm{ee}}(\omega) &= \frac{e^2|\beta|l^2}{72\pi\varepsilon_0 A}\left[\int_{\varrho_0/2}^{\sqrt{3}}\left(\frac{\varrho_6^2-3}{\varrho_6^2}\right)^2\frac{\varrho_6}{4\beta^2\varrho_6^2-\hbar^2\Omega^2}\frac{dk}{d\varrho_6}d\varrho_6\right. \\ &\qquad \left.+\int_{\varrho_\mathrm{g}/2}^{\sqrt{3}}\left(\frac{\varrho_5^2-3}{\varrho_5^2}\right)^2\frac{\varrho_5}{4\beta^2\varrho_5^2-\hbar^2\Omega^2}\frac{dk}{d\varrho_5}d\varrho_5\right] \\ &= S\left[\int_{\varrho_0/2}^{\sqrt{3}}\left(\frac{\varrho_6^2-3}{\varrho_6^2}\right)^2\frac{\varrho_6}{4\beta^2\varrho_6^2-\hbar^2\Omega^2}\frac{-\varrho_6 d\varrho_6}{\sqrt{(\varrho_\mathrm{o}^2/4-\varrho_6^2)(-\varrho_\mathrm{g}^2/4+\varrho_6^2)}}\right. \\ &\qquad \left.+\int_{\varrho_\mathrm{g}/2}^{\sqrt{3}}\left(\frac{\varrho_5^2-3}{\varrho_5^2}\right)^2\frac{\varrho_5}{4\beta^2\varrho_5^2-\hbar^2\Omega^2}\frac{\varrho_5 d\varrho_5}{\sqrt{(\varrho_\mathrm{o}^2/4-\varrho_5^2)(-\varrho_\mathrm{g}^2/4+\varrho_5^2)}}\right] \\ &= 4S\int_{\varrho_\mathrm{g}/2}^{\varrho_0/2}\left(\frac{\varrho^2-3}{\varrho}\right)^2\frac{1}{4\beta^2\varrho^2-\hbar^2\Omega^2}\frac{d\varrho}{\sqrt{(\varrho_\mathrm{o}^2-4\varrho^2)(-\varrho_\mathrm{g}^2+4\varrho^2)}} \end{aligned} \tag{E.1}$$

$$, \quad S=\frac{e^2|\beta|l}{18\pi\varepsilon_0 A}.$$

Introducing

$$a^2 = (\varrho_0^2-\varrho_\mathrm{g}^2)\beta^2 = E_0^2-E_\mathrm{g}^2, \tag{E.2a}$$

$$b^2 = \varrho_\mathrm{g}^2\beta^2-\hbar^2\Omega^2 = E_\mathrm{g}^2-\hbar^2\Omega^2, \tag{E.2b}$$

$$x^2 = \frac{4\varrho^2-\varrho_\mathrm{g}^2}{\varrho_0^2-\varrho_\mathrm{g}^2}, \tag{E.2c}$$

one obtains

$$\begin{aligned}
\chi^{(1)}_{xx,\mathrm{ee}}(\omega) &= 64|\beta|^3 S \int_0^1 \frac{\left(2x^2-1\right)^2}{(a^2x^2+E_\mathrm{g}^2)(a^2x^2+b^2)} \frac{dx}{\sqrt{(1-x^2)(a^2x^2+E_\mathrm{g}^2)}} \\
&= \frac{256|\beta|^3 S}{a^4 E_\mathrm{g}} \int_0^1 \left[1 + \frac{\left(b^2+\frac{a^2}{2}\right)^2}{b^2\left(E_\mathrm{g}^2-b^2\right)\left(1+\frac{a^2}{b^2}x^2\right)} \right. \\
&\qquad \left. + \frac{\left(E_\mathrm{g}^2+\frac{a^2}{2}\right)^2}{E_\mathrm{g}^2\left(b^2-E_\mathrm{g}^2\right)\left(1+\frac{a^2}{E_\mathrm{g}^2}x^2\right)} \right] \frac{dx}{\sqrt{(1-x^2)\left(1+\frac{a^2}{E_\mathrm{g}^2}x^2\right)}} \\
&= \frac{256|\beta|^3 S}{a^4 E_\mathrm{g}} \left[F\left(-\frac{a^2}{E_\mathrm{g}^2}\right) + \frac{\left(b^2+\frac{a^2}{2}\right)^2}{b^2\left(E_\mathrm{g}^2-b^2\right)} \Pi\left(-\frac{a^2}{b^2}, -\frac{a^2}{E_\mathrm{g}^2}\right) \right. \\
&\qquad \left. + \frac{\left(E_\mathrm{g}^2+\frac{a^2}{2}\right)^2}{E_\mathrm{g}^2\left(b^2-E_\mathrm{g}^2\right)} \Pi\left(-\frac{a^2}{E_\mathrm{g}^2}, -\frac{a^2}{E_\mathrm{g}^2}\right) \right]. \qquad \text{(E.3)}
\end{aligned}$$

Use of the relation $\left(E_0^2+E_\mathrm{g}^2\right)/2 = 3E_0E_\mathrm{g}$ and inclusion of the odd-odd contribution leads to Eq. (8.64).

F Short-axis Linear Optical Susceptibility of PPP

Inserting Eqs. (8.60) and (8.61) in Eq. (8.12), one obtains

$$\begin{aligned}
\chi^{(1)}_{yy,\mathrm{PPP}}(\omega) &= S \int_{\varrho_\mathrm{g}/2}^{\varrho_0/2} \left(\frac{\left(1-\varrho^2\right)^2 - 2(1-\varrho)^2}{\varrho(1+\varrho)} \right) \times \\
&\qquad \frac{1}{\beta^2(1+\varrho)^2 - \hbar^2\Omega^2} \frac{\varrho d\varrho}{\sqrt{(\varrho_\mathrm{o}^2-4\varrho^2)(-\varrho_\mathrm{g}^2+4\varrho^2)}} \qquad \text{(F.1)} \\
&\quad , \quad S = \frac{4e^2|\beta|l}{3\pi\varepsilon_0 A}.
\end{aligned}$$

In the limit of zero damping, one has

$$\mathrm{Im}\left\{ \frac{1}{\beta^2(1+\varrho)^2 - \hbar^2\Omega^2} \right\} \propto \delta\left(\beta^2(1+\varrho)^2 - \hbar^2\omega^2\right). \qquad \text{(F.2)}$$

Assuming that the slowly varying part is constant during differentiation, one therefore has the following for the imaginary part of Eq. (F.1):

$$\chi^{(1)''}_{yy,\mathrm{PPP}} \simeq S\frac{\left(1-z^2\right)^2-2(1-z)^2}{z(1+z)}\times \mathrm{Im}\left\{\int_{\varrho_\mathrm{g}/2}^{\varrho_0/2}\frac{1}{\beta^2(1+\varrho)^2-\hbar^2\Omega^2}\frac{\varrho d\varrho}{\sqrt{(\varrho_\mathrm{o}^2-4\varrho^2)(-\varrho_\mathrm{g}^2+4\varrho^2)}}\right\} \quad \text{(F.3)}$$

$$, \; z=\begin{cases} \frac{\varrho_\mathrm{g}}{2} & \text{for } \hbar\omega<|\beta|\left(1+\frac{\varrho_\mathrm{g}}{2}\right) \\ \frac{\hbar\omega-|\beta|}{|\beta|} & \text{for } |\beta|\left(1+\frac{\varrho_\mathrm{g}}{2}\right)\le\hbar\omega\le|\beta|\left(1+\frac{\varrho_0}{2}\right) \\ \frac{\varrho_0}{2} & \text{for } \hbar\omega>|\beta|\left(1+\frac{\varrho_0}{2}\right) \end{cases},$$

where Im indicates the imaginary part.

Using Eqs. (E.2a), (E.2c) and

$$d_\pm = 2|\beta|\pm 2\hbar\Omega, \quad \text{(F.4)}$$

the integral in Eq. (F.3) can be written

$$\begin{aligned}
&\int_0^1 \frac{1}{\left(2|\beta|+\sqrt{a^2x^2+E_\mathrm{g}^2}\right)^2-4\hbar^2\Omega^2}\frac{dx}{\sqrt{1-x^2}} \\
&= \frac{1}{4\hbar\Omega}\int_0^1\left[\frac{1}{d_-+\sqrt{a^2x^2+E_\mathrm{g}^2}}-\frac{1}{d_++\sqrt{a^2x^2+E_\mathrm{g}^2}}\right]\frac{dx}{\sqrt{1-x^2}} \\
&= \frac{1}{4\hbar\Omega}\left[\frac{d_-^2}{E_\mathrm{g}(E_\mathrm{g}^2-d_-^2)}\,\Pi\left(\frac{a^2}{-E_\mathrm{g}^2+d_-^2},-\frac{a^2}{E_\mathrm{g}^2}\right)\right. \\
&\quad -\frac{\pi}{2}\frac{d_-}{\sqrt{a^2+E_\mathrm{g}^2-d_-^2}\sqrt{E_\mathrm{g}^2-d_-^2}} \\
&\quad -\frac{d_+^2}{E_\mathrm{g}(E_\mathrm{g}^2-d_+^2)}\,\Pi\left(\frac{a^2}{-E_\mathrm{g}^2+d_+^2},-\frac{a^2}{E_\mathrm{g}^2}\right) \\
&\quad \left.-\frac{\pi}{2}\frac{d_+(E_\mathrm{g}^2+d_+^2)}{\sqrt{a^2+E_\mathrm{g}^2-d_+^2}\left(E_\mathrm{g}^2-d_+^2\right)^{3/2}}\right]. \qquad \text{(F.5)}
\end{aligned}$$

Writing Eq. (F.5) in full, one obtains Eq. (8.65).

Chapter 9

Electro-optic Susceptibility

This chapter treats the long-axis electro-optic properties of poly(*para*-phenylene) (PPP), since an improved understanding of these properties might ultimately serve to optimize the application of PPP in connection with polymer-based light emitting diodes, solar cells or photodetectors.

The chapter contains a derivation of an analytic, perturbative expression for the complex long-axis optical susceptibility of pristine, infinite, parallel and non-interacting chains of PPP in the presence of an electrostatic field directed along the long-axis of the polymer. The obtained expression is valid for photon energies in the vicinity of the band gap. To obtain the high-field electro-optic characteristics and to assess the applicability of the low-field perturbation expression, a numerical, non-perturbative tight-binding calculation of the high-field electro-optic susceptibility is also presented.

The results presented in this chapter have been published in Ref. [2].

9.1 Analytic Derivations

Consider a both static and spatially invariant electric field

$$\vec{F} = F\hat{x} \tag{9.1}$$

directed along the long-axis of the polymer.

According to Eq. (3.38), in an inversion-symmetrical PPP chain, one has the following perturbative[1] approximation to the long-axis electro-optic susceptibility:

$$\chi(F,\omega) \simeq \chi^{(1)}(\omega) + \chi^{(3)}(\omega)F^2, \tag{9.2}$$

[1] The field can be treated as a perturbation if it is sufficiently small for the higher-order corrections $\chi^{(5)}(\omega)F^4$, $\chi^{(7)}(\omega)F^6, \ldots$ to Eq. (9.2) to be relatively small.

in which the following shorthand notation has been used for the long-axis electro-optic function $\chi^{(3)}_{xxxx}$ and the long-axis linear optical susceptibility $\chi^{(1)}_{xx}$:

$$\chi^{(3)}(\omega) \equiv \chi^{(3)}_{xxxx}(\omega = \omega + 0 + 0), \tag{9.3a}$$

$$\chi^{(1)}(\omega) \equiv \chi^{(1)}_{xx}(\omega). \tag{9.3b}$$

According to Aspnes and Rowe [53], the electro-optic function $\chi^{(3)}$ can be derived from $\chi^{(1)}$ through

$$\chi^{(3)}(\omega) \simeq \frac{1}{3\hbar^2\Omega^2}\frac{e^2\hbar^2}{8\mu}\frac{\partial^3\left(\hbar^2\Omega^2\chi^{(1)}(\omega)\right)}{\partial(\hbar\Omega)^3} \quad , \quad \hbar\omega \approx E_{\mathrm{g}}, \tag{9.4}$$

where $e > 0$ is the elementary charge, μ is the reduced mass, E_{g} is the band gap, and where $\hbar\Omega = \hbar\omega + i\hbar\gamma$ includes the photon energy $\hbar\omega$ and the damping parameter γ. Eq. (9.4) is based on a two-band effective mass model and is therefore valid for photon energies in the vicinity of the band gap only.

The analytic tight-binding derivation of the linear optical susceptibility $\chi^{(1)}$, which is given in full detail in Chap. 8, follows the following outline: The derivation is made in the free-carrier π-electron dipole approximation, and local-field effects and inter-chain coupling is disregarded. In unevaluated form, the linear optical susceptibility is given by Eq. (8.12):

$$\chi^{(1)}(\omega) = \frac{2}{\pi\varepsilon_0 A}\sum_{\mathrm{c,v}}\int_{-\frac{\pi}{l}}^{\frac{\pi}{l}} |x_{\mathrm{cv}}(k)|^2 \frac{E_{\mathrm{cv}}(k)}{E^2_{\mathrm{cv}}(k) - \hbar^2\Omega^2}dk, \tag{9.5}$$

where ε_0 is the vacuum permittivity, $l = 4.26$Å is the lattice constant, $A = 21.5\text{Å}^2$ is the cross sectional area occupied by the PPP chain [30], $E_{\mathrm{cv}}(k) = E_{\mathrm{c}}(k) - E_{\mathrm{v}}(k)$ is the π-band excitation energy as a function of crystal momentum, and $x_{\mathrm{cv}}(k)$ is the x-component of the electric dipole matrix element between the valence band v and conduction band c.

The excitation energy E_{cv} is found by setting up a matrix eigenvalue problem using the atomic $2p_z$-orbitals as basis while disregarding wave function overlaps between neighbouring atomic sites and including nearest neighbour Hamilton matrix elements only. The obtained band structure and conduction and valence band expansion coefficients are then used to derive the electric dipole matrix elements through Eq. (8.10):

$$x_{\mathrm{cv}}(k) = \frac{-e}{E_{\mathrm{cv}}(k)}\sum_{n,p,q} \mathrm{c}^*_q(k)\mathrm{v}_p(k)e^{iknl}(x_{pn} - x_{q0})\left\langle q0\left|\hat{H}\right|pn\right\rangle, \tag{9.6}$$

where x_{pn} is the x-coordinate of the pth atomic site in the nth unit cell, $\mathrm{c}^*_q(k)$ and $\mathrm{v}_p(k)$ are the conduction and valence band expansion coefficients, respectively, and $\langle q0|\hat{H}|pn\rangle$ is the Hamilton matrix element between $2p_z$-orbitals on atomic sites $q0$ and pn.

As an example, for the dominant transitions between the highest valence band and lowest conduction band, Eqs. (8.46) and (8.56) show that

$$E_{\rm cv}(k) \;=\; 2|\beta|\sqrt{3-\sqrt{8}\cos\left(\frac{kl}{2}\right)}, \tag{9.7a}$$

$$x_{\rm cv}(k) \;=\; \frac{-el}{24}\frac{E_{\rm cv}^2-12\beta^2}{E_{\rm cv}^2}, \tag{9.7b}$$

where β is the Hamilton matrix element between any two neighbouring sites.

Finally, Eq. (9.5) is evaluated using the excitation energy $E_{\rm cv}$ as integration parameter, and one ultimately obtains the combination of Eqs. (8.30) and (8.64):

$$\begin{aligned}\chi^{(1)}_{\rm PPP}(\omega) \;\simeq\; & \frac{e^2 l}{4\pi\varepsilon_0 A}\frac{E_0}{\hbar^2\Omega^2}\left[\frac{\hbar^2\Omega^2}{9E_{\rm g}E_0}\,F\left(\frac{E_{\rm g}^2-E_0^2}{E_{\rm g}^2}\right)\right.\\ & \left.+\;\frac{\left(E_{\rm g}-\frac{\hbar^2\Omega^2}{3E_0}\right)^2}{\hbar\Omega\sqrt{E_{\rm g}^2-\hbar^2\Omega^2}}\,\arcsin\left(\frac{\hbar\Omega}{E_{\rm g}}\right)-1\right]\quad,\quad \hbar\omega\approx E_{\rm g},\end{aligned} \tag{9.8}$$

where E_0 is the total width of the π-bands, and $F(k)\equiv\int_0^1 \frac{dx}{\sqrt{(1-x^2)(1-kx^2)}}$ is the Complete Elliptic Integral of the First Kind. In Eq. (9.8), the contributions from odd eigenstates have been neglected due to their negligible contributions to the band edge susceptibility.

Inserting Eq. (9.8) in Eq. (9.4) and assuming that slowly varying factors are constant during differentiation, one obtains the following end result:

$$\begin{aligned}\chi^{(3)}_{\rm PPP}(\omega) \;\simeq\; & \frac{e^4 l E_0\left(E_{\rm g}-\frac{\hbar^2\Omega^2}{3E_0}\right)^2}{96\pi\varepsilon_0 A\mu\hbar\Omega^3}\frac{\partial^3\left(\frac{\arcsin\left(\frac{\hbar\Omega}{E_{\rm g}}\right)}{\sqrt{E_{\rm g}^2-\hbar^2\Omega^2}}\right)}{\partial(\hbar\Omega)^3}\\ =\; & \frac{e^4 l\left(3E_{\rm g}E_0-\hbar^2\Omega^2\right)^2}{864\pi\varepsilon_0 A\mu E_0\hbar\Omega^3}\left[\frac{4E_{\rm g}^4+7E_{\rm g}^2\hbar^2\Omega^2-11\hbar^4\Omega^4}{\left(E_{\rm g}^2-\hbar^2\Omega^2\right)^4}\right.\\ & \left.+\;\frac{3\hbar\Omega\left(3E_{\rm g}^2+2\hbar^2\Omega^2\right)\arcsin\left(\frac{\hbar\Omega}{E_{\rm g}}\right)}{\left(E_{\rm g}^2-\hbar^2\Omega^2\right)^{7/2}}\right]\quad,\quad \hbar\omega\approx E_{\rm g}.\end{aligned} \tag{9.9}$$

From Fig. 9.1, which shows a plot of $\chi^{(3)}_{\rm PPP}(\omega)$, it can be seen that the field-induced change in the susceptibility is appreciable for photon energies close to the band gap only. Notice in Fig. 9.1 the field-induced absorption tail below the band gap caused by field-induced tunnelling of electrons [51]. The present result demonstrates that analytic expressions for the electro-optic properties can be found for a conjugated polymer with a relatively complicated chemical structure such as PPP.

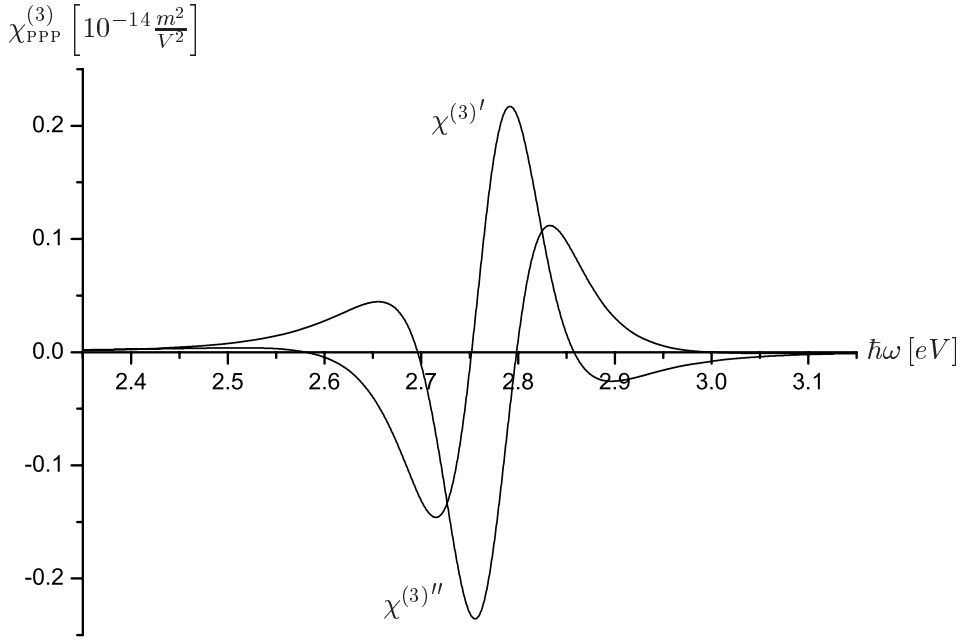

Figure 9.1: The real part $\chi^{(3)\prime}$ and imaginary part $\chi^{(3)\prime\prime}$ of the long-axis electro-optic function of poly(*para*-phenylene) for $E_{\rm g} = 2.8eV$, $E_0 = 16.2eV$, $\hbar\gamma = 0.1eV$, and $\mu = 0.07m_0$ [1].

9.2 Numerical Results

To assess the applicability of the analytic, perturbative approach presented in Sec. 9.1, a numerical, non-perturbative tight-binding evaluation of the electro-optic susceptibility has been made for comparison. The non-perturbative result is valid for arbitrary field strengths, while the perturbative result is valid in the low-field limit only. The numerical model is based on a PPP chain consisting of 100 unit cells and is in all other aspects identical to the PPP model used in the analytic derivation.

Fig. 9.2 shows a comparison of the analytic result in Fig. 9.1 with the numerical result $\Delta\chi_{\rm PPP}\left(F = 1\frac{mV}{\rm \AA}, \omega\right) \equiv \chi_{\rm PPP}\left(F = 1\frac{mV}{\rm \AA}, \omega\right) - \chi^{(1)}_{\rm PPP}(\omega)$, and Fig. 9.3 shows a plot of $\Delta\chi_{\rm PPP}\left(F = 2\frac{mV}{\rm \AA}, \omega\right)$. Inspection of Fig. 9.2 shows that the analytic, perturbative result of Eq. (9.9) is an excellent approximation to $\Delta\chi_{\rm PPP}(F, \omega)$ for fields smaller than $\sim 1\frac{mV}{\rm \AA}$. For fields larger than $\sim 1\frac{mV}{\rm \AA}$, however, Fig. 9.3 shows the emergence of oscillations above the band gap, which is characteristic of the non-perturbative Franz-Keldysh regime [51].

9.3 Discussion

Ref. [54] contains an analytic expression for $\chi^{(3)}$ derived using the Keldysh diagram technique in a one-electron two-band continuum linearized model of a

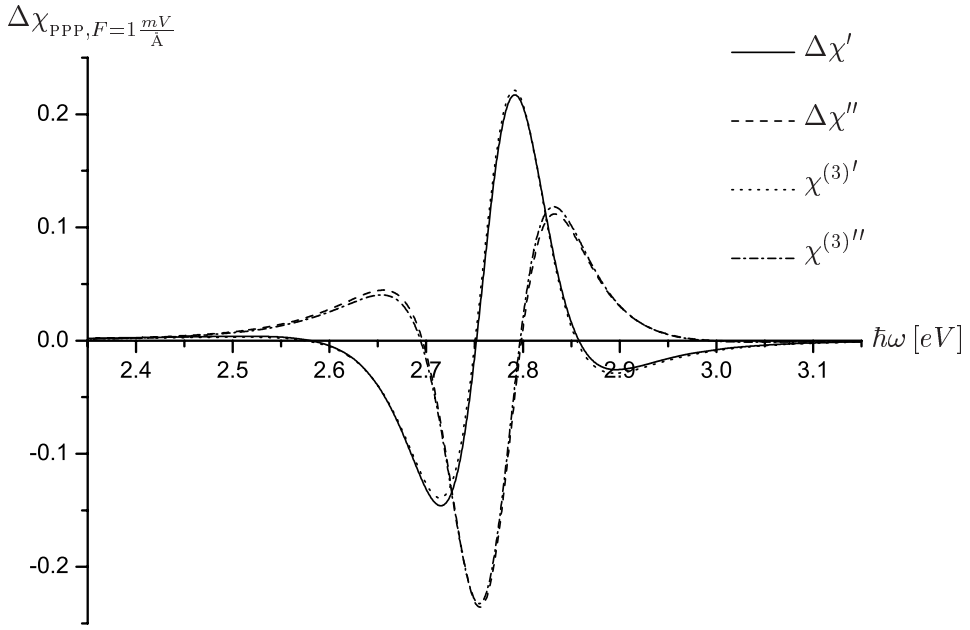

Figure 9.2: Comparison of the analytic result in Fig. 9.1 with the numerically obtained real part $\Delta\chi'$ and imaginary part $\Delta\chi''$ of $\Delta\chi_{\mathrm{PPP}}\left(F=1\frac{mV}{\mathrm{A}},\omega\right)$.

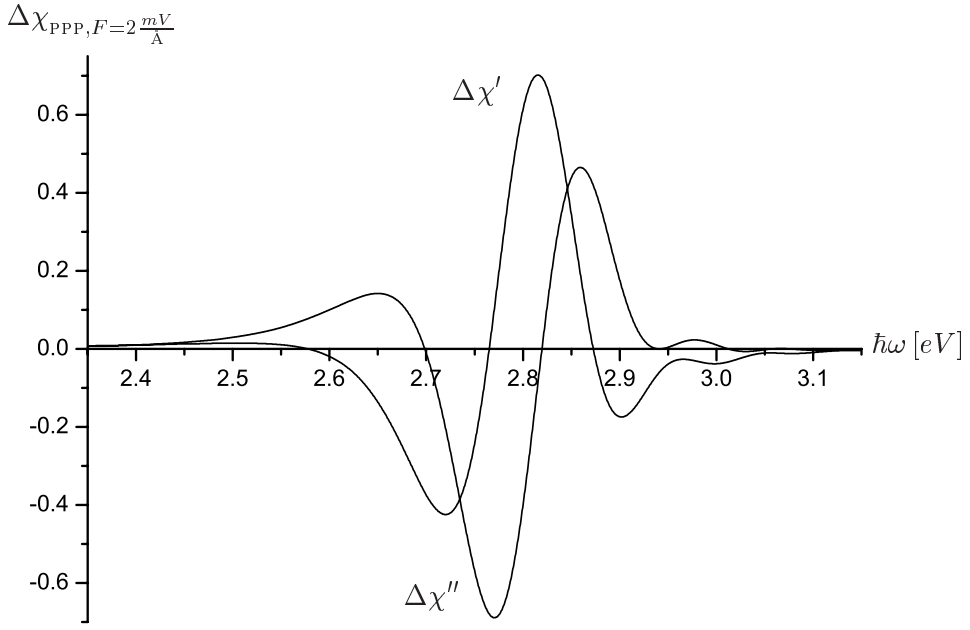

Figure 9.3: Numerically obtained real part $\Delta\chi'$ and imaginary part $\Delta\chi''$ of $\Delta\chi_{\mathrm{PPP}}\left(F=2\frac{mV}{\mathrm{A}},\omega\right)$ for $E_{\mathrm{g}}=2.8eV$, $E_0=16.2eV$, and $\hbar\gamma=0.1eV$.

conjugated polymer chain with constant dimerization. Comparison with the result in this work shows that the corresponding curves are quite similar, and that our expression is considerably simpler than the one given in Ref. [54]. Furthermore, comparison of Fig. 9.1 with the corresponding figure in Ref. [53] shows good agreement concerning the shape of the curves as well as the relative magnitudes of the peaks.

In Ref. [51], a non-perturbative, analytic expression for the electro-optic susceptibility of one-dimensional semiconductors is derived using the effective mass and constant momentum matrix element approximation (EM-CMMEA). Comparison of the second-order field-expansion of this expression with Eq. (9.9) of this work shows that the EM-CMMEA is valid for photon energies close to the band gap, as would be expected, but that for $\hbar\omega = 2.5eV$, say, the EM-CMMEA-induced error is 18%.

9.4 Conclusion

In this chapter, an analytic, approximate expression for the long-axis electro-optic function of poly(*para*-phenylene) has been derived. To test the applicability of this result in a perturbative expression for the electro-optic susceptibility, a non-perturbative, numerical evaluation has been performed for comparison. This comparison shows that the analytic, perturbative approximation to the electro-optic susceptibility of poly(*para*-phenylene) given by Eqs. (9.2) and (9.9) is valid for electric fields weaker than $\sim 1\frac{mV}{\text{Å}}$.

Part IV

DFTB Treatment of Phonons and Polarons

Chapter 10

Phonons

The treatment of phonons in extended systems such as conjugated polymers is computationally cumbersome within ab initio DFT. With this in view, this chapter confirms the applicability of the in Chap. 5 described computationally effective Density-Functional-based Tight-Binding (DFTB) approach to phonon dynamics in the conjugated polymers *trans*-polyacetylene (tPA) and poly(*para*-phenylene) (PPP).

Whereas the first theoretical treatments of vibrations in tPA [6, 55, 56, 57, 58, 59, 60, 61] and PPP [62, 63, 64, 65] date back several decades, the first ab initio LDA-DFT calculation of the in-plane phonon spectrum of tPA was performed in 1997 by Wu *et al.* [66] and extended in 1999 by Wu and co-workers [67] to include the out-of-plane phonon modes as well. A DFT-based vibrational treatment of the PPP oligomers biphenyle and terphenyle was presented in 2002 [68], but has yet to be seen for the polymer itself.

This chapter contains calculations of the equilibrium configuration, the phonon dispersion curves, the relative atomic displacements in the zone-centre modes, which are furthermore identified as being either Raman or infrared (IR) active, and finally the infrared absorption spectrum. The presented results are compared with experimental and calculated results from the literature.

While the general theoretical framework is based on Chap. 6, the presented model and computational approach is somewhat similar to the one applied by Sánchez-Portal and Hernández in their calculation of the vibrational properties of single-wall nanotubes [69]. The only required input in the present model is the parametrized Hamilton and overlap matrix elements. Calculations are performed on pristine, infinite and non-interacting polymer chains within the Born-Oppenheimer and harmonic approximations. Electron-phonon coupling is disregarded leaving important extensions to be considered in future work.

The results presented in this chapter have been published in Ref. [3].

10.1 The Model

10.1.1 Super Cell

The polymer chains are assumed to be infinitely long, but the sum in Eq. (6.14) is limited to a number of neighbouring unit cells constituting the so-called super cell, which is then subsequently reproduced periodically along the polymer chain. In choosing the size of this super cell, the tradeoff is between accuracy and computational efficiency. This work includes results obtained for different sizes of super cells.

10.1.2 Equilibrium Configuration

The equilibrium configuration $\vec{R}^0$ is found by minimizing the semiconductor equivalent of Eq. (5.4):

$$V(\vec{R}) = 2\sum_{\mathrm{v},k} \epsilon_{\mathrm{v}}\left(k, \vec{R}\right) + \sum_{i<j} V_{\mathrm{rep}}^{ij}\left(\left|\vec{R}_i - \vec{R}_j\right|\right) \tag{10.1}$$

to an accuracy of 0.01eV[1]. To impose molecular symmetries and thereby simplify the calculations, the Euclidian coordinates $\vec{R}$ are replaced by structural parameters in terms of bond lengths and angles as parameters for this minimization.

Notice that *trans*-polyacetylene differs from almost any other polymer in having two degenerate ground states with one ground state being as shown in Fig. 10.1 while the other is flipped 180° around the y-axis. This degeneracy gives rise to the intensively studied problem of solitons [5] which is disregarded in this work (for a short description see Sec. 7.3).

In order to reduce the size of the PPP unit cell, the torsion between alternating phenyl rings is ignored, and PPP is thus treated as a planar molecule with a unit cell as shown in Fig. 10.2. Isolated PPP chains have a torsion angle of about 26° [70], but in the polymer films used for experiments, solid state packing will strongly reduce this torsion angle making the approximation of planarity quite reasonable. That the two molecules are planar leads to a decoupling of the xy- and the z-components in the dynamical matrix. This permits in-plane (xy) and out-of-plane (z) calculations to be performed separately leading to an increased computational efficiency.

[1] Notice that Eq. (10.1) shows inter-atomic bond lengths to be the result of a compromise between on the one hand the lowering of the valence band energy resulting from an increased overlap of the electron clouds and on the other hand the increased nuclear repulsion caused by a decrease in the bond lengths.

10.1.3 Force Constant Matrix

Writing the elements of the force constant matrix $\overleftrightarrow{C}$ in terms of the atomic force vector and applying a harmonic approximation[2], one has for a small displacement d [71]:

$$C_{ij} = -\frac{\partial F_j}{\partial R_i}\bigg|_{\vec{R}^0} \simeq -\frac{F_j\left(\vec{R}^0 + d\vec{e}_i\right)}{d}, \tag{10.2}$$

where $\vec{e}_i$ is the unit vector corresponding to the ith degree of freedom.

To reduce the number of numerical steps required to solve for the band structure, the force component in Eq. (10.2) is expressed in terms of the derivatives of the Hamilton and overlap matrix elements $H_{\alpha\beta}$ and $S_{\alpha\beta}$ [45] (see the appendix):

$$F_j = \frac{2}{N_{\mathrm{sc}}} \sum_{\mathrm{v},k} \sum_{\alpha,\beta} \mathrm{v}^*_\alpha \mathrm{v}_\beta \left(\epsilon_\mathrm{v} \frac{\partial S_{\alpha\beta}}{\partial R_j} - \frac{\partial H_{\alpha\beta}}{\partial R_j} \right) - \frac{\partial V^{\mathrm{sc}}_{\mathrm{rep}}}{\partial R_j}. \tag{10.3}$$

When numerically approximating the derivatives of $X \in \{S_{\alpha\beta}, H_{\alpha\beta}, V^{\mathrm{sc}}_{\mathrm{rep}}\}$ via

$$\frac{\partial X}{\partial R_j} = \frac{X\left(\vec{R}^0 + d\vec{e}_i + d\vec{e}_j\right) - X\left(\vec{R}^0 + d\vec{e}_i - d\vec{e}_j\right)}{2d} \equiv \frac{\Delta X}{2d}, \tag{10.4}$$

one obtains

$$C_{ij} = \frac{1}{N_{\mathrm{sc}}} \sum_{\mathrm{v},k} \sum_{\alpha,\beta} \mathrm{v}^*_\alpha\left(\vec{R}^0_{d_i}\right) \mathrm{v}_\beta\left(\vec{R}^0_{d_i}\right) \left[\frac{\Delta H_{\alpha\beta}}{d^2} - \epsilon_\mathrm{v}\left(\vec{R}^0_{d_i}\right) \frac{\Delta S_{\alpha\beta}}{d^2} \right] + \frac{\Delta V^{\mathrm{sc}}_{\mathrm{rep}}}{2d^2}, \tag{10.5}$$

with

$$\vec{R}^0_{d_i} \equiv \vec{R}^0 + d\vec{e}_i. \tag{10.6}$$

In choosing the value of the displacement d, the following compromise is to be made: Inherently, d is to be small for the approximation in Eq. (10.2) to be valid. On the other hand, too small a displacement will lead to numerical instability, since taking the difference ΔX will amplify the inherent errors of the in that case almost identical values $X\left(\vec{R}^0 + d\vec{e}_i + d\vec{e}_j\right)$ and $X\left(\vec{R}^0 + d\vec{e}_i - d\vec{e}_j\right)$. In this work, the compromise landed on the value

$$d = 0.01\text{Å}. \tag{10.7}$$

In this connection, the "forward-backward"-approach of Eq. (10.4) in taking derivatives with respect to R_j is applied to reduce the errors resulting from the relatively large value of d. Furthermore, to compensate for anharmonicities, an average is made over positive and negative displacements d and $-d$ [69]. The k-sum in Eq. (10.5) is performed using a 10 point Gaussian quadrature.

[2] In the harmonic approximation, the force on an atom is proportional to the atom's displacement from its equilibrium position.

10.1.4 Symmetries

To avoid obtaining unphysical phonon spectra, all system symmetries are imposed on the force constant matrix. First of all, the force constant matrix is to be symmetrical. Secondly, for tPA the two CH bonds in the unit cell are identical, and corresponding force constant matrix elements should thus be identical also. The same argument holds for the CH interaction crosswise between the two CH bonds. These symmetries are imposed by simple averaging over the matrix elements in question. Similar considerations are made for PPP.

For small displacements from the equilibrium configuration, the ith component of the force acting on the pth atom is given by

$$F_{p_i} = -\sum_{q=1}^{N}\sum_{j} C_{q_j,p_i} d_{q_j} \quad , \quad j \in \{x,y,z\}, \tag{10.8}$$

where N is the number of atoms in a super cell, and where d_{q_j} is the displacement of the qth atom in the direction of the j-axis.

For a displacement of the entire system as a whole, ($d_{q_j} = d_j$) all atomic forces are zero, and hence

$$\sum_{q=1}^{N} C_{q_j,p_i} = 0 \quad , \quad \forall p,i,j. \tag{10.9}$$

This so-called acoustic sum rule is imposed by adjusting the 3×3 block diagonal force constant matrix elements corresponding to interactions of an atom with itself.

10.2 Results

10.2.1 Equilibrium Configuration

Figs. 10.1 and 10.2 show the equilibrium configurations of tPA and PPP, respectively. As can be seen from Tabs. 10.1 and 10.2, the obtained results are in good agreement with other results from the literature with the deviations being within a few percent.

10.2.2 Phonon Dispersion

Figs. 10.3 and 10.4 show the in-plane and out-of-plane tPA phonon dispersion curves, respectively, for a super cell consisting of 11 unit cells. The two in-plane modes around 3100cm^{-1} are CH bond stretching modes (see Fig. 10.7). As the phonon momentum q is a measure of the phase difference between vibrational displacements in different unit cells, the almost dispersionless nature of these modes indicates that CH bonds in different unit cells vibrate almost independently of one

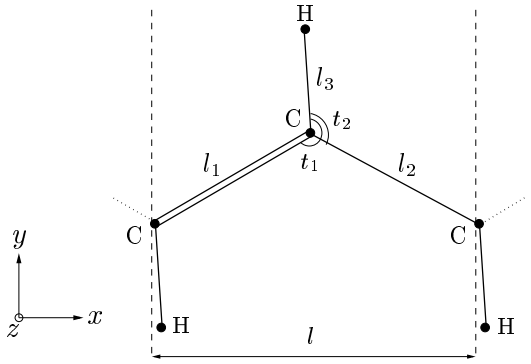

Figure 10.1: The *trans*-polyacetylene unit cell has the following structural parameters in the equilibrium configuration: $l_1 = 1.369$Å, $l_2 = 1.414$Å, $l_3 = 1.113$Å, $t_1 = 124.4°$ and $t_2 = 117.3°$ corresponding to a lattice constant of $l = 2.461$Å.

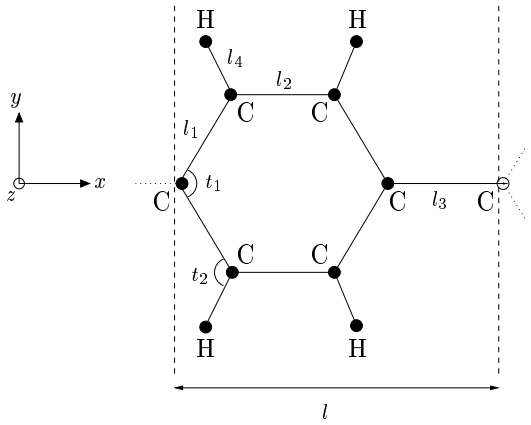

Figure 10.2: The poly(*para*-phenylene) unit cell has the following structural parameters in the equilibrium configuration: $l_1 = 1.399$Å, $l_2 = 1.380$Å, $l_3 = 1.463$Å, $l_4 = 1.113$Å, $t_1 = 117.8°$ and $t_2 = 118.9°$ corresponding to a lattice constant of $l = 4.286$Å.

Table 10.1: Comparison of the calculated equilibrium configuration of *trans*-polyacetylene with calculated [72, 73, 74, 75] and observed [76] results from the literature. The columns marked with % show the deviation of the present results with respect to the references indicated. The symbol ≡ indicates that the value has been fixed.

	This work	[72]	[73]	[74]	[75]	[75]%	[76]	[76]%
l_1	1.369Å	1.377Å	1.377Å	1.327Å	1.35Å	*1.4%*	1.36Å	*0.7%*
l_2	1.414Å	1.434Å	1.434Å	1.477Å	1.42Å	*-0.4%*	1.45Å	*-2.5%*
l_3	1.113Å	1.08Å	≡ 1.08Å	1.085Å	1.10Å	*1.2%*	1.09Å	*2.1%*
t_1	124.4°	≡ 120°	≡ 120°	124.2°	124.53°	*-0.1%*		
t_2	117.3°				117.01°	*0.3%*		
l	2.461Å	2.435Å	2.435Å	2.479Å	2.443Å	*0.7%*		

Table 10.2: Comparison of the calculated equilibrium configuration of poly(*para*-phenylene) with calculated results from Ref. [70]. The column marked with % shows the deviation of the present results with respect to Ref. [70].

	This work	[70]	[70]%
l_1	1.399Å	1.407Å	*-0.6%*
l_2	1.380Å	1.388Å	*-0.6%*
l_3	1.463Å	1.465Å	*-0.1%*
l_4	1.113Å	1.103Å	*0.9%*
t_1	117.8°	117.5°	*0.3%*
t_2	118.9°	119.2°	*-0.3%*
l	4.286Å	4.31Å	*-0.6%*

another. The high frequencies indicate that the CH bond stretching is decoupled from the motion of the carbon backbone.

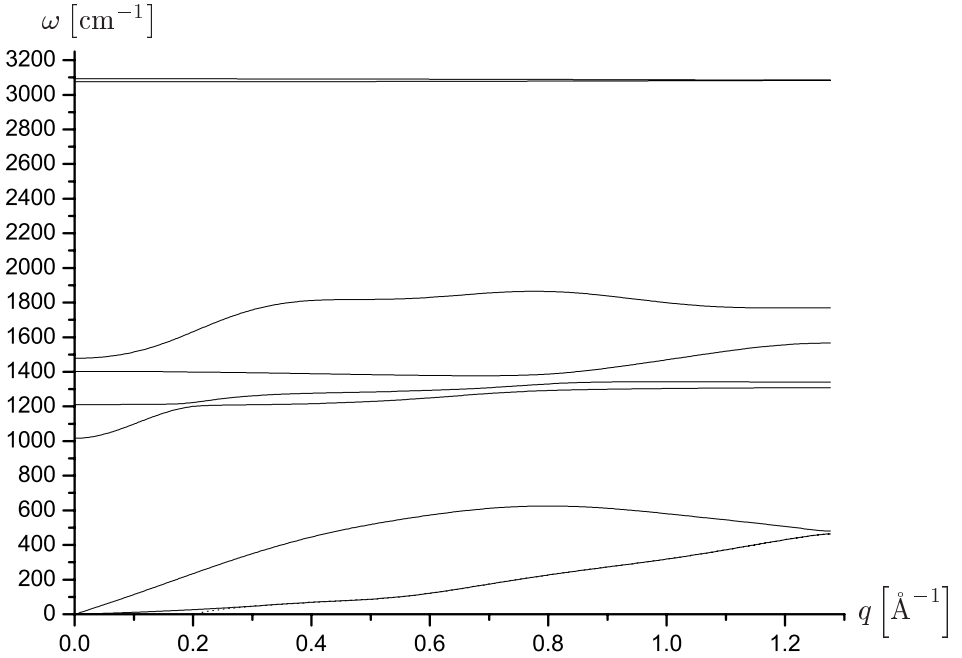

Figure 10.3: The in-plane phonon dispersion curves of *trans*-polyacetylene for a super cell consisting of 11 unit cells.

Comparison of the spectra in Figs. 10.3 and 10.4 with corresponding spectra based on a super cell consisting of 3 unit cells will reveal substantial differences, especially when it comes to the lower phonon bands. This demonstrates that 3 unit cells is insufficient as a tPA super cell. In this work, phonon dispersion curves have been calculated for super cells containing 3, 5, 7, 9 and 11 unit cells with results showing a steady convergence towards the phonon dispersion curves displayed in Figs. 10.3 and 10.4.

The lowest in-plane tPA phonon band is imaginary for low q-values corresponding to negative solutions for ω_i^2 in Eq. (6.13). This unphysical behavior has been minimized by imposing the system symmetries mentioned in Sec. 10.1.4. That force constant matrix elements representing identical physical interactions are made identical does not ensure, however, that the force constant matrix elements are not assigned unphysical values. To correct the imaginary frequencies, the lowest phonon band in Fig. 10.3 is cut around $q = 0.3\text{Å}^{-1}$ and the part of the band containing the imaginary frequencies replaced by a parabolic fit. The original phonon band is seen as a dotted curve. The problem of unphysical phonon bands decreases as the size of the super cell is increased. Hence, all the results for tPA presented below are for a super cell consisting of 11 unit cells.

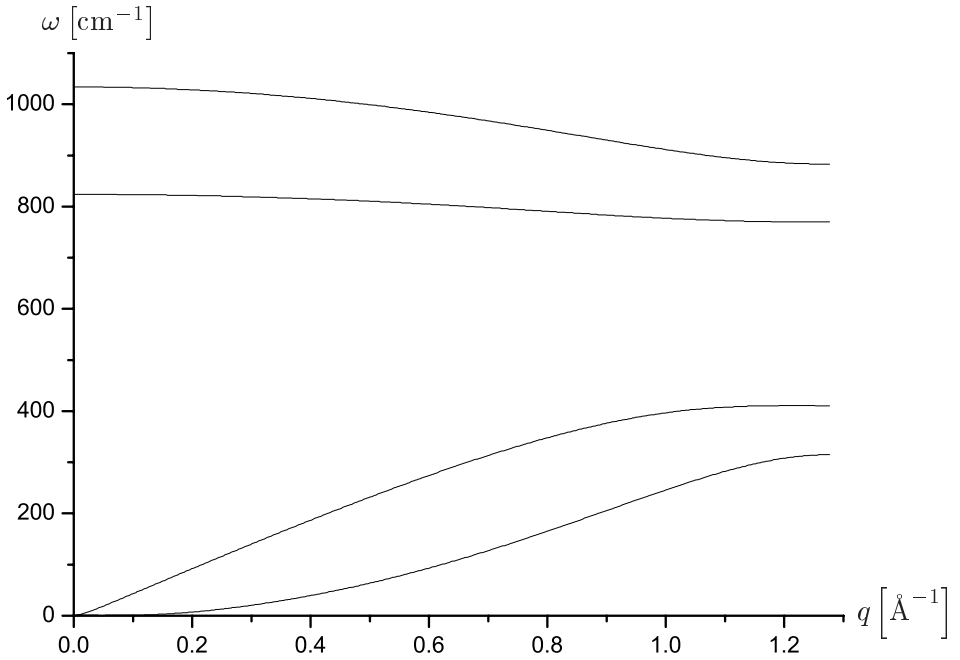

Figure 10.4: The out-of-plane phonon dispersion curves of *trans*-polyacetylene for a super cell consisting of 11 unit cells.

For PPP, a super cell consisting of 3 unit cells is found to be sufficient. Figs. 10.5 and 10.6 show the in-plane and out-of-plane PPP phonon dispersion curves, respectively. The lowest phonon band in Fig. 10.6 has been corrected for imaginary frequencies in the same manner as described above. Notice again the presence of the dispersionless high-frequency CH modes which serve as a hallmark for carbohydrate molecules.

The literature contains numerous calculations of the phonon dispersion curves of tPA [6, 55, 56, 58, 59, 61, 66, 67] and PPP [62, 63, 64, 65]. Among these, Refs. [6, 67] and [62, 64] present the out-of-plane as well as the in-plane dispersion curves. For tPA, comparison shows good agreement between the present results and the results obtained in Ref. [67] via an ab initio LDA-DFT calculation as well as with the results in Ref. [6] which were obtained by fitting the force constants to experimental phonon frequencies.

For PPP, comparison shows reasonable agreement with the results obtained for a planar PPP molecule in Refs. [62] and [64]. In Ref. [62], force constants were transferred from the toluene molecule, and in Ref. [64], a quadratic simplified valence force field was used.

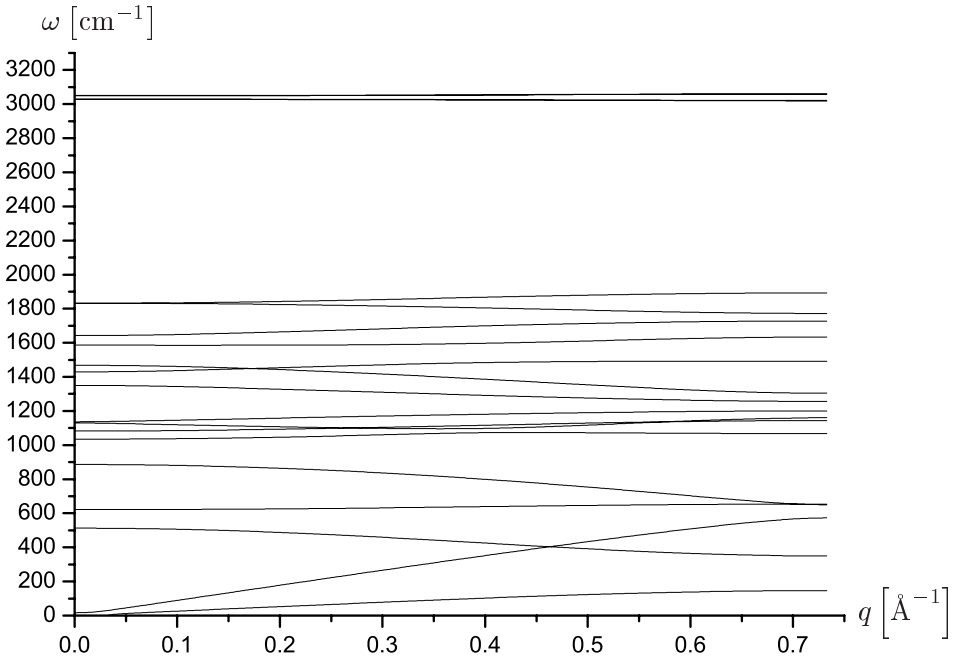

Figure 10.5: The in-plane phonon dispersion curves of poly(*para*-phenylene) for a super cell consisting of 3 unit cells.

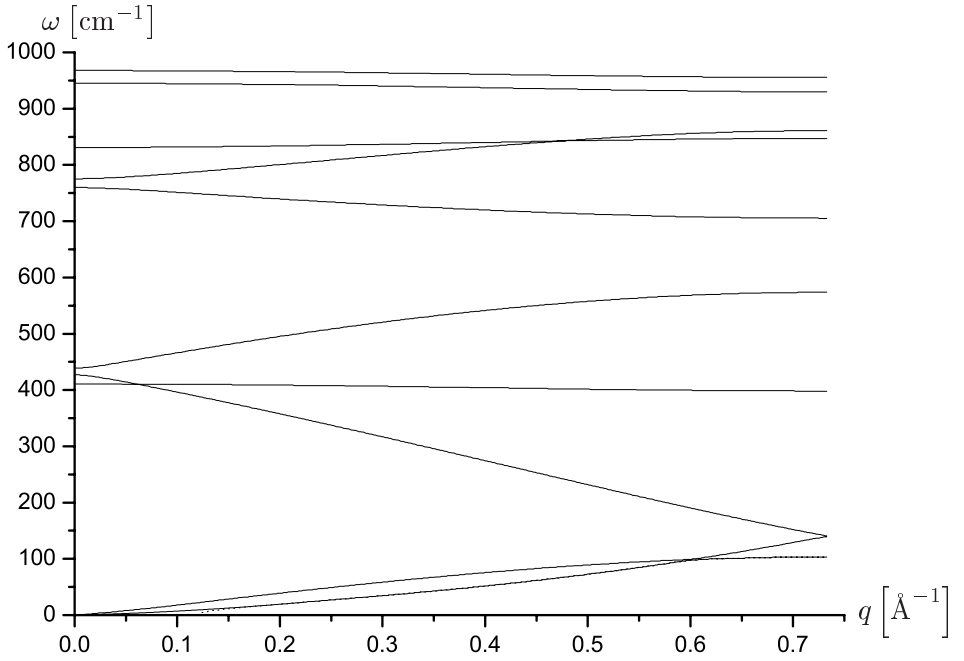

Figure 10.6: The out-of-plane phonon dispersion curves of poly(*para*-phenylene) for a super cell consisting of 3 unit cells.

10.2.3 Zone-centre Modes

Figs. 10.7-10.9 show a graphical representation of the relative atomic displacements $Q_i\vec{X}_i(q=0)$ associated with the different zone-centre modes. Different Q_i's have been chosen for the different modes in order to obtain a useful length scale of the arrows. Notice how the Raman active modes preserve inversion symmetry.

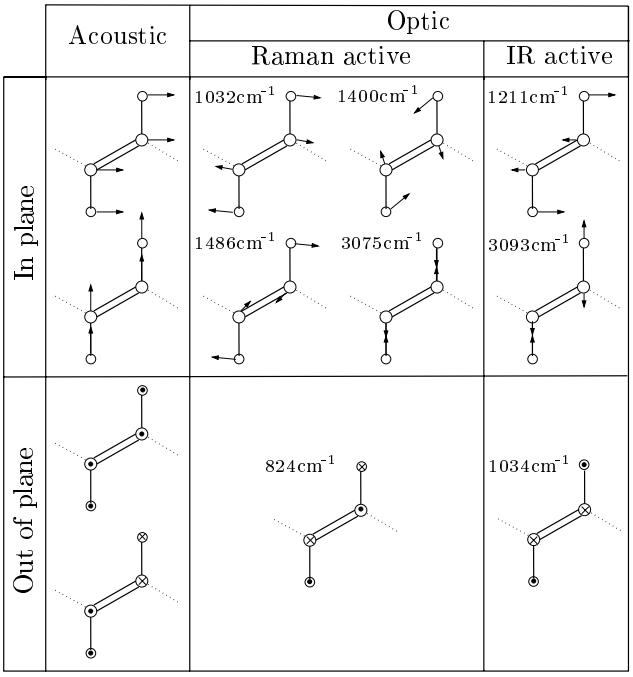

Figure 10.7: The relative displacements of the zone-centre phonon modes of *trans*-polyacetylene.

Comparison of Fig. 10.7 with the calculated tPA phonon mode displacements in Refs. [57, 59, 60] shows good agreement on the relative displacements. Furthermore, Tab. 10.3 shows a reasonably good agreement between the calculated tPA zone-centre frequencies of this work and the calculated and observed frequencies in Ref. [60] and Refs. [57, 59, 67, 77], respectively. Notice that for in-plane tPA phonon frequencies larger than 1400cm^{-1}, the frequencies of this work are consistently larger.

Comparison of Fig. 10.8 with the calculated below 2000cm^{-1} in-plane PPP phonon mode displacements in Ref. [64] shows a handful of modes for which the agreement is less than good. It has not been possible to find other calculations with which to compare. Since it has not been possible to find other calculations of the relative displacements of the out-of-plane PPP modes either, the results in Fig. 10.9 seem to be the first of their kind. Tab. 10.4 shows a comparison of the calculated PPP zone-centre frequencies of this work with calculated frequencies found in the literature. Inspection shows good correspondence for phonon

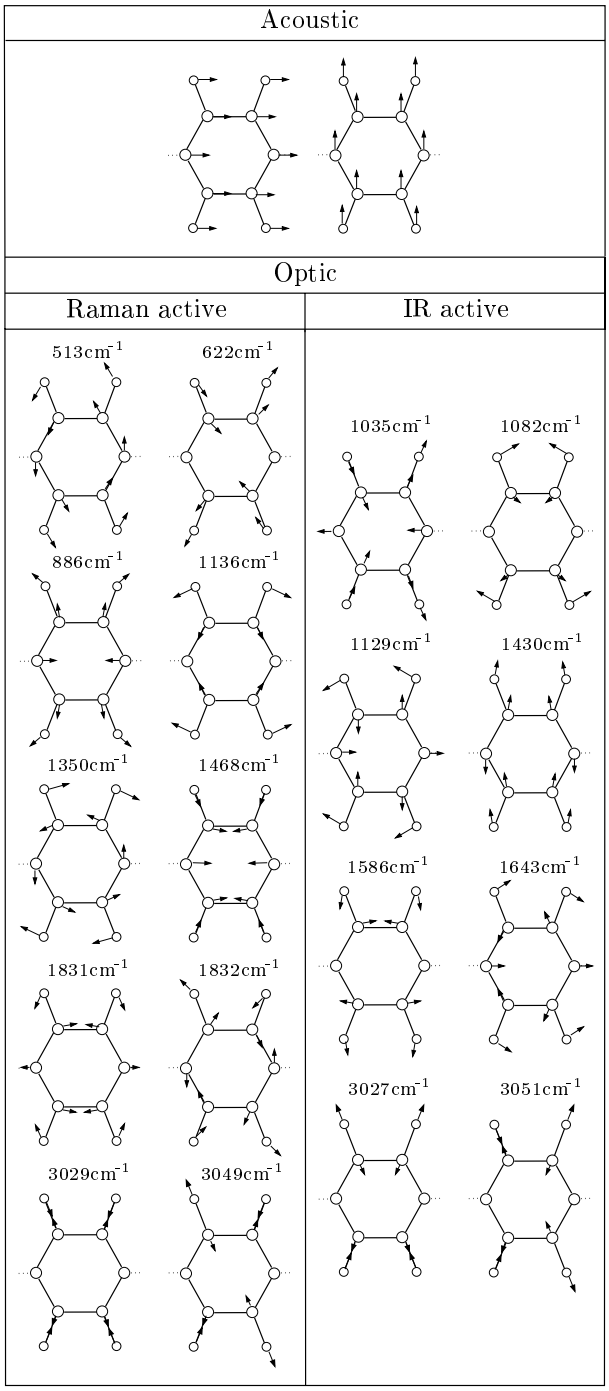

Figure 10.8: The relative displacements of the in-plane zone-centre phonon modes of poly(*para*-phenylene).

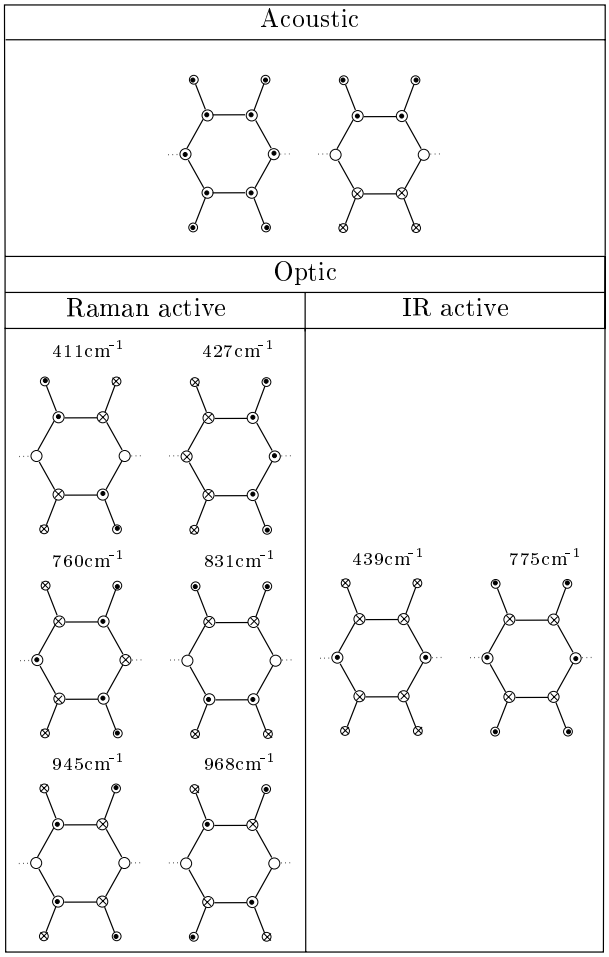

Figure 10.9: The relative displacements of the out-of-plane zone-centre phonon modes of poly(*para*-phenylene).

Table 10.3: Comparison of the calculated zone-centre phonon frequencies of *trans*-polyacetylene with calculated [60] and observed [57, 59, 67, 77] frequencies from the literature. $R_\perp$ indicates an out-of-plane Raman active mode, and all frequencies are in units of cm^{-1}. The columns marked with % show the deviation of the present results with respect to the references indicated.

	This work	[60]	[57]	[57]%	[59]	[67]	[67]%	[77]	[77]%
$R_\perp$	824	915				884	*-6.8%*		
$R_\parallel$	1032	1163	1060	*-2.6%*	1064	1012	*2.0%*		
$I_\perp$	1034	999				1066	*-3.0%*	1015	*1.9%*
$I_\parallel$	1211	1284				1170	*3.5%*	1292	*-6.3%*
$R_\parallel$	1400	1278	1285	*9.0%*		1294	*8.2%*		
$R_\parallel$	1486	1639	1450	*2.5%*	1456	1457	*2.0%*		
$R_\parallel$	3075	2979	2990	*2.8%*					
$I_\parallel$	3093	3010						3013	*2.7%*

frequencies below about $1400cm^{-1}$ and above $3000cm^{-1}$, whereas the present in-plane frequencies in the intermediate interval are consistently larger than the corresponding frequencies from the references. It should be noted that the above-mentioned deviating phonon mode displacements are evenly distributed among the below $2000cm^{-1}$ in-plane modes so that no apparent connection between the displacement and frequency deviations can be ascertained.

10.2.4 Infrared Absorption Spectrum

Figs. 10.10 and 10.11 show the IR absorption spectra of tPA and PPP, respectively, calculated from Eqs. (6.27) and (6.42). As can be deduced from symmetries in the vibrational modes presented in Figs. 10.7-10.9, the IR active modes contribute to either α_{xx}, α_{yy} or α_{zz}.

As can be seen from Fig. 10.10, observed IR spectra for tPA [60, 77] show a strong absorption line around $1000cm^{-1}$, a weak line around $3000cm^{-1}$ and an almost undiscernably weak line around $1300cm^{-1}$. Fig. 10.10 shows good agreement on the resonant frequencies in question, but a poor agreement on the relative amplitudes of the absorption lines. It is perhaps worth noting that in the calculated IR spectrum in Ref. [60], the absorption line at $1284cm^{-1}$ is nearly as strong as the line at $999cm^{-1}$.

Being based on Eq. (6.42) and thus on the approximation in Eq. (6.40), one would expect that the IR spectra could be made more accurate by taking the derivative of Eq. (6.39) numerically. However, doing so results in a huge, unphysical amplification of the CH bond stretching modes around $3000cm^{-1}$. This amplification can be attributed to the lack of self-consistency in the model, since this means that the full prize in energy is not paid for a perturbation of the electron distribution. The simultaneous CH bond stretching and compression

Table 10.4: Comparison of the calculated zone-centre phonon frequencies of poly(*para*-phenylene) with calculated frequencies from the literature. $R_\perp$ indicates an out-of-plane Raman active mode, and all frequencies are in units of cm^{-1}. The columns marked with % show the deviation of the present results with respect to the references indicated.

	This work	[62]	[62]%	[64]	[64]%
$R_\perp$	411	399	*3.0%*	401	*2.5%*
$R_\perp$	427	408	*4.7%*	402	*6.2%*
$I_\perp$	439	415	*5.8%*	458	*-4.2%*
$R_\parallel$	513	435	*17.9%*	460	*11.5%*
$R_\parallel$	622	605	*2.8%*	602	*3.3%*
$R_\perp$	760	740	*2.7%*	760	*0.0%*
$I_\perp$	775	788	*-1.7%*	790	*-1.9%*
$R_\perp$	831	805	*3.2%*	834	*-0.4%*
$R_\parallel$	886	847	*4.6%*	846	*4.7%*
$R_\perp$	945	944	*0.1%*	945	*0.0%*
$R_\perp$	968	969	*-0.1%*	961	*0.7%*
$I_\parallel$	1035	1016	*1.9%*	968	*6.9%*
$I_\parallel$	1082	1045	*3.5%*	1075	*0.7%*
$I_\parallel$	1129	1076	*4.9%*	1051	*7.4%*
$R_\parallel$	1136	1169	*-2.8%*	1127	*0.8%*
$R_\parallel$	1350	1298	*4.0%*	1328	*1.7%*
$I_\parallel$	1430	1316	*8.7%*	1268	*12.8%*
$R_\parallel$	1468	1335	*10.0%*	1289	*13.9%*
$I_\parallel$	1586	1347	*17.7%*	1440	*10.1%*
$I_\parallel$	1643	1469	*11.8%*	1510	*8.8%*
$R_\parallel$	1831	1609	*13.8%*	1661	*10.2%*
$R_\parallel$	1832	1665	*10.0%*	1654	*10.8%*
$I_\parallel$	3027	3055	*-0.9%*		
$R_\parallel$	3029	3059	*-1.0%*		
$R_\parallel$	3049	3064	*-0.5%*		
$I_\parallel$	3051	3067	*-0.5%*		

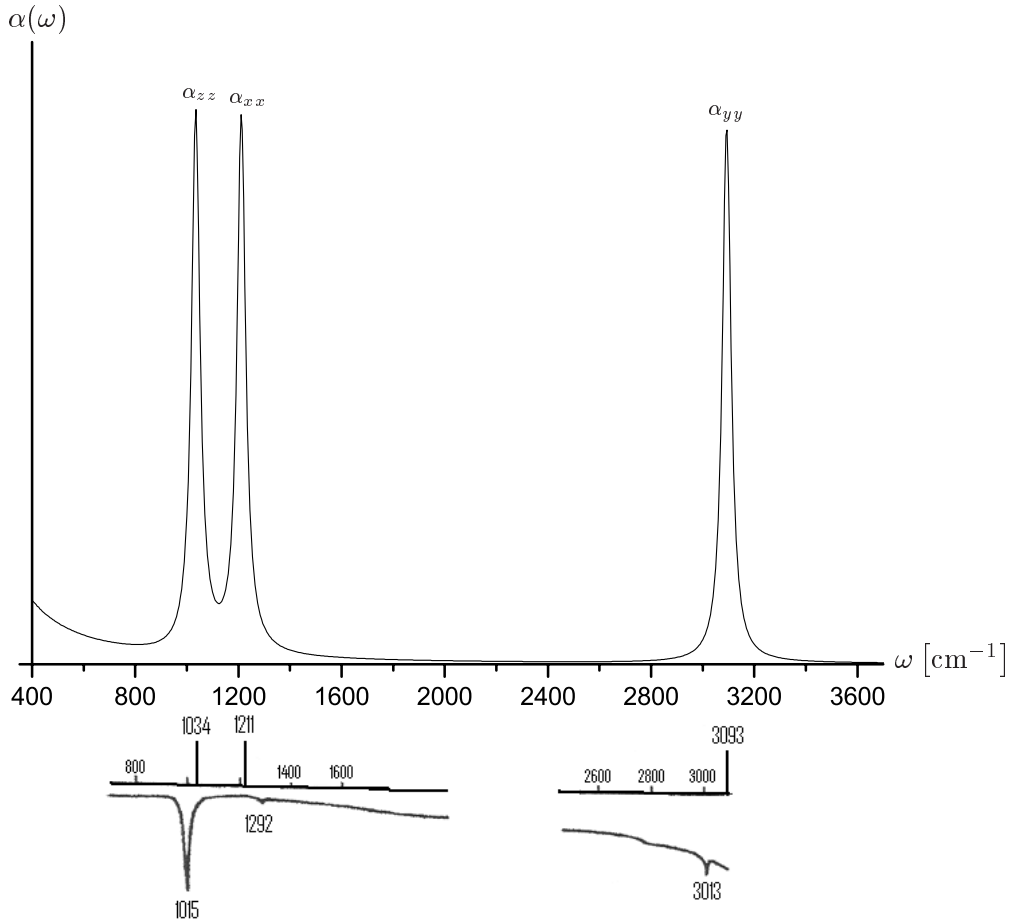

Figure 10.10: The infrared absorption spectrum $\alpha(\omega) = \alpha_{xx}(\omega) + \alpha_{yy}(\omega) + \alpha_{zz}(\omega)$ of *trans*-polyacetylene (top) compared with the experimental spectrum of Ref. [60] (bottom). The vertical bars in the bottom figure mark the infrared active zone-centre frequencies obtained in this work, while the frequencies 1015cm^{-1}, 1292cm^{-1}, and 3013cm^{-1} are from Ref. [60].

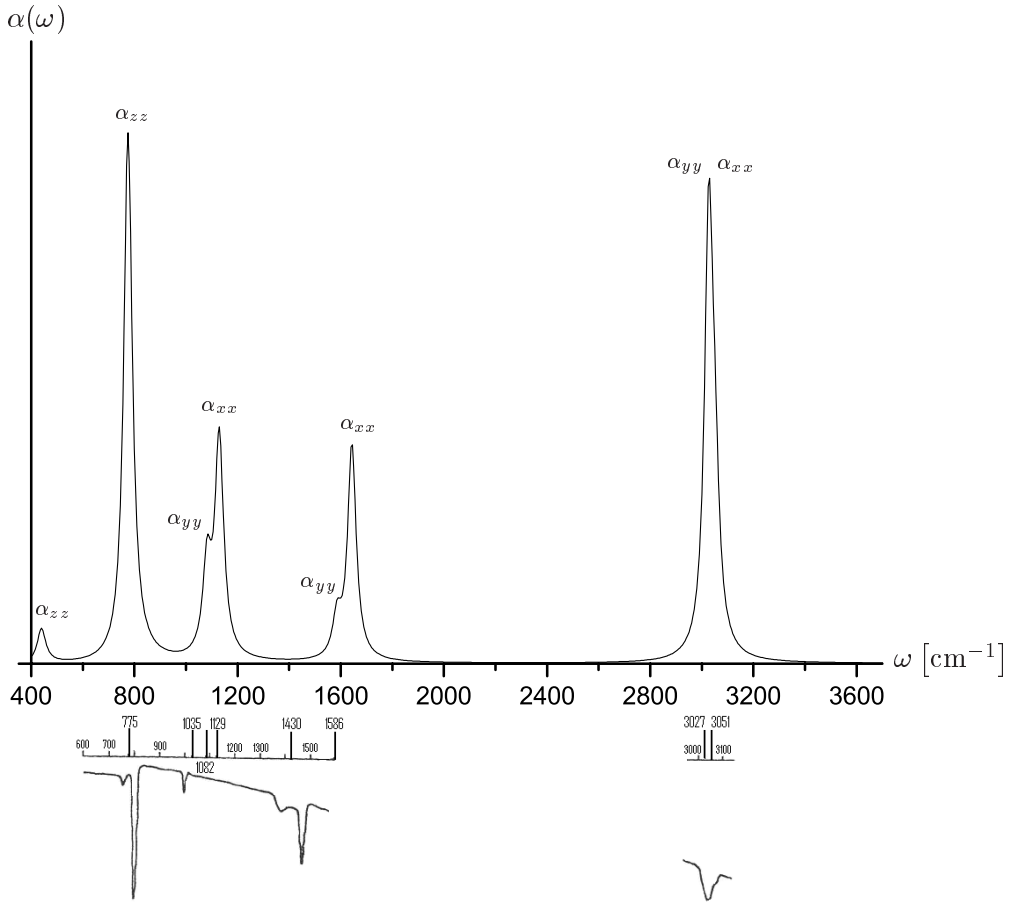

Figure 10.11: The infrared absorption spectrum $\alpha(\omega) = \alpha_{xx}(\omega) + \alpha_{yy}(\omega) + \alpha_{zz}(\omega)$ of poly(*para*-phenylene) (top) compared with the experimental spectrum of Ref. [62] (bottom). The vertical bars in the bottom figure mark the infrared active zone-centre frequencies obtained in this work. The α_{zz}- and α_{xx}-contributing modes lying outside the scale of the bottom figure are at 439cm^{-1} and 1643cm^{-1}, respectively. According to Fig. 10.8, there is an α_{xx}-contributor at 1035cm^{-1} and an α_{yy}-contributor at 1430cm^{-1} which are too weak to appear on the scale of the top figure.

thus leads to an unphysically large oscillatory change in the electron distribution within the molecule resulting in the induction of a huge change in the dipole moment. This effect necessitates the use of the quite crude approximation stated in Eq. (6.40).

For PPP [62, 78, 79], three weak absorption lines are observed around 775cm^{-1}, 1000cm^{-1} and 1400cm^{-1}, one medium absorption line is observed around 3050cm^{-1}, and two strong absorption lines are observed around 800cm^{-1} and 1475cm^{-1}. As can be seen from Fig. 10.11, this work has two strong absorption lines at 775cm^{-1} and 3027-3051cm^{-1}, two medium absorption lines at 1082-1129cm^{-1} and 1586-1643cm^{-1}, and one weak absorption line at 439cm^{-1}. The poor agreement on IR absorption intensities should not be surprising considering that DFTB, as mentioned above, due to its lack of self-consistency has a poor description of vibrationally induced perturbations of the electron distribution.

Besides the various approximations contained in the present model, the most significant deviation from experimental reality is probably the fact that the model treats a single molecule or, equivalently, a number of perfectly aligned, non-interacting molecules, whereas experiments are performed on films containing somewhat entangled molecules. Such entanglement would expectedly lead to a weakening of especially the high frequency CH modes around 3000cm^{-1} and might therefore at least partly explain the enhancement of these modes in the present IR spectra. Furthermore, this model disregards electron-phonon coupling, the torsion in the PPP molecules and the soliton effect in tPA, and parameters such as temperature and pressure, which have a role to play in experiments, are also disregarded.

10.3 Conclusion

In this chapter, the applicability of the DFTB model has been tested by calculating equilibrium configurations, phonon dispersion curves, zone-centre phonon mode displacements and IR absorption spectra for the two conjugated polymers *trans*-polyacetylene (tPA) and poly(*para*-phenylene) (PPP).

When it comes to IR absorption intensities, DFTB is not able to provide reasonable results due to its lack of self-consistency. Otherwise, the results for tPA show good agreement with results from the literature, and for PPP the agreement with the few other available results is reasonably good. As long as one does not try to describe properties that are sensitive to the lack of self-consistency, DFTB is seen to be a highly efficient computational method with which reasonable results can be obtained for the vibrational properties of extended systems such as infinite chains of conjugated polymers.

Appendix

A Derivation of the Force Component

Using Eq. (10.1) while omitting the configuration parameter $\vec{R}$ for notational reasons, the jth component of the force vector is given by[3]

$$\begin{aligned} F_j &= -\frac{1}{N_{\rm sc}}\frac{\partial V}{\partial R_j} \\ &= -\frac{2}{N_{\rm sc}}\sum_{{\rm v},k}\frac{\partial \epsilon_{\rm v}(k)}{\partial R_j} - \frac{\partial V_{\rm rep}^{\rm sc}}{\partial R_j} \quad , \quad j \in \{1,2,\ldots,3N\}, \end{aligned} \tag{A.1}$$

where $N_{\rm sc}$ and N is the number of super cells in the chain and the number of atoms in a super cell, respectively, and where

$$V_{\rm rep}^{\rm sc} = \frac{1}{N_{\rm sc}}\sum_{p<q} V_{\rm rep}^{pq}\left(\left|\vec{R}_p - \vec{R}_q\right|\right), \tag{A.2}$$

with p and q running over all atoms in the chain. $V_{\rm rep}^{\rm sc}$ is thus the repulsive potential of one super cell.

According to Eq. (2.28a), one has

$$|{\rm v}k\rangle = \frac{1}{\sqrt{N_{\rm sc}}}\sum_{\beta,n} {\rm v}_\beta(k) e^{iknL}|\beta n\rangle, \tag{A.3}$$

where $|\beta n\rangle$ is an atomic orbital in the nth super cell, and where L is the length of a super cell.

Use of Eq. (A.3) leads to

$$\begin{aligned} \frac{\partial \epsilon_{\rm v}}{\partial R_j} &= \frac{\partial \left\langle {\rm v}k \left| \hat{H} \right| {\rm v}k \right\rangle}{\partial R_j} \\ &= \sum_{\alpha,\beta}\left[\frac{\partial {\rm v}_\alpha^*}{\partial R_j}{\rm v}_\beta H_{\alpha\beta} + {\rm v}_\alpha^*\frac{\partial {\rm v}_\beta}{\partial R_j}H_{\alpha\beta} + {\rm v}_\alpha^*{\rm v}_\beta\frac{\partial H_{\alpha\beta}}{\partial R_j}\right], \end{aligned} \tag{A.4}$$

where $\hat{H}$ is the one-electron Kohn-Sham Hamiltonian of Eq. (5.7), and where

$$H_{\alpha\beta} = \sum_n e^{iknL}\left\langle \alpha 0 \left| \hat{H} \right| \beta n \right\rangle, \tag{A.5a}$$

$$S_{\alpha\beta} = \sum_n e^{iknL}\left\langle \alpha 0 | \beta n \right\rangle \tag{A.5b}$$

[3] The factor $N_{\rm sc}^{-1}$ occurs in Eq. (A.1) since a change in R_j implies the displacement of not just one atom but of all the $N_{\rm sc}$ identical atoms that correspond to the jth degree of freedom.

are the one-dimensional equivalents of the Hamilton and overlap matrix elements presented in Eqs. (2.35).

Applying $\langle\alpha 0|$ from the left on $\hat{H}|\mathrm{v}k\rangle = \epsilon_\mathrm{v}|\mathrm{v}k\rangle$ and $|\beta 0\rangle$ from the right on $\langle\mathrm{v}k|\hat{H} = \epsilon_\mathrm{v}\langle\mathrm{v}k|$, one obtains

$$\sum_\beta \mathrm{v}_\beta H_{\alpha\beta} = \epsilon_\mathrm{v} \sum_\beta \mathrm{v}_\beta S_{\alpha\beta}, \tag{A.6a}$$

$$\sum_\alpha \mathrm{v}^*_\alpha H_{\alpha\beta} = \epsilon_\mathrm{v} \sum_\alpha \mathrm{v}^*_\alpha S_{\alpha\beta}. \tag{A.6b}$$

With the help of Eqs. (A.6), Eq. (A.4) can be rewritten

$$\frac{\partial \epsilon_\mathrm{v}}{\partial R_j} = \sum_{\alpha,\beta} \left[\epsilon_\mathrm{v} \left(\frac{\partial \mathrm{v}^*_\alpha}{\partial R_j} \mathrm{v}_\beta + \mathrm{v}^*_\alpha \frac{\partial \mathrm{v}_\beta}{\partial R_j} \right) S_{\alpha\beta} + \mathrm{v}^*_\alpha \mathrm{v}_\beta \frac{\partial H_{\alpha\beta}}{\partial R_j} \right]. \tag{A.7}$$

Using the fact that $\langle\mathrm{v}k|\mathrm{v}k\rangle = 1$ implies

$$\frac{\partial}{\partial R_j} \sum_{\alpha,\beta} \mathrm{v}^*_\alpha \mathrm{v}_\beta S_{\alpha\beta} = 0, \tag{A.8}$$

one obtains

$$\frac{\partial \epsilon_\mathrm{v}}{\partial R_j} = \sum_{\alpha,\beta} \mathrm{v}^*_\alpha \mathrm{v}_\beta \left(\frac{\partial H_{\alpha\beta}}{\partial R_j} - \epsilon_\mathrm{v} \frac{\partial S_{\alpha\beta}}{\partial R_j} \right), \tag{A.9}$$

in which dependence on k and $\vec{R}$ is implicit.

Insertion of Eq. (A.9) in Eq. (A.1) yields Eq. (10.3).

Chapter 11

Polarons

As described in Chap. 7, the question of polaron formation is of importance when describing the principles of operation for semiconductor devices based on conjugated polymers (CP). Such devices include polymer-based solar cells and polymer light emitting diodes (PLED). Due to the inherently large electron-phonon coupling in organic compounds, the a priori expectation would be that of polaron formation. And polaron formation has indeed been predicted for a variety of CP in early Su-Schrieffer-Heeger (SSH)-based calculations [80, 81, 82, 83] as well as in self-consistent calculations at the Hartree-Fock (HF) level [84, 85] (see Chap. 4). However, more recent ab initio DFT calculations [86] using the BLYP functional on hole-injected oligothiophenes have shown delocalization where a corresponding HF calculation predicts the formation of a polaron. If one goes beyond pure DFT, BHandH Hybrid DFT and MP2 calculations have indicated polaron formation in hole-injected oligothiophenes [87]. There is thus seen to be a discrepancy on this point between different theoretical approaches.

As Density-Functional-based Tight-Binding (DFTB) (see Chap. 5) is a DFT method that shares the TB approach with the SSH scheme, it is hard to give an a priori prediction of whether or not DFTB will predict the formation of polarons in CP. The purpose of this chapter is to provide the answer to this question. This is done by presenting the polaron binding energies and lattice deformations of differently sized oligomers of *trans*-polyacetylene (tPA), poly(*para*-phenylene) (PPP) and poly(*para*-phenylene vinylene) (PPV). Calculations have been performed on finite oligomers partly because of the complexity of treating an infinite chain with broken periodicity due to an excess charge. But in fact finite oligomers are probably the entity of most practical interest, since, in real polymers, chain breaks and conjugation defects limit the conjugation lengths to the range of 10-100Å [88]. Furthermore, this chapter presents the first comparative study of electron and hole polaron binding energies in oligomers of tPA, PPP and PPV.

tPA has been chosen because of its status as an extensively studied model polymer, and PPP and PPV have been chosen because of their potentialities in

connection with PLED and solar cells [9, 10, 27]. Treating both linear and phenyl-based polymers, one obtains a reasonable basis for generalizing the qualitative results to all CP. Due to its degenerate ground state, tPA can contain topological "kink" solitons [89] (see Sec. 7.3) in addition to the non-topological polarons treated in this work. Polarons, however, are generic and concern all CP, and even in tPA, at low doping levels the formation of polarons (a bound charged/neutral soliton pair) is favoured over that of topological solitons [90].

The results presented in this chapter have been published in Ref. [4].

11.1 The Model

The electron and hole polaron binding energies are defined as the decrease in energy associated with the atomic configuration being allowed to adapt to the presence of an added electron and hole, respectively. In a system with the nuclei at rest, the total energy E_{tot} is given by the nuclear potential in Eq. (5.4). The equilibrium configuration $\vec{R}^0$ and the adjusted equilibrium configuration upon carrier injection $\vec{R}^0_{\mathrm{inj}}$ are found by minimization of Eq. (5.4), and the polaron binding energy is thus given by

$$E_{\mathrm{pol}} = E_{\mathrm{tot}}\left(\vec{R}^0\right) - E_{\mathrm{tot}}\left(\vec{R}^0_{\mathrm{inj}}\right), \tag{11.1}$$

where E_{tot} includes the excess carrier.

The oligomers are treated as quasi-1D structures, and interchain interaction is thus disregarded along with the torsion between adjacent phenyl rings, which in the solid phase is assumed to be small due to solid state packing.

11.2 Results

Figs. 11.1-11.3 show the electron and hole polaron binding energies in oligomers of tPA, PPP and PPV. The non-zero polaron binding energies show that for the finite oligomer chains, the ionized states have a different atomic configuration than the neutral state. The numerical value of the binding energies are a measure of the degree of deformation. Notice that the smaller polaron binding energies for the phenyl-based polymers PPP and PPV are due to the larger rigidity of a phenyl backbone compared with a linear chain such as tPA.

Figs. 11.4-11.5 show the changes in bond lengths resulting from electron injection. Corresponding figures for hole injection show qualitatively the same features with slightly weaker deformations. In Fig. 11.4 notice how the excess charge causes the bond length alternation between single and double bonds to be smoothed out. In pristine tPA, this Peierls distortion of the bond lengths occurs as the result of a compromise between a lowering of the π-valence band (increased ionization energy) and an increase in the elastic energy of the atomic

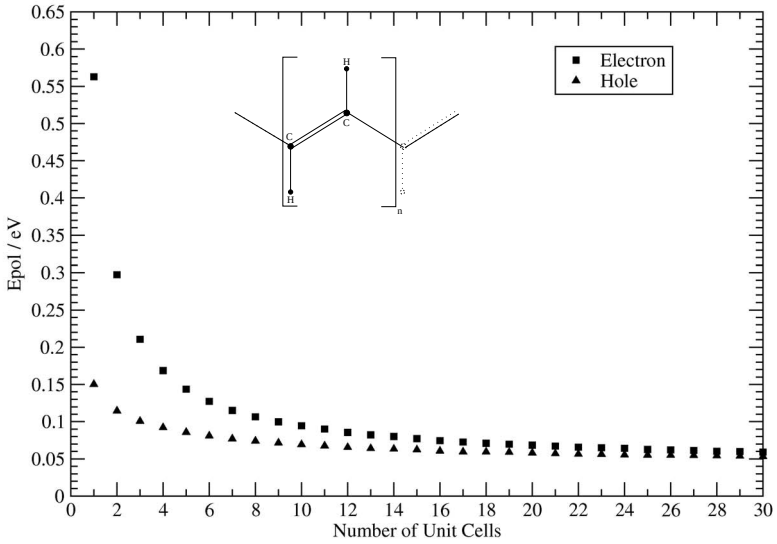

Figure 11.1: The electron and hole polaron binding energies for oligomers of *trans*-polyacetylene as a function of the number of unit cells.

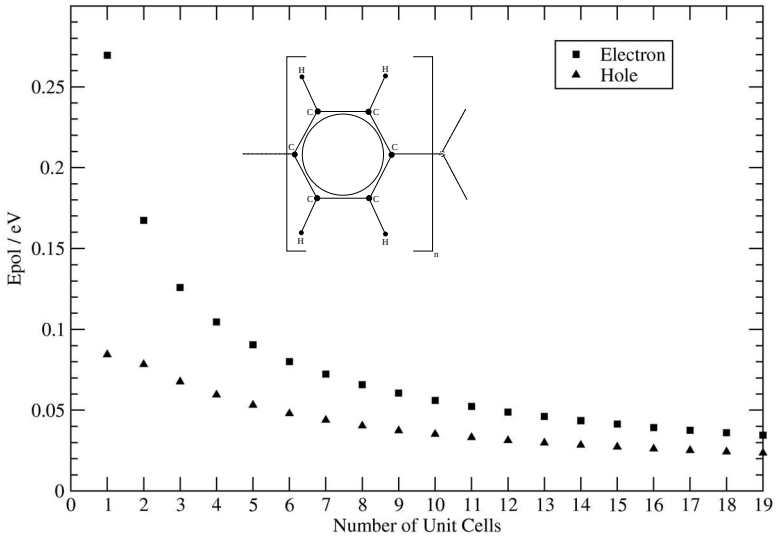

Figure 11.2: The electron and hole polaron binding energies for oligomers of poly(*para*-phenylene) as a function of the number of unit cells.

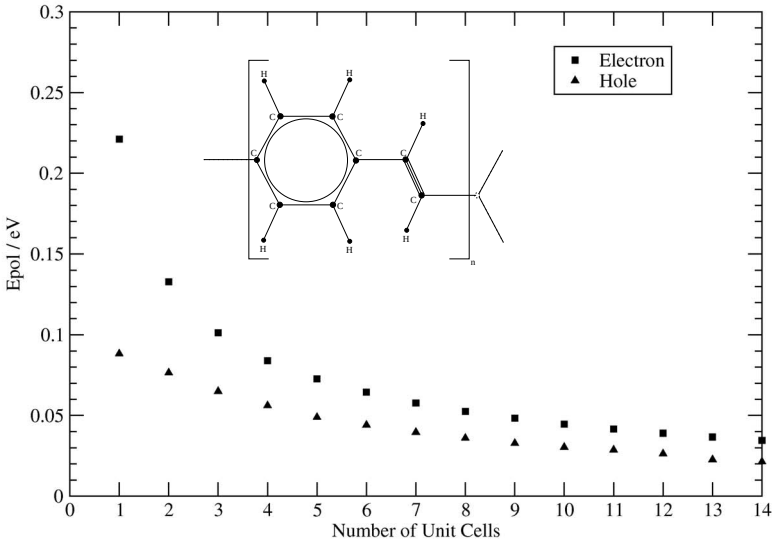

Figure 11.3: The electron and hole polaron binding energies for oligomers of poly(*para*-phenylene vinylene) as a function of the number of unit cells.

cores. However, the lowering of the π-valence band is accompanied by a corresponding elevation of the π^*-conduction band (decreased electron affinity), and this makes the dimerization less favourable in the presence of an injected electron, even though the electron is injected into a polaron energy level split of from the π^*-band and not into the π^*-band itself. In Fig. 11.5 notice how the excess charge changes the structure from a somewhat benzenoid (aromatic) to a more quinoid-like structure (see Fig. 11.6). This structural change occurs because the smaller ionization energy and larger electron affinity associated with a quinoid structure more than compensates for the elastic energy required to form the quinoid segment.

The deformations displayed in Figs. 11.4 and 11.5 show the hallmarks of a polaron, and at a first glance, the polaron binding energies in Figs. 11.1-11.3 do not seem to approach zero and thus seemingly indicate the presence of polarons in the corresponding parent polymers. But when the chain length is increased, the deformation spreads out as examplified in Figs. 11.7 and 11.8 which show the delocalized deformation of an electron-injected tPA 30-mer and PPP 19-mer, respectively. The deformation, and thus the charge, is concentrated at the middle of the chain, but as the chain becomes longer, so does the extension of the deformation. As an example, the deformation in Fig. 11.8 extends over about 11 unit cells, whereas similar figures for PPP 29- and 49-mers show deformations extending over about 13 and 15 unit cells, respectively, with the electron polaron

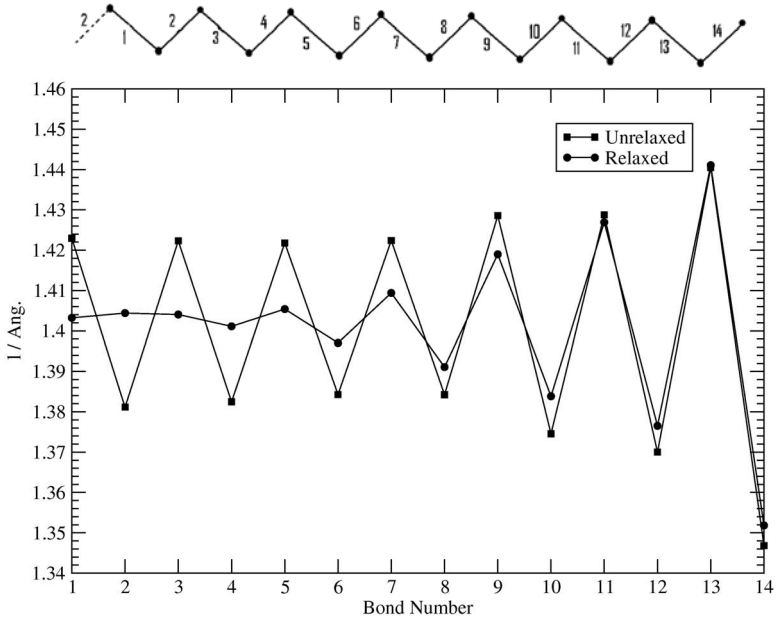

Figure 11.4: The relaxed and unrelaxed bond lengths of an electron-injected *trans*-polyacetylene 14-mer as a function of bond number (see inset). Due to symmetry, only half of the bonds are shown.

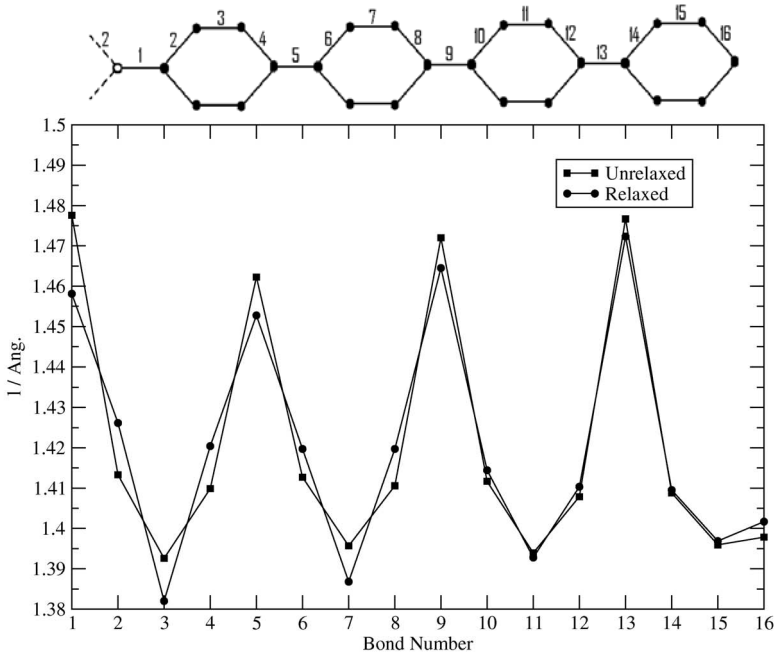

Figure 11.5: The relaxed and unrelaxed bond lengths of an electron-injected poly(*para*-phenylene) 8-mer as a function of bond number (see inset). Due to symmetry, only half of the bonds are shown.

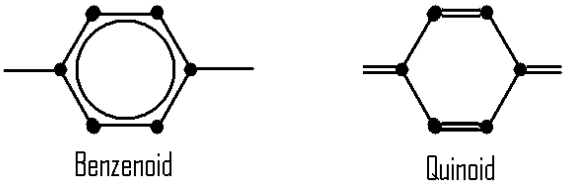

Figure 11.6: The benzenoid (aromatic) and quinoid structures.

binding energy reaching $0.019eV$ for a PPP 49-mer. For comparison, Brédas et al. reported a PPP polaron extension of 4 unit cells [82].

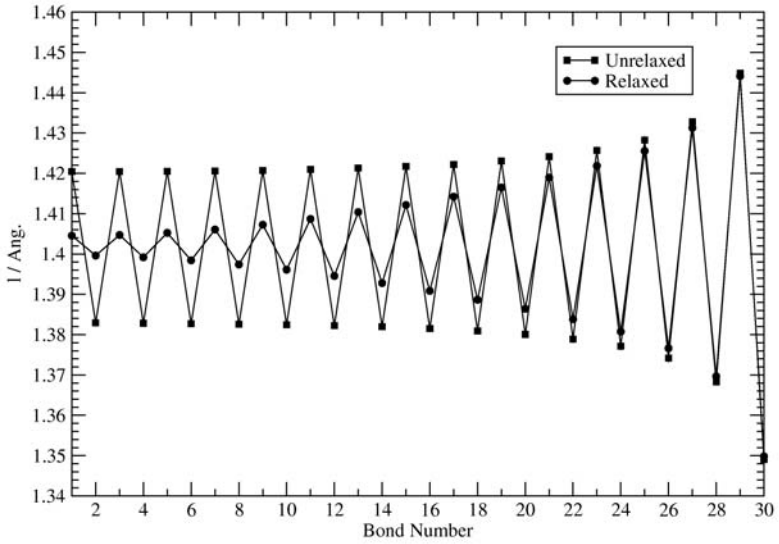

Figure 11.7: The relaxed and unrelaxed bond lengths of an electron-injected *trans*-polyacetylene 30-mer as a function of bond number (see inset to Fig. 11.4). Due to symmetry, only half of the bonds are shown.

This qualitative picture of deformation spreading is seen for all three polymers for electron as well as for hole injection. This means that in the limit where the chains become infinite, there will be no deformation, and thus the polaron binding energies in Figs. 11.1-11.3 do in fact approach zero, however slowly. The deformation leading to the non-zero polaron binding energies for the oligomers is due to the finite lengths of the oligomer chains and is not a sign of the self-localization associated with polarons. When it comes to the question of polaron formation, DFTB is thus seen to be in qualitative accordance with ab initio DFT.

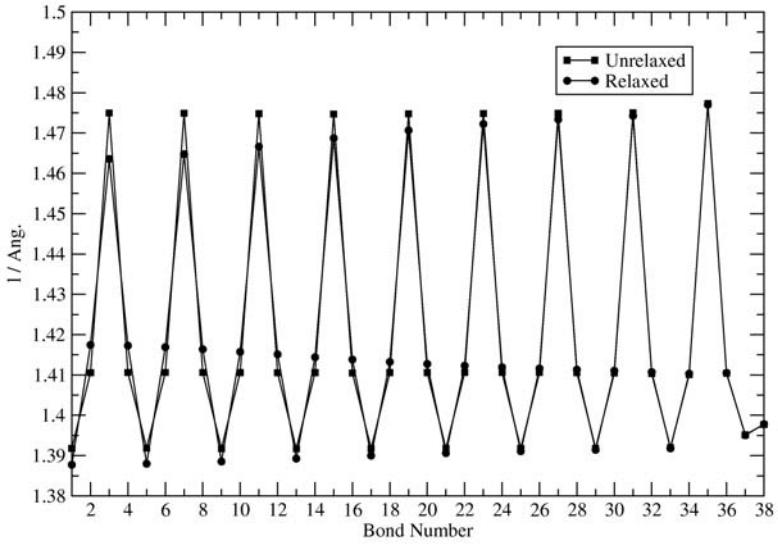

Figure 11.8: The relaxed and unrelaxed bond lengths of an electron-injected poly(*para*-phenylene) 19-mer as a function of bond number (see inset to Fig. 11.5). Due to symmetry, only half of the bonds are shown.

In this connection it should be noted that similar calculations for bipolarons (two excess electrons or two excess holes) show qualitatively the same features as mentioned above, e.g. with the electron bipolaron binding energy decreasing from $0.131eV$ in a PPP 29-mer over $0.121eV$ in a PPP 39-mer to $0.116eV$ in a PPP 49-mer.

Calculations similar to the ones presented here using the more sophisticated Self-Consistent-Charge (SCC) extension to DFTB [91] yields the following results: For tPA, one finds the same qualitative picture with $E_{\rm pol}^{\rm SCC}$ being on the order of $0.01eV$ larger than the here presented $E_{\rm pol}$. For the phenyl-based polymers, the $E_{\rm pol}^{\rm SCC}$ is of the order of $0.01eV$ smaller than the present value of $E_{\rm pol}$, and as shown in Fig. 11.9, the self-consistency in the electron charge distribution causes the charge, and thus the deformation, to disperse evenly over all but the outmost unit cells. Similar calculations performed within the spin-polarization extension to SCC-DFTB [92] show results that are in practice indistinguishable from the SCC-DFTB results.

11.3 Conclusion

In this chapter, the electron and hole polaron binding energies in oligomers of *trans*-polyacetylene (tPA), poly(*para*-phenylene) (PPP) and poly(*para*-phenylene

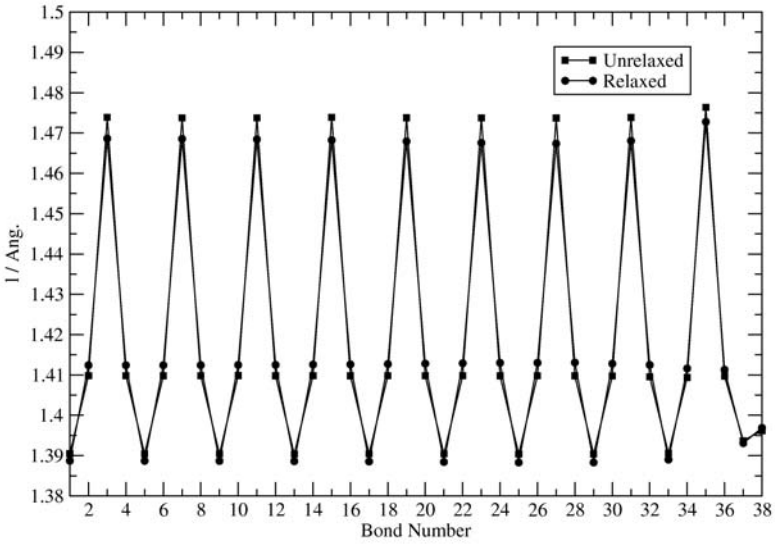

Figure 11.9: The SCC-DFTB equivalent of Fig. 11.8.

vinylene) (PPV) have been calculated using the computationally efficient DFTB method. The calculations show that the injection of an excess charge into the corresponding infinite parent polymers does not lead to the formation of a polaron. Instead the excess charge spreads out over the chain. In this prediction, DFTB is in accordance with ab initio DFT. In the finite oligomers, the boundary induced deformations show the same qualitative features as would be seen in the case of a polaron: In oligo-tPA the dimerization is smoothed out, whereas in oligo-PPP and -PPV, the structure changes from a benzenoid-like to a quinoid-like structure. The present comparative study of a linear polymer such as tPA with phenyl-based polymers such as PPP and PPV also shows the larger rigidity of the phenyl-backbone as indicated by the smaller polaron binding energies of the phenyl-based polymers.

Part V

Concluding Remarks

Summary of Conclusions

Besides presenting analytic closed-form expressions for the linear optical susceptibility tensor of *trans*-polyacetylene (tPA) along with the long-axis linear optical susceptibility and the imaginary part of the short-axis linear optical susceptibility of poly(*para*-phenylene) (PPP), Chap. 8 lead to an analytic closed-form expression for the long-axis linear optical susceptibility of a general conjugated polymer (CP) valid for photon energies in the vicinity of the band gap. In Chap. 9, an analytic, perturbative expression for the electro-optic susceptibility of PPP was derived and its applicability assessed by comparison with a numerical evaluation.

Chap. 10 demonstrated the applicability of the computationally highly efficient Density Functional-based Tight-Binding (DFTB) approach to phonon dynamics in CP. This was done by calculating equilibrium configurations, phonon dispersion curves, zone-centre phonon mode displacements and IR absorption peaks of tPA and PPP. The shortcoming of the non-self-consistent DFTB approach in calculating IR absorption intensities was also demonstrated. Besides presenting the first comparative study of electron and hole polaron binding energies in oligomers of tPA, PPP and poly(*para*-phenylene vinylene) (PPV), Chap. 10 showed that DFTB, in accordance with ab initio density functional theory, does not predict polaron formation in CP. The finite oligomers show the polaron-like deformations, but as the chain lengths are increased, the deformations become smeared out.

Outlook

This work leaves a large number of possible continuations and improvements. Besides improving the model limitations listed in Sec. 1.2, obvious extensions would be to consider excitonic (electron-electron coupling) and polaronic (electron-phonon coupling) effects when treating the optical properties and to combine

the phonon and polaron results by including polaronic effects in the treatment of phonon dynamics. Another interesting extension would be to include static electric fields in the treatment of both phonons and polarons. This short list is by no means exhaustive.

Bibliography

Bibliography

[1] T. B. Lynge and T. G. Pedersen. *Phys. Rev. B*, 67:075206, 2003.

[2] T. B. Lynge and T. G. Pedersen. *Synth. Met.*, 138:329, 2003.

[3] T. B. Lynge and T. G. Pedersen. *Phys. Status Solidi B*, 241:1005, 2004.

[4] T. B. Lynge and T. G. Pedersen. *Comp. Mat. Sci.*, 30:212, 2004.

[5] A. J. Heeger, S. Kivelson, J. R. Schrieffer, and W.-P. Su. *Rev. Mod. Phys.*, 60:781, 1988.

[6] K. Shimamura, F. E. Karasz, J. A. Hirsch, and J. C. W. Chien. *Makromol. Chem., Rapid Commun.*, 2:473, 1981.

[7] M. Pope, M. Kallmann, and P. Magnante. *J. Chem. Phys.*, 38:2042, 1963.

[8] C. K. Chiang, C. R. Fincher Jr., Y. W. Park, A. J. Heeger, H. Shirakawa, E. J. Louis, S. C. Gau, and A. G. MacDiarmid. *Phys. Rev. Lett.*, 39:1098, 1977.

[9] N. S. Sariciftci, L. Smilowitz, A. J. Heeger, and F. Wudl. *Science*, 258:1474, 1992.

[10] R. H. Friend, R. W. Gymer, A. B. Holmes, J. H. Burroughes, R. N. Marks, C. Taliani, D. D. C. Bradley, D. A. Dos Santos, J. L. Brédas, M. Lögdlund, and W. R. Salaneck. *Nature (London)*, 397:121, 1999.

[11] A. Kraft, A. C. Grimsdale, and A. B. Holmes. *Angew. Chem. Intl. Ed.*, 37:402, 1998.

[12] M. Wohlgenannt, E. J. W. List, C. Zenz, G. Leising, W. Graupner, and Z. V. Vardeny. *Synth. Met.*, 116:353, 2001.

[13] S. Ramasesha and I. D. L. Albert. *Chem. Phys. Lett.*, 196:287, 1992.

[14] N. Tessler. *Adv. Mat.*, 11:363, 1999.

[15] G. Horowitz. *Adv. Mat.*, 10:365, 1998.

[16] C. Cojan, G. P. Agrawal, and C. Flytzanis. *Phys. Rev. B*, 15:909, 1977.

[17] C. R. Fincher Jr., M. Ozaki, M. Tanaka, D. Peebles, L. Lauchlan, A. J. Heeger, and A. G. MacDiarmid. *Phys. Rev. B*, 35:9708, 1987.

[18] D. Baeriswyl, G. Harbeke, H. Kiess, E. Meier, and W. Meyer. *North Holland*, 1983.

[19] T. K. Lee and S. Kivilson. *Phys. Rev. B*, 29:6687, 1984.

[20] J. L. Brédas, B. Thémans, J. G. Fripiat, and J. M. André. *Phys. Rev. B*, 29:6761, 1984.

[21] J. Fink and G. Leising. *Phys. Rev. B*, 34:5320, 1986.

[22] J. Fink. *Synth. Met.*, 21:87, 1987.

[23] E. C. Ethridge and J. L. Fry. *Phys. Rev. B*, 53:3662, 1996.

[24] M. Rohlfing and S. G. Louie. *Phys. Rev. Lett.*, 82:1959, 1999.

[25] C.-S. Neumann and R. von Baltz. *Phys. Rev. B*, 35:9708, 1987.

[26] J. H. Burroughes, D. D. C. Bradley, A. R. Brown, R. N. Marks, K. Mackay, R. H. Friend, P. L. Burns, and A. B. Holmes. *Nature (London)*, 347:539, 1990.

[27] G. Grem, G. Leditzky, B. Ullrich, and G. Leising. *Synth. Met.*, 51:383, 1992.

[28] G. Grem, G. Leditzky, B. Ullrich, and G. Leising. *Adv. Mat.*, 4:36, 1992.

[29] A. W. Grice, D. D. C. Bradley, M. T. Bernius, M. Insebasekaran, W. W. Wu, and E. P. Woo. *App. Phys. Lett.*, 73:629, 1998.

[30] C. Ambrosch-Draxl, J. A. Majewski, P. Vogl, and G. Leising. *Phys. Rev. B*, 51:9668, 1995.

[31] R. B. Capaz and M. J. Caldas. *J. Mol. Struc.*, 464:31, 1999.

[32] T. B. Boykin and P. Vogl. *Phys. Rev. B*, 65:035202, 2001.

[33] W. Heisenberg. *Z. Physik*, 33:879, 1925.

[34] E. Schrödinger. *Ann. Phys. (Leipzig)*, 79:361, 1926.

[35] M. Born and J. R. Oppenheimer. *Ann. Phys.*, 84:457, 1927.

[36] L. H. Thomas. *Proc. Cambridge Phil. Soc.*, 23:542, 1927.

[37] E. Fermi. *Atti. Accad. Naz. Lincei, Cl. Sci. Fis. Mat. Nat. Rend*, 6:602, 1927.

[38] D. R. Hartree. *Proc. Cambridge Phil. Soc.*, 24:89, 1928.

[39] V. Fock. *Z. Physik*, 61:126, 1930.

[40] J. C. Slater. *Phys. Rev.*, 35:210, 1930.

[41] P. Hohenberg and W. Kohn. *Phys. Rev. B*, 136:864, 1964.

[42] P. A. M. Dirac. *Proc. Cambridge Phil. Soc.*, 26:376, 1930.

[43] W. Kohn and L. J. Sham. *Phys. Rev. A*, 140:1133, 1965.

[44] D. Porezag, Th. Frauenheim, Th. Köhler, G. Seifert, and R. Kaschner. *Phys. Rev. B*, 51:12947, 1995.

[45] D. Porezag. *PhD Thesis*. Technical University of Chemnitz-Zwickau, 1997.

[46] J. P. Perdew and A. Zunger. *Phys. Rev. B*, 23:5048, 1979.

[47] J. C. Slater and G. F. Koster. *Phys. Rev.*, 94:1498, 1954.

[48] H. Eschrig. *Phys. Status Solidi B*, 96:329, 1979.

[49] S. Ikehata, J. Kaufer, T. Woerner, A. Pron, M. A. Druy, A. Sivak, A. J. Heeger, and A. G. McDiarmid. *Phys. Rev. Lett.*, 45:1123, 1980.

[50] M. Peo, S. Roth, K. Dransfeld, B. Tieke, J. Hocker, H. Gross, A. Grupp, and H. Sixl. *Solid State Commun.*, 35:119, 1980.

[51] T. G. Pedersen and T. B. Lynge. *Phys. Rev. B*, 65:085201, 2002.

[52] N. W. Ashcroft and D. N. Mermin. *Solid State Physics, International Edition*. Saunders College, Philadelphia, 1976.

[53] D. E. Aspnes and J. E. Rowe. *Phys. Rev. B*, 5:4022, 1972.

[54] K. A. Pronin, R. H. Friend, and D. D. C. Bradley. *Synth. Met.*, 71:1689, 1995.

[55] F. Inagaki, M. Tasumi, and T. Miyazawa. *J. Raman Spec.*, 3:335, 1975.

[56] E. J. Mele and M. J. Rice. *Sol. State Comm.*, 34:339, 1980.

[57] F. B. Schügerl and H. Kuzmany. *J. Chem. Phys.*, 74:953, 1981.

[58] E. J. Mele. *Mol. Cryst. Liq. Cryst.*, 77:25, 1981.

[59] D. Jumeau, S. Lefrant, E. Faulques, and J. P. Buisson. *J. Physique*, 44:819, 1983.

[60] D. Raković, I. Božović, S. A. Stepanyan, and L. A. Gribov. *Phys. Rev. B*, 28:1997, 1983.

[61] G. Zannoni and G. Zerbi. *J. Mol. Struct.*, 100:485, 1983.

[62] D. Raković, I. Božović, S. A. Stepanyan, and L. A. Gribov. *Sol. State Comm.*, 43:127, 1982.

[63] C. Menéndez and F. Guinea. *Phys. Rev. B*, 28:2183, 1983.

[64] G. Zannoni and G. Zerbi. *J. Chem. Phys.*, 82:31, 1985.

[65] V. Hernandez, J. Soto, and J. T. Lopez Navarrete. *Synth. Met.*, 55-57:4461, 1993.

[66] C. Q. Wu, R. T. Fu, Z. Q. Li, and Y. Kawazoe. *J. Phys.: Condens. Matter*, 1997.

[67] J. Miao, C. Q. Wu, X. Sun, R. T. Fu, Z. Q. Li, and Y. Kawazoe. *Synth. Met.*, 101:314, 1999.

[68] W. Förner and W. Utz. 2002.

[69] D. Sánchez-Portal and E. Hernández. *Phys. Rev. B*, 66:235415, 2002.

[70] R. B. Capaz and M. J. Caldas. *J. Mol. Struct.*, 464:31, 1999.

[71] W. Frank, C. Elsässer, and M. Fähnle. *Phys. Rev. Lett.*, 74:1791, 1995.

[72] E. C. Ethridge, J. L. Fry, and M. Zaider. *Phys. Rev. B*, 53:3662, 1996.

[73] J. W. Mintmire and C. T. White. *Phys. Rev. B*, 28:3283, 1983.

[74] A. Karpfen and J. Petkov. *Solid State Commun.*, 29:251, 1979.

[75] R. Fu, M. H. Lee, and M. C. Payne. *J. Phys.: Condens. Matter*, 8:2539, 1996.

[76] H. Kahlert, O. Leitner, and G. Leising. *Synth. Met.*, 17:467, 1987.

[77] H. Shirakawa and S. Ikeda. *Polym. J.*, 2:231, 1971.

[78] L. W. Shacklette, R. R. Chance, D. M. Ivory, G. G. Miller, and R. H. Baughman. *Synth. Met.*, 1:307, 1979.

[79] M. Hanfland, A. Brillante, K. Syassen, M. Stamm, and J. Fink. *J. Chem. Phys.*, 90:1930, 1989.

[80] W.-P. Su and J. R. Schrieffer. *Proc. Natl. Acad. Sci. USA*, 77:5626, 1980.

[81] D. K. Campbell and A. R. Bishop. *Phys. Rev. B*, 24:4859, 1981.

[82] J. L. Brédas, R. R. Chance, and R. Silbey. *Mol. Cryst. Liq. Cryst.*, 77:319, 1981.

[83] S. Stafström and K. A. Chao. *Phys. Rev. B*, 30:2098, 1984.

[84] D. S. Boudreaux, R. R. Chance, J. L. Brédas, and R. Silbey. *Phys. Rev. B*, 28:6927, 1983.

[85] J. L. Brédas, B. Thémans, J. G. Fripiat, J. M. André, and R. R. Chance. *Phys. Rev. B*, 29:6761, 1984.

[86] G. Moro, G. Scalmani, U. Cosentino, and D. Pitea. *Synth. Met.*, 108:165, 2000.

[87] V. M. Geskin, A. Dkhissi, and J. L. Brédas. *Int. J. Quantum Chem.*, 91:350, 2003.

[88] H. A. Mizes and E. M. Conwell. *Phys. Rev. Lett.*, 70:1505, 1993.

[89] A. J. Heeger, S. Kivelson, J. R. Schrieffer, and W.-P. Su. *Rev. Mod. Phys.*, 60:781, 1988.

[90] J. L. Brédas, R. R. Chance, and R. Silbey. *Phys. Rev. B*, 26:5843, 1982.

[91] M. Elstner, D. Porezag, G. Jungnickel, J. Elsner, M. Haugk, Th. Frauenheim, S. Suhai, and G. Seifert. *Phys. Rev. B*, 58:7260, 1998.

[92] C. Köhler, G. Seifert, U. Gerstmann, M. Elstner, H. Overhof, and Th. Frauenheim. *Phys. Chem. Chem. Phys.*, 3:5109, 2001.

Dansk resume

Denne ph.d.-afhandling omhandler konjugerede polymerer, der udgør et forskningsområde i hastig vækst. I dag indgår konjugerede polymerer i forskningen inden for bla. plastikbaserede solceller, fotodetektorer og lysdioder, og sådanne plastikbaserede komponenter udgør allerede i dag et alternativ til de tilsvarende traditionelle siliciumbaserede halvlederkomponenter. Hvis plastikbaserede halvlederkomponenter som ventet inden for en overskuelig fremtid bliver i stand til at kombinere høj kvalitet med relativt begrænsede produktionsomkostninger, vil plastikkomponenter komme til at spille en betydelig rolle i fremtidens elektronikindustri.

I denne afhandling behandles specifikt de tre konjugerede polymerer *trans*-polyacetylen (tPA), poly(*para*-phenyl) (PPP) og poly(*para*-phenyl vinyl) (PPV). Afhandlingens forskningsresultater, som er opnået inden for tight-binding-modellen, består af to dele. I den ene del udledes analytiske udtryk for polymerernes optiske egenskaber udtrykt ved den optiske susceptibilitet såvel i tilstedeværelsen som i fraværet af et statisk elektrisk felt. I den anden del anvendes den beregningsmæssigt effektive DFTB-model (tæthedsfunktionalbaseret tight-binding-model) til at beskrive fononer og polaroner i de ovennævnte polymerer. Afhandlingens første del indeholder de teoretiske forudsætninger for en gennemgang af de præsenterede forskningsresultater.